Smartphone to Smartphone Visible Light Communications

Rayana Boubezari
Faculty of Engineering and Environment
Northumbria University

This dissertation is submitted for the degree of
Doctor of Philosophy

March 2018

To my loving parents, Amel and Abdelhafid,

to my siblings, Yousra, Abderrahim and Djouhaina, and their respective families,

this humble work is a sign of my love to you ...

Declaration

I hereby declare that except where specific reference is made to the work of others, the contents of this thesis containing 32081 words are original and have not been submitted in whole or in part for consideration for any other degree or qualification in this, or any other university.

Rayana Boubezari

March 2018

Acknowledgements

Firstly, I would like to apologise in case I have missed anyone, this was certainly not intentional.

Secondly, I would like to acknowledge the financial support received from Northumbria University in the form of a full PhD studentship, laboratory equipment and several travel grants to attend international conferences. I would also like to acknowledge the financial support received from Intel-NTU during my internship in their research centre, from Qatar University during my stay in Doha, as well as the travel grant received from the European Cooperation in Science and Technology to attend the Opticwise Summer School in Istanbul, Turkey.

Now I would like to thank all the individuals that contributed to this outstanding PhD experience.

The first person I would like to thank is my principal supervisor, Dr. Hoa Le-Minh, for guiding me through my PhD and giving me constructive feedback to help me achieve the work presented in this thesis and several publications. He also provided valuable opportunities for me to travel and collaborate with other research groups.

Then, I would like to thank the head of the Optical Communications Research Group (OCRG), Pr. Fary Ghassemlooy for his support, guidance, constant enthusiasm, dedication and professionalism. Working with him was an immense privilege.

Additionnaly, I would like thank my second supervisor, Pr. Ahmed Bouridane,

for his full confidence, his critical feedback and also for believing in me before the PhD journey even started.

I would like to offer special thanks to Hsin-Mu Tsai from National Taiwan University, also known as Michael, for welcoming me in his research group, and giving me the opportunity to visit Taiwan. I absolutely loved travelling there and working with you and your students and I am forever grateful for this life-changing experience. You are a role model in terms of professionalism and dedication.

I would also like to thank Dr. Somaya Al-Maadeed, for welcoming me in her research group in Qatar University. You gave me the opportunity to live an enriching experience and I enjoyed every minute.

To my parents, Amel and Abdelhafid Boubezari, thank you for being there for me and supporting me my entire life. Making you proud is the biggest achievement and I hope I fulfilled this ambition with this thesis.

Thank you to my sister Yousra, you already know how much I appreciate everything you have done and do for me every single day.

To Zina, Abderrahim, Djouhaina, Hind, Zakaria, Samy, Faycal, Yacine, Affaf and all the others, thank you for being in my life. A family like ours is all that one can wish for.

To Redouane Boukadoum, thank you for providing an endless support and for making me laugh every day although remotely.

To Louiza Oudni and Remy Peyret, my technical and personal advisors and two of the smartest people I have ever met, thank you for your priceless contributions to this work and to my life in general. I wish you all the success that you deserve and I hope I will be there for you as much as you were there for me.

Arezoo Amirkhalili, going through the whole PhD journey with you was an absolute delight. I loved sharing my life with you during the process of us becoming

doctors, and I cannot wait to experience many more adventures with you. Plus, no words can describe everything you did for me, so thank you …

Abstract

Visible light communications (VLC) is an emerging technology of optical wireless communications, which has been in the research spotlight recently, thanks to the remarkable development of light emitting diodes. Furthermore, optical camera communications, a timely VLC topic, has earned a great share of researchers'interest in the last few years, given the wide availability of digital cameras.

This thesis proposes to merge two separate technologies: image processing and VLC, to create a camera-based VLC system. Moreover, the work presented in this thesis describes a short-range mobile-to-mobile communication link, where the transmitter and the receiver are the smartphone's screen and camera, respectively. In addition, the data is encoded into images and subsequently beamed out of the transmitter's screen, and the receiver's camera captures consecutive frames containing the transmitter's screen to extract the data.

The proposed system offers inherent advantages in terms of portability and simplicity of implementation as it uses available screens and smartphone cameras. Additionally, the system is software-based and does not require any hardware modifications on the devices, thus making a high potential for millions of consumers.

The system proposed in this thesis is designed for mobile users. Therefore, high performance in dynamic environments is required. Moreover, combining image processing and VLC for smartphone to smartphone VLC is an innovative topic and very few works reported similar communication links. As such, it is imperative to

investigate the impact of computer vision challenges on the system's performance, such as the detection of the transmitter by the receiver's camera, in dynamic conditions. Consequently, this work focuses on the development of an effective algorithm to capture frames containing the transmitter as well as other objects in the background, detect the transmitter contained in the received frames, and then finally extract the originally transmitted information.

The end-to-end system is fully implemented on a mobile platform and a range of experiments are carried out in order to evaluate the system's performance. It is proved that the system is able to achieve very high success rate that reaches 98% data recovery of transmitted images under test conditions, demonstrating a practical link with a possible 100 kbps data transmission capability.

Table of contents

List of figures

List of tables

Nomenclature

Acronyms

ANT	**A**daptive **N**etwork **T**echnology
ASCII	**A**merican **S**tandard **C**ode for **I**nformation **I**nterchange
ASK	**A**mplitude **S**hift **K**eying
BER	**B**it **E**rror **R**ate
BSR	**B**it **S**uccess **R**ate
CCD	**C**harged **C**oupled **D**evice
CDMA	**C**ode **D**ivision **M**ultiple Access
CMOS	**C**omplementary **M**etal **O**xid **S**emiconductor
CSK	**C**ode **S**hift **K**eying
dB	**D**ecibels
DOB	**D**egree **O**f **B**lur
FOV	**F**ield **O**f **V**iew
FSO	**F**ree **S**pace **O**ptics

HSI	**H**ue **S**aturation **I**ntensity
HSV	**H**ue **S**aturation **V**alue
HT	**H**ard **T**hresholding
IM/DD	**I**ntensity **M**odulation **D**irect **D**etection
IoT	**I**nternet of **T**hings
IR	**I**nfra **R**ed
LCD	**L**iquid **C**rystal **D**isplays
LED	**L**ight **E**mitting **D**iode
LOS	**L**ine **O**f **S**ight
MIMO	**M**ultiple **I**nput **M**ultiple **O**utput
NFC	**N**ear **F**ield **C**ommunications
NRZ	**N**on **R**eturn to **Z**ero
OCC	**O**ptical **C**amera **C**ommunications
OFDM	**O**rthogonal **F**requency **D**ivision **M**ultiplexing
OOK	**O**n **O**ff **K**eying
OWC	**O**ptical **W**ireless **C**ommunications
PAM	**P**ulse **A**mplitude **M**odulation
RFID	**R**adio **F**requency **ID**entification
RF	**R**adio **F**requency

RGB	**R**ed **G**reen **B**lue
Rx	**R**eceiver
S2SVLC	**S**martphone **TO S**martphone **V**isible **L**ight **C**ommunications
ST	**S**oft **T**hresholding
SURF	**S**peeded **U**p **R**obust **F**eatures
Tx	**T**ransmitter
VLC	**V**isible **L**ight **C**ommunications
WMAN	**W**ireless **M**etropolitan **A**rea **N**etwork

Symbols

B_H	Screen High Brightness Level
B_L	Screen Low Brightness Level
F_b	Bright frame
F_d	Dark frame
T_b	Bright frame duration
T_d	Dark frame duration

Chapter 1

Introduction

1.1 Background

The human visual system is composed of two functional parts: the eye which operates like a sensor and part of the brain which processes the received information. The optic nerve transfers the information between the eye and the brain [2]. Figure 1.1 shows the cross section of the human eye ball. Moreover, a healthy human eye reacts when exposed to visible light arrays of a scene, and sends an electric signal to the brain, reflecting the perceived scene [3]. The human visual system was an inspiration for the camera invention as it is one of the most effective image processing and analysis system.

Light travels on a straight line. However, when the light beams penetrate through a small hole, the beams are not diffused but they form an inverted image on a flat surface parallel to the hole. This is the most fundamental optic law on which the human eye and the camera systems are based. Throughout time, cameras have evolved based on this concept until digital cameras were created, where an array of optical sensors capture light and form a digital image. Moreover, digital cameras have known such a phenomenal development since the first ever digital camera

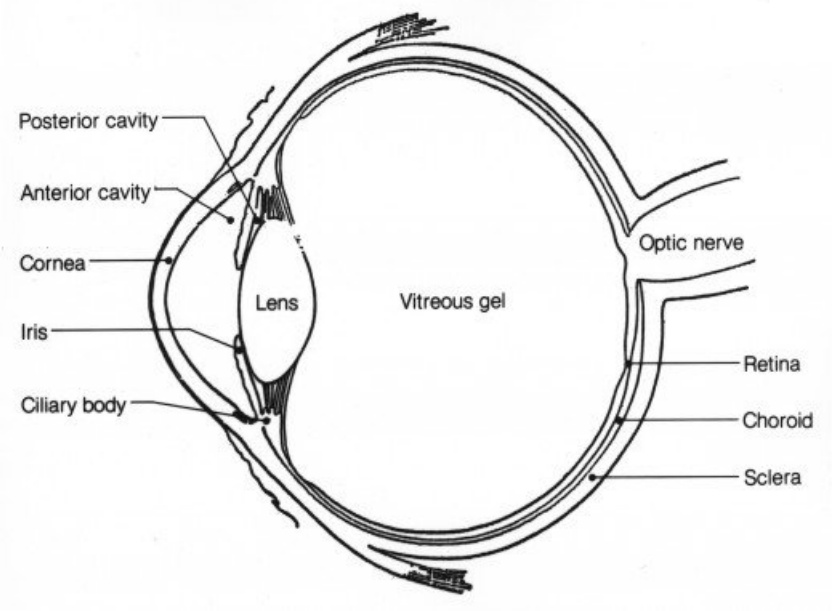

Figure. 1.1 Cross section of the human eye ball [1]

created by Kodak in 1975, that high resolution cameras are now available in everywhere in all public and private places, on personal devices such as laptops and smartphones, on building and store entrances etc. Furthermore, a picture is worth a thousand words. Therefore, it was only a matter of time before these widely available high rate cameras were combined with extremely fast light sources and high definition screens to develop a new born technology called camera communications.

In summary, camera communication takes advantage of the extremely technologized environment to create a complementary communication option to fulfill the constant need of communicating more and faster.

1.2 Research motivations

The ever increasing growth in telecommunication networks has led to a huge bandwidth requirement provoking thus a spectrum saturation. In fact, radio frequency

(RF) technologies are extensively used in wireless based communications systems. RF applications vary from short range indoor communications such as near field communications (NFC), Wi-Fi or Bluetooth to mobile cellular networks [4] up to medium-to-long range links such as millimeter wave back-hauling [5] and satellite-to-Earth communications [6], respectively. The explosion in mobile devices usage over the last decade has led to the ever increasing usage of the limited and expensive radio spectrum. For instance, wireless and mobile devices will exceed traffic from wired devices by 2016 (54%) [7]. In Europe, the total frequency spectrum for public mobile communications is now over 500 MHz [8], with the additional spectrum becoming available in the future at higher-frequency carriers. The spectrum has become rather a limited resource when considering the rapid growth in the number of interconnected mobile users and the emergence of Internet of things (IoT) paradigm. RF based technologies are facing a substantial demand for the capacity that simply cannot be met with current spectral allocations [9]. This had led researchers in communication technologies to seek a powerful complementary technology to respond to the users' needs in terms of high rate wireless communications demand [10]. Moreover, some research works reported the possible harmful sides of RF waves on human beings' health due to electromagnetic hypersensitivity [11][12]. Although, studies carried out in this subject are mainly short term investigations and no formal conclusions have been made yet [13].

One of the viable solutions that has emerged in recent years is moving the wireless communications to the optical domain where extra bandwidth could be provided in parallel with the conventional RF technology. Optical communication development started when the first laser was invented in the early 1960s. This device pushed researchers to dig deeper in the optical spectrum capacities with its operational characteristics, in order to extend RF spectrum. Many complex issues were

faced as research progressed making the achievement of such a large broadband harder than expected. In fact, optical wireless communications (OWC) provide a promising medium to complement RF technologies, offering a huge potential of bandwidth. In this approach, namely OWC, the optical light beam is directional and interference free with other radiation sources thus offering higher quality link (low bit-error-rate) and providing some degrees of physical security as the light beam does not emit outside the designated area. OWC offers a huge bandwidth and capacity, thus providing a viable and attractive option for over 1 Gbps highly secure and rapidly deployable wireless data transmission [14]. Additionally, on top of the unlimited spectrum as currently unregulated and the immunity to RF interference [15], OWC offers a low cost technology in terms of manufacturing and power consumption [16]. It is one of the main areas in optical communications, and includes itself three major subsets: Infrared fibre, free-space communications (FSO) as well as VLC [17]. Given all the previously cited advantages, OWC is widely applicable to many scenarios [18]. For instance, OWC systems started being deployed for urban networks use more than a decade ego where multiple atmospheric turbulence challenges had to be tackled [19]. Moreover, OWC is used in other applications such as ground to train communications for high speed broadband services on fast moving trains [20], or for last-mile free space optical links [21]. Moreover, in the short range communications domain, a 100 Tbps link (up to 1 m) was demonstrated in [22] with strong atmospheric turbulences. Additionally, the authors in [23] have reported a 100 Tbit/s link using three dimensional multiplexing.

OWC operate in two different environments with different challenges (see Figure 1.2), and involves two separate technology categories, the first one being infrared (IR) communications. It corresponds to the range 700 nm to 1mm wavelength [24]. In fact, even at its early stages, IR technology showed a high potential

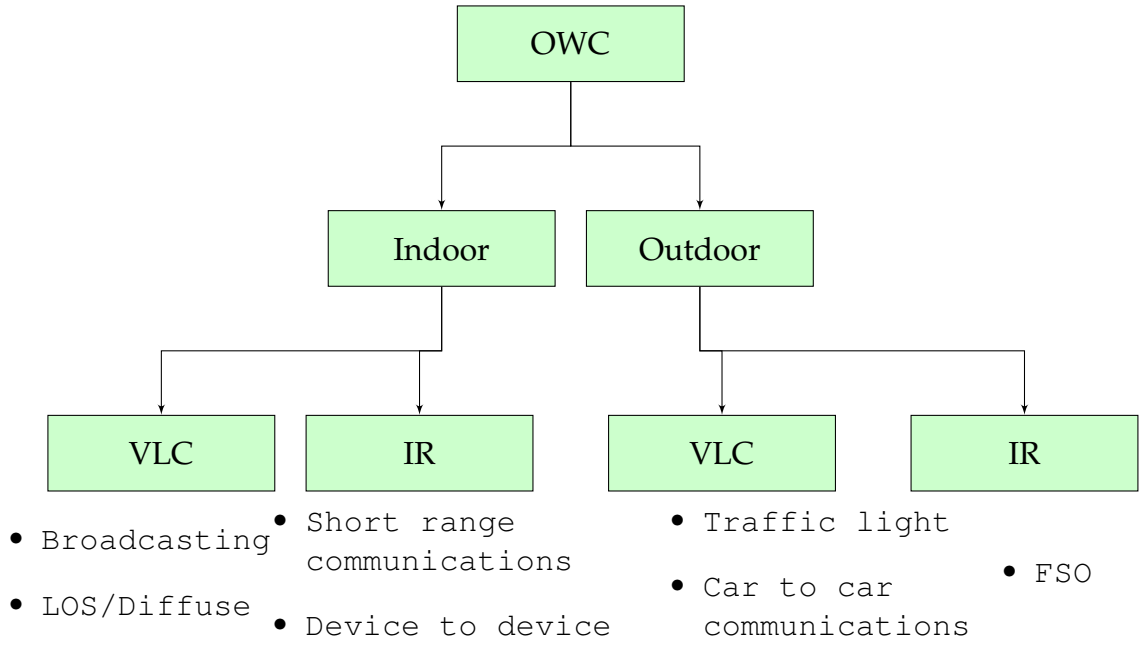

Figure. 1.2 Classification of optical wireless communications

in terms of high speed data transmission (1 Gbps) using the link demonstrated in [25] revealed in 1996. The progress in this area in the following twenty years was spectacular as a high speed laser link was demonstrated in [26] reaching 80 Gbps data transmission rate.

The other category that lies under the wide OWC umbrella is VLC. VLC is one of the key candidates to solve the so-called capacity crunch in certain applications, as it potentially offers 10,000 times more bandwidth capacity than the RF based technologies [27]. It operates within the (380 – 780 nm) wavelength range. The VLC technology is mostly based around the intensity modulation of white light emitting diodes (LEDs) (in-organic [28] and organic [29]), which can be switched on and off at a very high rate [30], thus enabling data communications, illuminations, sensing as well as indoor localization [31]. VLC is an emerging technology of OWC and has been in the spotlight recently [32] thanks to the remarkable development of light emitting diodes (LED) technology [33]. LEDs offer multiple advantages. In fact,

in addition to their low cost, high efficiency, wide availability, long life expectancy [34] and low energy consumption, LEDs allow both illumination and high speed wireless communication simultaneously [35]. VLC also can be preferable over RF communications technologies for other advantages such as confinement resulting in simpler security since light does not travel through the wall which also allows re-usability of spectrum and equipment by nearby systems as well as license free operation. Therefore, VLC offers benefits both ecological and financial [36]. Moreover, LEDs are widely used in everyday infrastructures including homes, offices, street and traffic lights and smartphones [37], which encouraged the VLC development.

Furthermore, many high speed VLC systems were developed demonstrating effective VLC links for data transmission. In fact, modern modulation techniques are now applied to VLC in order to increase the communication throughput such as MIMO and OFDM [38]. For instance, the work presented in [39] achieved using ZnSe-Baed white LEDs, where 400 Mbps error free data transmission was demonstrated. Another high speed link was presented in [40] where 1 Gbps using a micro light-emitting diode array.

Among the various VLC systems variations, the image sensing based systems were granted a considerable share in terms of research recently [41]. With LED and LCD screens being broadly available, as well as high speed cameras, applications of camera based communications are wide.

In this thesis, one of the camera based communications, which is smartphone to smartphone visible light communications, is investigated. It falls within the short range communication category. Such a technology would be extremely useful in providing the opportunity to exchange data such as coupons, brochures and maps, in public spaces, where the lack of privacy and security is prominent. In fact, the

visible range of a phone can be limited to a few inches using the screen's brightness as well as the viewing angle. Playing with these parameters could provide more control over the broadcasting range. Moreover, smartphones are designed for usage in a dynamic environment. Consequently, a system such as S2SVLC is required to provide mobility to the user. In other words, the user should be able to exchange data with minimal constraints on the position (distance, viewing angle) in which the link is established. Besides, a system implemented on smartphone platforms is intuitive and easy to use, and does not rely on Internet infrastructures. Additionally, only a few works have been reported in the area and they are still at the early development stages. Therefore, the main research objective of this thesis is to study the achievability of a smartphone to smartphone visible light communication system, focusing on the detection of the transmitter (Tx) by the receiving camera in dynamic conditions.

1.3 Research objectives

This research work aims at investigating the possibility of a smartphone to smartphone VLC system conception, including the design and implementation on a mobile platform as well as its performance evalutation. Using the smartphone's screen, this system targets to offer the user the ability to transmit exchange video, image and audio files at a high data rate, without any major hardware changes on the mobile phone, under dynamic conditions. The project lies within a complete novel network framework where information is conveyed using only visible light.

The proposed research will address existing Smartphone limitations due to slow hardware response and increase its capacity by modulating the light beam intensity, colour and position, taking advantage of the existing high resolution smartphone screens. A smart receiving system will be employed to maintain the Tx's detection

and the link connectivity in all mobility conditions. In this context, this research presents multiple novel aspects such as:

- All-optical communications capability utilizing the available hardware with no extra modifications, which represents the main advantage over already existing short range communication technologies such as NFC and Bluetooth. For instance, these technologies are not available on all smartphones. Instead, this link will be developed taking advantage of the high rate built-in cameras;

- Develop an adaptive communication strategy to convey information in dynamic conditions;

The research hypothesis will be achieved by satisfying the following key objectives:

1. To identify the key issues in the realisation of such a system and propose an efficient approach for integrating VLC into mobile applications;

2. To investigate and develop a modulation scheme that controls the smartphone screen light beam properties including the intensity, the colour and the position;

3. Develop a VLC system on a mobile platform using mobile applications to handle data transmission and reception;

4. Apply object recognition solutions to the Tx's detection challenges, as well as other image processing and computer vision algorithms to optimise the transmission throughput.

5. Adapt the adequate data extraction on the receiving side for an optimised data recovery.

1.4 Original Contributions to Knowledge

The key contributions to knowledge of this research derived in this thesis are presented as follows:

- The main focus of this thesis being the smartphone's mobility during the communication, the R's is required to know the Tx's position throughout the whole communication time, in order to successfully receive the transferred data. This work presents several solutions not only for the Tx's detection, but also for the received images enhancement in case of signal attenuation;

- Although the work investigated in the thesis is a communication system development, all the tools used to achieve its implementation are image processing and computer vision based. Therefore, one of the main contributions of this work is establishing the analogy between the distinct image processing and communication domains, by translating the different noises present in the channel, such as inter symbol interference, into image processing problems whilst providing the necessary solutions.

- Mobility being the main requirement in this scope, it can be translated into multiple parameters such as: distance, rotation and viewing angles. The channel attenuation due to these parameters is studied through theoretically, including the attenuation due to the perspective correction. The latter is described as a combination of two geometric transformations: a translation and a rotation. Other parameters can cause the signal's attenuation through the free-space channel, such as inter-symbol interference which is provoked by the increase in the distance between the Tx and the receiver (Rx).

- The main challenge in S2SVLC is the accurate detection of the four borders of the Tx on the received frames. Chapter 4 presents an object detection based

method for the Tx's detection. It uses the speeded up robust feature (SURF) detector and descriptor to detect and recognise a detection frame pre-learnt by both sides of the communication. This method being over-complicated for the purpose of this scheme, it then evolved to a detection method much simpler to implement and more appropriate to this scope. The new method involved a flashing screen, which is then used to perform a frame subtraction on the receiving side, thus enabling the Tx's detection on the captured frames. Both these methods include a quantization method used for cell reconstruction to reduce the inter symbol interference effect on the signal.

- In Chapter 5 the S2SVLC link demonstrates a link capacity of 100 kbps under standard home/office lighting conditions. The system also shows its immunity regarding the Tx's rotation over the [0°, 360°] range, and proves to have a 90° field of view, as it reaches a high bit success rate over the Tx's tilting angle range [-45°, 45°].

- Chapter 6 presents the Android design and implementation of the end to end fully functioning system. The implementation included the development of a transmitting application with a user interface that allows to enter a text which is then encoded into a series of black and white cells that are then displayed on the flashing screen. An application for data reception was also developed with a user interface that enables to start and stop data acquisition. The images captured are stored in the Rx's memory and then processed. The implementation on Android also showed a VLC link capable of transmitting 100 kbps over short distances (10 to 50 cm). The link also demonstrated its immunity to the Tx's rotation and translation within the Rx's field of view (FOV), and allows a reasonable tilting angle during the communication. The evaluation of all these parameters showed that the overall system provides a

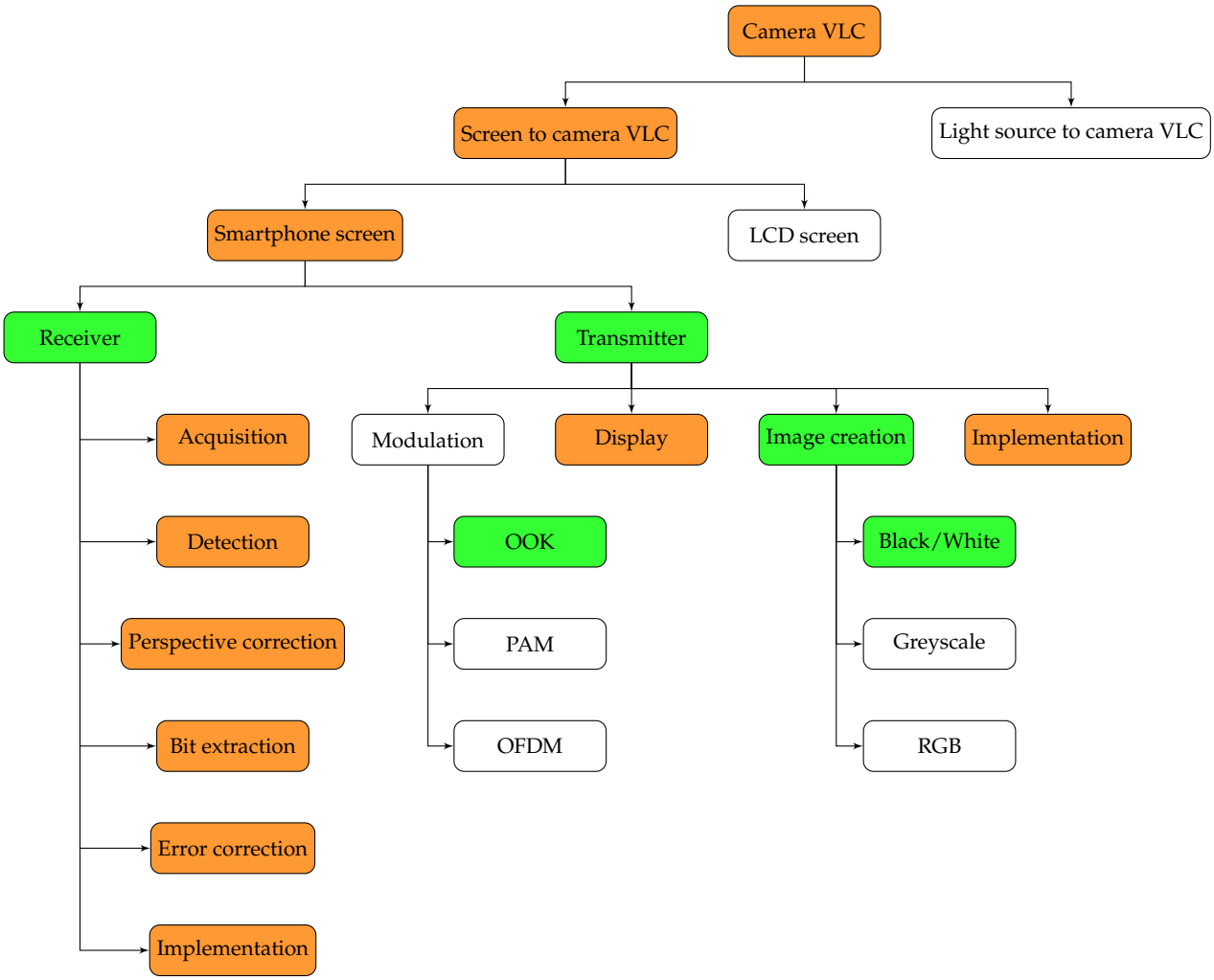

Figure. 1.3 Camera communications domains and the challenges tackled

reasonable mobility level.

1.5 List of publications

1.5.1 Peer reviewed journal papers

1. R. Boubezari, H. Le Minh, Z. Ghassemlooy, and A. Bouridane, "Smartphone Camera Based Visible Light Communication," *Journal of Lightwave Technology*, vol. 34, pp. 4121-4127, 2016. Impact factor: 2.862.

1.5.2 Peer reviewed conference papers

1. R. Boubezari, H. L. Minh, Z. Ghassemlooy, and A. Bouridane, "Novel detection technique for smartphone to smartphone visible light communications," in *2016 10th International Symposium on Communication Systems, Networks and Digital Signal Processing* (CSNDSP), 2016, pp. 1-5.

2. R. Boubezari, M. Hoa Le, Z. Ghassemlooy, A. Bouridane, and A. T. Pham, "Data detection for Smartphone visible light communications," in *2014 9th International Symposium on Communication Systems, Networks & Digital Signal Processing (CSNDSP)*, 2014, pp. 1034-1038.

3. Hsin-I Wu, Yu-Lin Wei, Han-Chung Wang, Hsin-Mu Tsai, Kate Ching-Ju Lin, Rayana Boubezari, Hoa Le Minh, and Zabih Ghassemlooy, “LiCompass: Extracting Orientation from Polarized Light” *IEEE International Conference on Computer Communications (INFOCOM)*, 1-4 May, 2017.

1.5.3 Submitted journal papers

1. Rayana Boubezari, Hoa Le Minh, Zabih Ghassemlooy, and Ahmed Bouridane "Design and implementation of a smartphone to smartphone visible light communications system," *IEEE Journal on Selected Areas in Communications*. Impact factor: 4.138. (submitted)

2. Hsin-I Wu, Yu-Lin Wei, Han-Chung Wang, Hsin-Mu Tsai, Kate Ching-Ju Lin, Rayana Boubezari, Hoa Le Minh, and Zabih Ghassemlooy, *IEEE Journal on Selected Areas in Communications*.Impact factor: 4.138. (submitted)

1.6 Thesis Organisation

This thesis is organized in 7 chapters as follows:

Chapter one – Introduction

A complete introduction to VLC technology, as well as camera communications. The research aims and objectives, as well the problem statement are also presented.

Chapter two – Background theory

This chapter overviews all the concepts involved in the creation of smartphone to smartphone VLC. It includes an introduction to RF technology, OWC and VLC. It also provides information about the history of the telephone and basic information on current smartphone technologies. The final section is dedicated to image processing and computer vision, comprising elementary notions for a better understanding of the following chapters.

Chapter three – Fundamentals of smartphone to smartphone visible light communications

This chapter exposes the existing works in the camera communications domain. It presents work involving light source to camera or screen to camera communications. It also depicts the advantages and benefits in the S2SVLC study, as well as the practical challenges of its development. Chapter 3 presents the first experimental work which consists of the smartphone screen's characterization. Additionally, it provides a mathematical study of the channel attenuation.

Chapter four – Smartphone to smartphone visible light communication system description

Chapter 4 is devoted to the S2SVLC system developed in this work. It presents the most commonly used modulation schemes in VLC and presents the analogy with the signal modulation used in S2SVLC. It also provides information about the Tx's detection by presenting the two methods developed in this scheme. It finally intro-

duces the data recovery process and presents the different image processing tools used for this matter.

Chapter five – Static S2SVLC evaluation

The system exposed in Chapter 4 is implemented on Matlab and the performance is evaluated. The OOK modulation scheme is used since a random and equally distributed binary stream is converted to black and white cells to constitute an image to be displayed on the transmitting screen. The receiving camera captures the data, and the acquired frames are processed off-line. Different mobility parameters are varied and the system's performance is evaluated using the bit success rate (BSR) parameter, which consists of the number of bits correctly recovered.

Chapter six – Dynamic S2SVLC evaluation

This chapter outlines the main objective of the work presented in this thesis, which is the implementation of a S2SVLC system. The practical design and implementation of this system is outlined in this chapter. As was the case in Chapter 5, the system is evaluated through several mobility tests using the BSR parameter, and the results are presented.

Chapter seven – Conclusions and future works

Finally, the summary and the key findings of this work are presented in this chapter. It also outlines the major future works and investigations that can be achieved based on the work presented in this thesis.

Chapter 2

Theory

2.1 Introduction

The system presented in this thesis is a S2SVLC. It is a camera based communication system that emerged from the combination of several fundamental concepts which are introduced in this chapter. Firstly, an overview of wireless communications is given, including radiofrequency technologies, wireless optical communications as well as short range communication systems such as Bluetooth and NFC. Secondly, the smartphone technology summary, general information about smartphone screens, software platforms and the device processors are discussed. Finally, the third major area that contributed to the creation of camera communication is the image processing and computer vision area which will be presented. Notions about digital images and cameras are presented, alongside basic principles of computer vision.

2.2 Wireless Communications

Wireless communications networks consist of microcells that connect people with pocket size devices, telephones pagers personal digital assistant modems [42]. In this section, fundamentals related to the major wireless communication technologies are presented.

2.2.1 RF technology

RF technology is a communication technology that transmits electromagnetic signals. The signal is conveyed through radio waves with radio frequencies expanding between 3 Hz and 300 GHz. RF communication systems are wireless and the signal is transmitted and received through antennas. which define the system's performance and application. The complete range of electromagnetic radiation is known as the radio spectrum which is the name given to the types of electromagnetic waves that can be used for communication purposes [43]. It includes all aspects

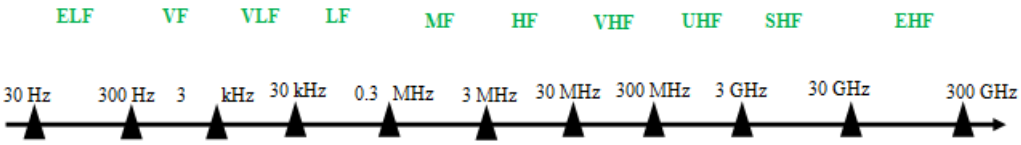

Figure. 2.1 Electromagnetic spectrum

related to radio propagation. RF bands are represented in Figure 2.1. International and national regulations are to be considered before any specific use of the radio spectrum.

Radio waves are radiated from the transmitting antenna to the receiving antenna, and through different routes which can be highlighted as [44]:

- Ground wave propagation: It presents a canonical case of a flat and homogeneous terrain [45] and the most investigated issues include earth curvatures

and irregularities [46]. It is used for broadcasting in the medium and lower frequencies, it has recently gained interest in the high frequency domain for wireless communications [47].

- Ionosphere wave propagation: It uses high frequency (HF) radio waves, and takes advantage of the ionosphere refraction for wave propagation over long distances [48].

- Troposphere dispersion wave propagation: The troposphere is the Earth's atmosphere lowest layer [49]. It transmits waves between VHF and UHF [50] and faces a limiting factor related to the variation of the refractive index [51].

Radio waves utilization for telecommunications purposes began in 1895 when the Italian engineer GM Marconi and the Russian physicist AS Popov independently introduced the first wireless transmission of telegraph signal through earth's atmosphere [52]. Wireless RF communications represent an outstanding achievement. The idea originated from the discovery of 'magic stones' that applied force on each other at a certain distance, using them magnetic field force. Later on, electrically charged bodies showed similar effect and the scientist Faraday established that an electric field could be generated by a time varying magnetic field [53].

RF technology is extensively used in wireless based communications systems and its applications are illustrated in Figure 2.2.

2.2.2 Optical wireless communications

OWC enables data transfer through infrared (> 750 nm), visible or ultraviolet (< 400 nm) bands using electromagnetic waves at very high frequencies [54]. In the optical domain, the wavelength notion is preferable to the frequency as it describes the waves in the electromagnetic space rather than their time variations. The infrared

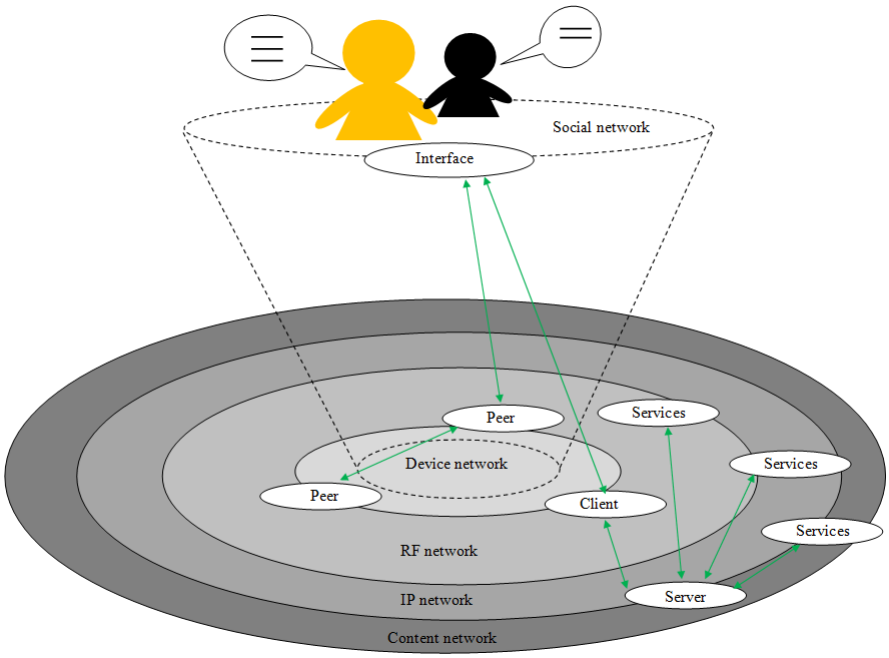

Figure. 2.2 RF Technology applications

interval is composed of multiple subsets. However, in communication applications, near-infrared is more suitable (0.75-3µm) [55] as mid and far infrared wavelengths present non desired thermal effects. Currently, the main transmitters used in OWC are LEDs and lasers [56]. [57] refers to signalling through smoke and semaphore telegraph as the historical father of OWC. Centuries later, Alexander Graham Bell invented the photophone in 1880, the first wireless phone in history, as it transmitted speech using a light beam [57]. As stated in Chapter 1, the world is running out of spectrum and investing new communication technologies to complement the RF networks has become a necessity. Therefore, OWC has seen enormous progress since the first photophone, and its applications include indoor and outdoor environments, allowing data transmission over short range links between two mobile systems (remotes, telephones, laptops etc.) as well as wider scale systems for high rate data transmission between buildings (WMAN networks) or spatial transmissions (Earth-satellite links).

The following section is dedicated to the visible spectrum domain, where LEDs are used for both communication and illumination. It is called visible light communication, and the work presented in this thesis involves a major subset of VLC.

2.2.3 Visible light communications

The VLC technology is mostly based around the intensity modulation of white light emitting diodes (LEDs) (in-organic [30] and organic [58]), which can be switched on and off at a very high rate [59]. Figure 2.3 represents a typical VLC system, where the data is modulated and beamed out of a light source through the free space channel, and a photodetector is used for data reception.

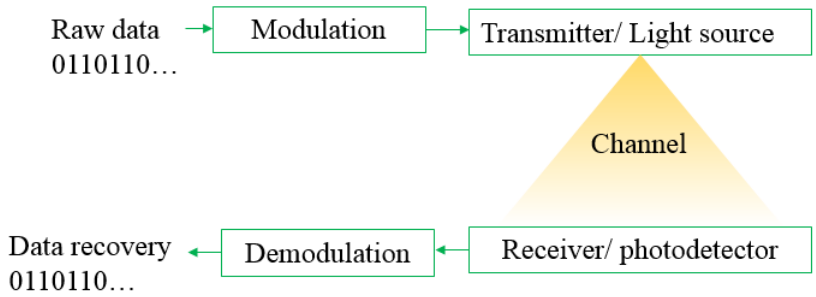

Figure. 2.3 Typical VLC system

LEDs are widely used in everyday infrastructures including homes, offices, street and traffic lights and smartphones [37]. In display devices such as smartphones or computers, the individual elements of the large pixel arrays can be independently modulated [58] and captured using a camera (i.e., optical camera communication (OCC)) in order to recover the transmitted information [60]. Camera communications are considered under the VLC topic because the two typical systems are very similar. In fact, a communication system is composed of a Tx, a Rx and a channel. In standard VLC, a Tx can be a blue LED with phosphor coating to produce white light or a red, green and blue LEDs combination. In camera communication, it is

either a light source or a digital screen, which is composed of an array of LEDs. The Rx on the other side, is a photodetector in typical VLC, which is a semiconductor device that converts the received light into current. In camera communication on the other hand, the Rx is an image sensor, which is available on most mobile devices cameras, such as smartphones. The image sensor is a matrix of multiple photodetectors. Finally, the channel is free space in both camera communication and standard VLC.

VLC is a relatively recent technology that has only emerged over the past 20 years. The huge focus of researchers on this technology gave it a boost which is leading to its commercialization. In fact, the IEEE 802.15.7 task group is currently working towards a global VLC standard, in which several dimming approaches are proposed [61].

More VLC information relevant to the work developed in this thesis is given in the next chapter, dedicated to camera communications, and smartphone visible light communications specifically.

2.2.4 Short range communications

The system developed in this work is aimed to transmit data over short distances. Figure 2.4 illustrates short range communication systems applications and this section will discuss some of the major short range communication systems.

- **Bluetooth**

  A communication technology for data exchange using UHF radio waves covering distances between 1 and 100 meters [62].

- **ANT+**

  A wireless technology that harvests and monitors data in sensor networks.

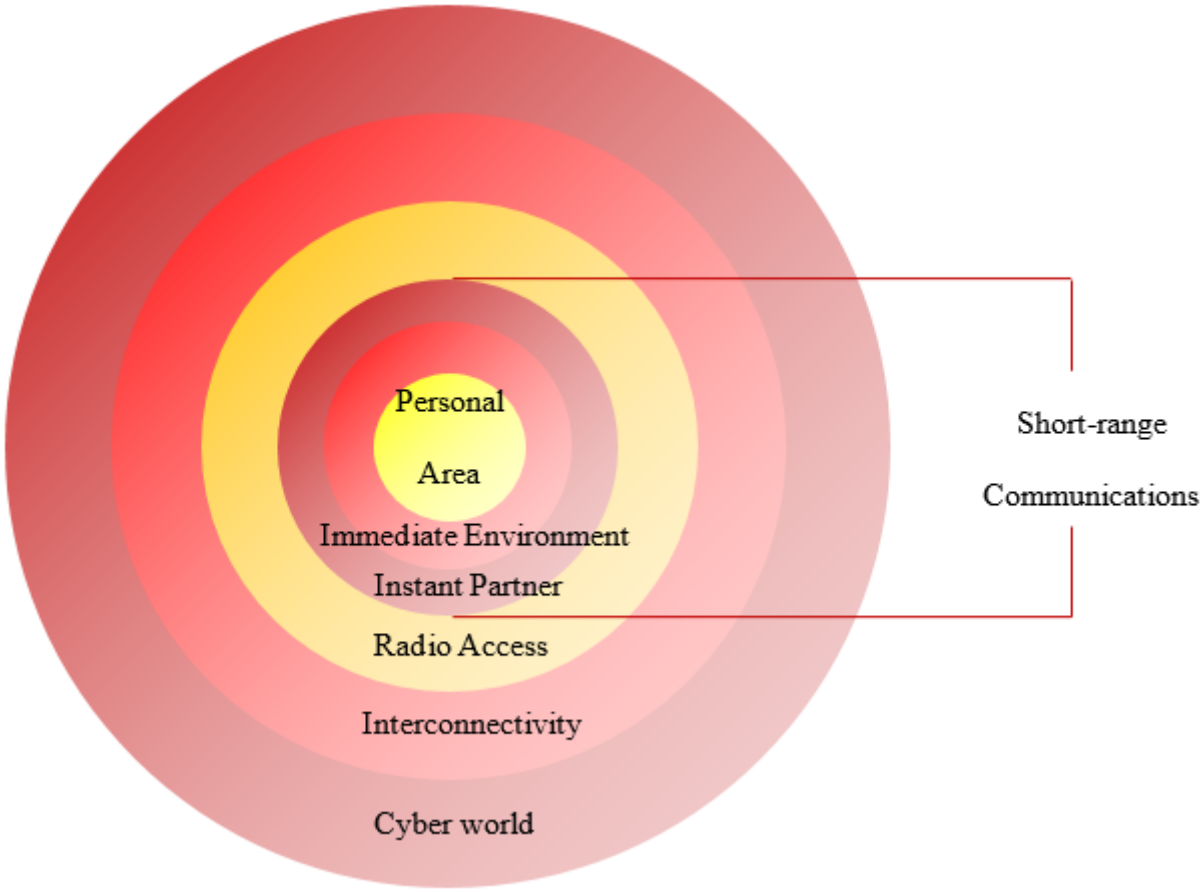

Figure. 2.4 Short range communications applications

It operates over links shorter than 10 m, and its applications are mainly for wearable devices [63].

- **NFC**

  A communication system based on magnetic field induction, for data transfer between two devices touching each other or at a distance below 30 cm from each other [64].

- **RFID**

  Or RF identification, uses electromagnetic fields for tag identification and tracking, and operates over below-1m distances [65].

2.3 Smartphones

2.3.1 Telephone history

Figure 2.5 represents the key dates in the telephone history timeline. In 1876, the Scottish scientist Alexander Graham Bell gives birth to a new technology, a telephone. He patens an electrical transmission system, that conveys sound waves through a wire over an 800m link. Later on, improvements were made to the original Bell's telephone, and earphones were added as well as a pick up/ hang up system in 1903. Moreover, the Marty telephone offered a handset in 1910, and the PTT24 appeared in 1922, the first dial phone. While the phone cases were made out of wood, the evolved to a robust plastic make in 1941, and a Bakelite was added. It only in 1970 that the new era of 'phones for everyone' started, and phones were available households. The year 1980 notices the evolution from a Bakelite to a keyboard to compose numbers. Additionally, advances progress in telephone technology resulted in the creation of wireless phones, that transmit information through radio waves, in 1990. In the beginning of the millennial, professionals were conquered by cellular mobile phones, which later on became more popular among people from the general public. Although advances smart phones based on highly evolved applications were developed in the early years 2000, the actual smartphone advent started in 2007 where the iPhone was released, and became more popular with the first Android phones in 2008.[66]

2.3.2 Smartphone

Smartphones represent a mobile phone category that provides advanced capabilities beyond standard mobile phones, such as access to the internet. They run under a specific operating system software and offer interface and platform for applica-

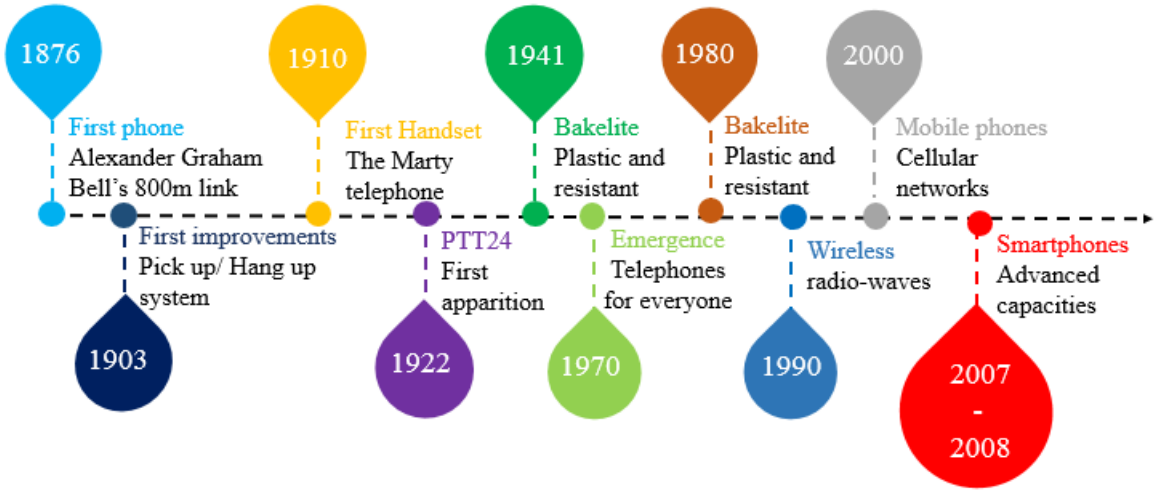

Figure. 2.5 Telephone history timeline

tion developers. The number of smartphone users reached the 2 billion in 2017 and is expected to exceed the 2.3 billion by 2017 [67].

2.3.3 Smartphone sensors

Most smartphones nowadays are equipped with a wide range of powerful sensors in order to broaden their abilities and the services they can offer. The most common sensors are:

- Accelerometer: detects orientation changes, and distinguishes the smartphone's up from down;
- Digital compass: based on a magnetometer, it provides the smartphone with an orientation relatively to the earth's magnetic field.
- Gyroscope: While the accelerometer measures a linear acceleration movement, the gyroscope measures the angular rotational velocity.
- Global positioning system (GPS): which is a radio navigation system, that receives localization information from satellites [68].

Model	Screen technology	Size Resolution	
Sony Xperia z5 premium	4K Ultra HD	154.4 x 76.0 mm	3840 x 2160
Samsung Galaxy S7 edge	HD Super AMOLED	150.9 x 72.6 mm	1440 x 2560
OnePlus 3	Optic AMOLED	152.7 x 74.7	1080 x 1920
Motorola Moto G 4 Play	IPS LCD	144.4 x 72	720 x 1280
iPhone 7	Retina display	138.3 x 67.1 mm	1334 x 750

Table 2.1 Examples of the most sophisticated smartphone screens available on the market

- Proximity sensor: emits electromagnetic radiation in order to detect the presence of objects, by observing the changes in its electromagnetic field.

2.3.4 Smartphone Screens

The work developed in this system used a smartphone screen as a Tx. The size and resolution of the screen are important features that affect the system's performance. In Table 2.1, a summary of the most sophisticated smartphone screens available on the market, that states the screen technology as well as the size and resolution.

2.3.5 Smartphones Processors

Smartphones adoption is spreading at a dramatic speed every day [69]. As they are becoming the linchpin of basic computing [70], it is only natural that researchers focus on improving these devices capacities by improving their processors'performances as they represent the core components. The smartphone's processor determines its working speed, therefore allowing it to offer more features to the user. Table 2.2 summarizes the processor specifications of the most powerful smartphones released in 2016.

Device	Processor
OnePlus 3	SNAPDRAGON 820
Huawei P9	KIRIN 955
Pixel c	TEGRA X1
Samsung Galaxy S7 Edge	EXYNOS 8890
Iphone 7 plus	Apple A10 Fusion

Table 2.2 Examples of the most sophisticated smartphone processors available on the market

2.3.6 Smartphones operating systems

The rapid growth in smartphone feature development put pressure on researchers to improve the services provided by these personal devices. Therefore, Smartphone platforms have become a battleground in order to satisfy more users [71]. The major smartphone operating systems: Android, Ios, Symbian, Blackberry and Windows.

Android emerges as the leading platform for mobile devices. It hit the 88% market share in November 2016 with over 328 million Android devices purchased worldwide [72]. The open-source side of this operating system led this work to be developed on Android.

In addition, applications developed for smartphone become a significant part of the growth of smartphone usage and convenience. In this research, two applications will be developed for the Tx and Rx for sending and detecting data, respectively, which enables S2SVLC without additional requirement of hardware for the smartphones.

2.4 Image processing and computer vision

2.4.1 Digital cameras

Digital camera mechanism

Photography relies on three pillars which are aperture, shutter speed and ISO. This section presents an overview on these basic parameters that govern the camera mechanism.

Aperture The aperture of a digital camera refers to the lens diaphragm opening that allows the light to travel inside the camera. The larger the opening, the more amount of light is captured by the camera. Figure 2.6 illustrates a digital camera aperture.

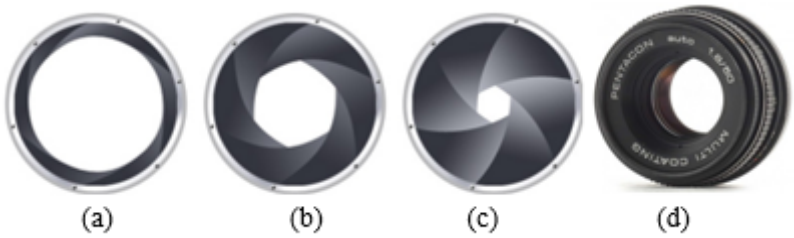

Figure. 2.6 Digital camera aperture (a) large (b) medium (c) small (d) example of a real digital camera aperture

It is specified in terms of an f-stop value, and the opening area descreases as the f-stop increases. Some examples are depicted on Figure 2.7.

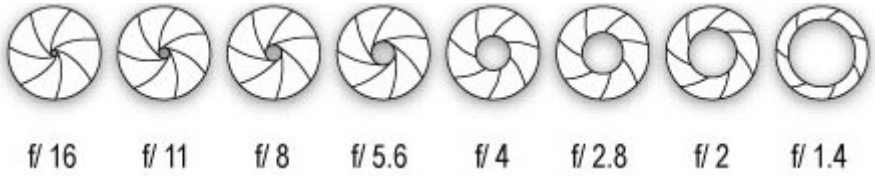

Figure. 2.7 Aperture versus f-stop value

Shutter and shutter speed The digital camera shutter can be described as a curtain that covers the camera sensors allows the captured light to go through the aperture. The light falls on the image sensor when the shutter is open, and the array composing the image is formed inside the camera.

The camera shutter has two major parameters, the shutter speed and the shutter time. While the shutter speed can be defined as the number of times the shutter is opened and closed, the shutter time consists of the time the shutter remains open whilst exposing the sensor to the extern light.

There is an inversely proportional relationship between the shutter time and the shutter speed, as when the shutter speed increases, the shutter time decreases and vice versa.

ISO The camera ISO factor is a number that denotes the camera's sensitivity to light. If this number is decreased, the camera is less sensitive to light and the image is darker. If this number is increased on the other hand, the captured image is brighter.

Digital camera optical system

Energy In order to capture images, the camera needs to translate what it sees into a measurable energy, or light brightness in this particular case. Light is physically an electromagnetic wave, it has no mass, a photon, with sinusoidal electric and magnetic fields. A photon can be described by its energy E, its frequency f and its wavelength λ. There three notations are connected through the speed of light c and Planck's constant h:

$$\lambda = \frac{c}{f}, \tag{2.1}$$

and

$$E = h.f, \tag{2.2}$$

Therefore

$$\lambda = \frac{h.c}{E}. \tag{2.3}$$

Sensors In digital cameras, the key component is its image sensors. It determines the captured image size and resolution, low light performance, depth of field, the dynamic range etc. In fact, every digital camera contains an array of image sensors, that absorbs the photons that travel through the camera lens, and convert these photons to an electrical signal with an amplitude proportional to the captured photon's energy. The two types of image sensors used in digital cameras are CCD (charge-coupled device) sensors and CMOS (complementary metal-oxide semiconductor) sensor.

Resolution The resolution of an image expresses the amount of details that can be seen in an image. It depends mainly on the number of pixels in an image which is defined by the number of sensors a camera has. Figure 2.8 depicts an image showing colourful baboon, and the size of a part of this image is increased to show its details.

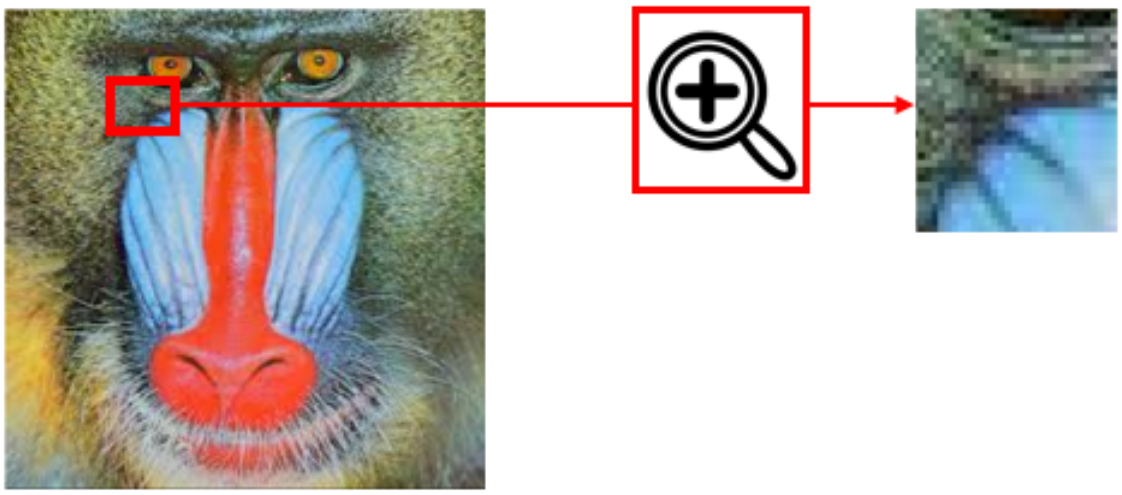

Figure. 2.8 Zoomed-in picture

2.4.2 Digital imaging

Definition and purpose of digital image processing

Digital image processing is described as the manipulation of digital images through a digital computer, using a comprehensive set of standard algorithms. It is a subfield of signal processing. It focuses on developing systems that perform operations on the input image, and provide low level processing with an image as an output, such as noise suppression, mid-level processing with image attributes as an output, such as object recognition, or high level processed outputs, such as autonomous navigation.

Digital image processing has several purposes; among which we can mention some keys ones:

- Image digitization for an easier visualisation and transmission.
- Image enhancement, sharpening and restauration.
- Image segmentation and description for object detection and pattern recognition.

- Computer aided diagnosis.
- Images reconstruction and synthesis for 2D and 3D scene reconstruction.
- Data compression for size reduction of computer files containing images.

Digital images

A digital image I [M, N] described in a discrete 2D space is obtained through a sampling process of an analogue image I (x, y) in a 2D continuous space. This process is referred to as digitization. The analogue image is in fact divided into M rows and N columns and the intersection of a row and a column is called a pixel. Every pair of coordinates [m, n] is assigned a value a [m, n] with m ranging between 0 and M-1 and n ranging between 0 and N-1. Figure 2.9 represents a continuous image divided into 13 columns and 13 rows. A digital image can be obtained by simply averaging the signal amplitudes contained in the intersection and assigning the nearest integer value to the pixel.

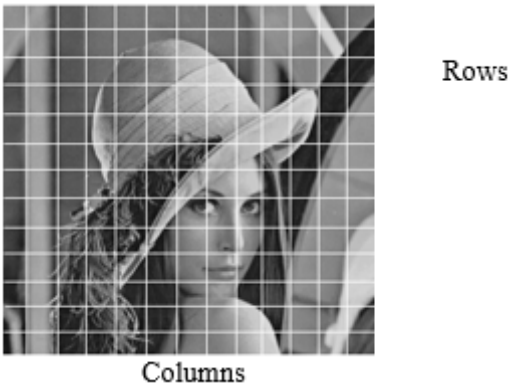

Figure. 2.9 Digitization of a continuous image

A signal, by definition, is a mathematical function that conveys information about the behaviour or attributes of some phenomenon. Therefore, a digital image is indeed a signal.

Image sampling

Image sampling is a signal processing technique that allows the conversion of analogue images to digital images, a format that permits the processing of images on computers [73], and therefore fulfilling the need in the multimedia-riche applications [74]. Let the original image be a continuous function $f(x,y)$. In order to obtain the appropriate discrete data structure, which is a grid of sampling points in the plane in this case, f is sampled at points $x = j\,\Delta x$, $y = k\,\Delta y$, for $j = 1, \ldots, M$, $k = 1, \ldots, N$ [75]. Δx represents the distance between two neighbouring samples along the x axis and Δy along the y axis, these two parameters are calls sampling intervals. The resulting matrix constitutes the discrete image. The Dirac function is a handy tool to represent it, as the following impulse train can be used:

$$s(x,y) = \sum_{j=1}^{M} \sum_{k=1}^{N} \delta(x - j\Delta x, y - k\Delta y) \tag{2.4}$$

And the sampled image $f_s(x,y)$ is the product of the continuous function $f(x,y)$ and the sampling function $s(x,y)$:

$$f_s(x,y) = f(x,y)s(x,y) \tag{2.5}$$

Therefore:

$$f_s(x,y) = f(x,y) \sum_{j=1}^{M} \sum_{k=1}^{N} \delta(x - j\Delta x, y - k\Delta y) \tag{2.6}$$

Pixels

A pixel, short for Picture Element, is the basic unit of programmable colour numerical displays such as computer screens and digital images. The physical size of a pixel determines the display's resolution.

Black and white images

A black and white image is a bi-dimensional array of pixels, where each pixel is represented by its gray level. It spans the full black-to-white range as it varies between 0 and 255, see Figure 2.10.

Figure. 2.10 Black and white image pixel colour range

A black and white image can be modelled with the following mathematical function. For an image I of M rows and N columns:

$$I : s \rightarrow \Omega(i;j) \rightarrow I(i;j) \tag{2.7}$$

where $s = 1,..,M$ and $\Omega = 1,2,3,...,255$.

Colour images

Colour is an important feature in the human visual perception [76]. It is connected to the objects' ability to reflect electromagnetic waves of different wavelengths [77]; the chromatic spectrum extents approximately from 400 nm to 700 nm [78]. The human visual system detects colours as a combination of the primary colours red, green and blue, and standards wavelengths have been defined for these colours, 700 nm, 546.1nm and 435.8nm respectively [79].

In colour images, each pixel is represented by three colour components, red, green and blue. Any colour can be created by mixing the correct amount of red, green and blue lights. Each one of these components ranges between 0 and 255, and

can be stored in 8 bits. Therefore, every pixel in a colour image can be represented by 24 bits (3 bytes). In fact, every pixel is represented by a three-dimensional vector (r, g, b) that provides the colour intensity of each component, where a black colour is represented by (0, 0, 0) and (255, 255, 255) is white, (255, 0, 0) is pure red for example [75]. Figure 2.11 represents a colour image, separated into its three colour components.

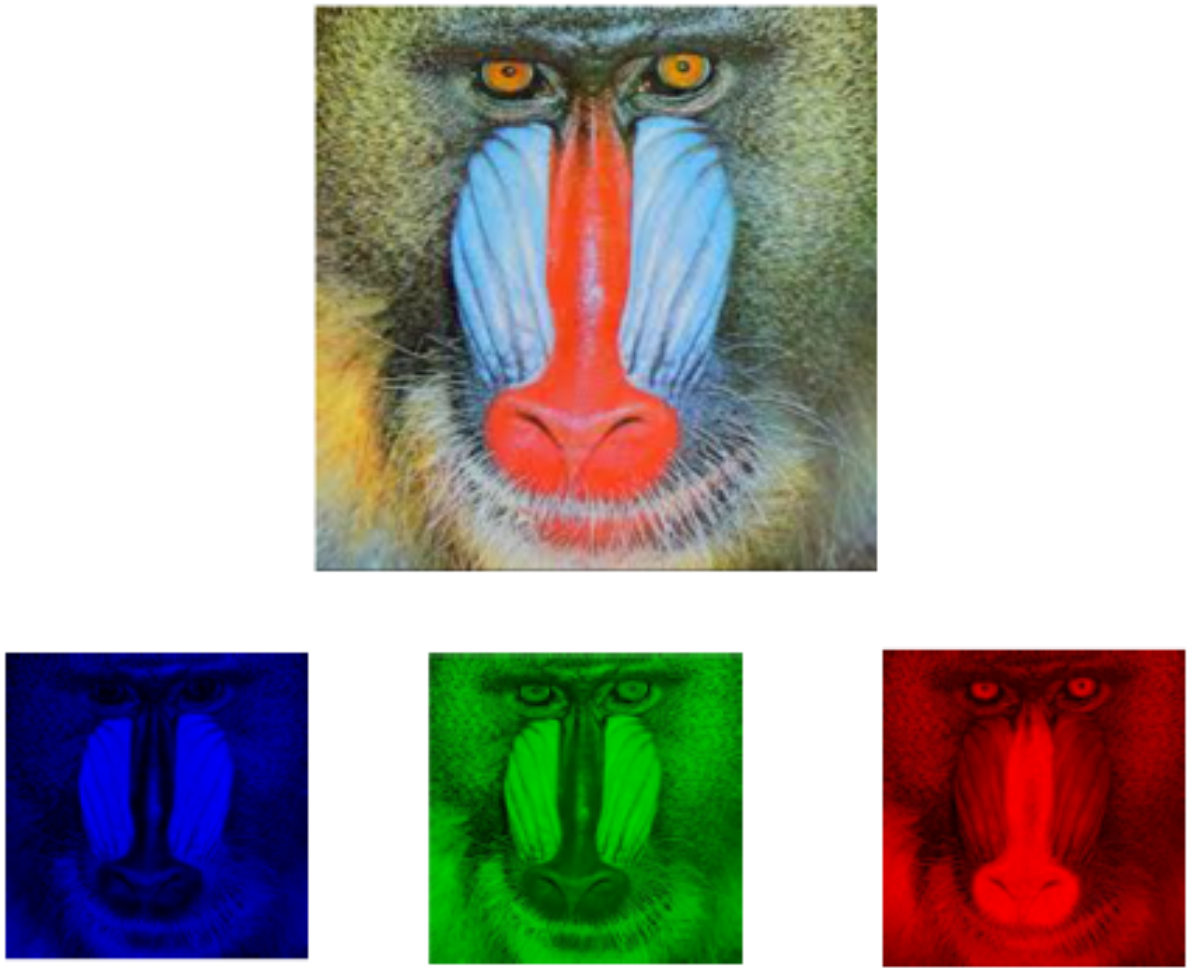

Figure. 2.11 Example of a RGB image and its three components

Colour spaces

In the previous section, the RGB colour space was described, where every pixel is represented by a combination of three hues. It is the most common space to use in image processing [80], [81]. However, there are other colour spaces available and widely used in image processing such as YUV [82] [83], HSV [84] or HSI [85]. These spaces provide information about hue, saturation and brightness that cannot be obtained through the RGB format, as the red, green and blue components are highly correlated [86].

HSI The HSI colour space (hue, saturation and intensity) is an attempt to produce a more intuitive representation of colours. The I axis represents the luminance information, whereas the H and S are polar coordinates on a plane orthogonal to I. H is the angle, the colour red is the absolute reference as its angle $h = 0^\circ$, green is represented by $h = 120^\circ$ and blue at $h = 240^\circ$ (see Figure 2.12). In other words, h represents what the human eye understands as colour. The saturation S on the other hand refers to the amount of white contained in a colour.

HSV The HSV colour space (hue saturation value) is similar to the HSI colour space, and the difference remains in the conversion from or to the RGB colour space as the polar coordinates are expressed differently.

YUV The Y in YUV stands for "luma" which is brightness, whereas the U and V components provide Chroma apperception information. The Y component is independent from the other two Chroma components [87].

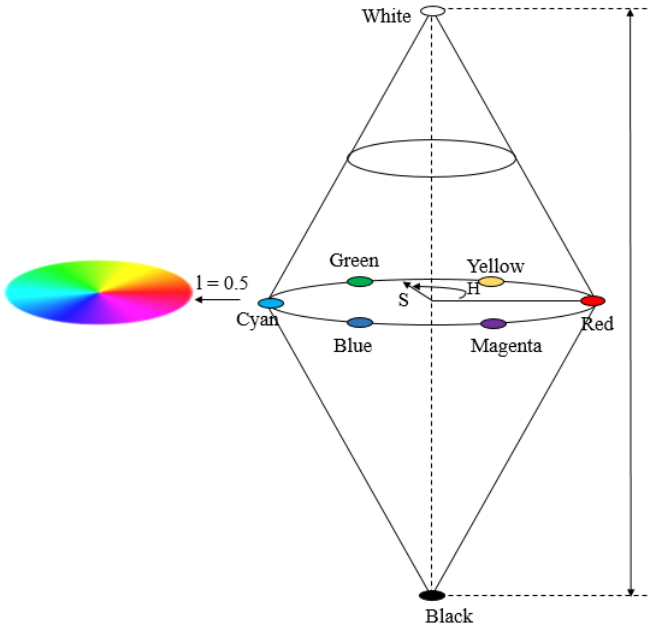

Figure. 2.12 Double Hexcone HSI Colour Model

Noise

There are various types of noise that a digital image can contain. These noises create random errors and cause a degradation in the image. They can occur during image capture, transmission or processing. They can be either multiplicative and therefore dependent of image content, or additive and independent, as it can be seen in standard signal processing. Table 2.3 (b) shows an image with additive constant mean and variance, Table 2.3 (c) shows an image with a multiplicative noise and Table 2.3 (d) shows an image with an impulse noise that alters at random the values of some pixel. This noise is called salt and pepper.

2.4.3 Computer Vision

Definition

Modern signal processing capabilities constantly improve at a dramatic speed every day, and offers economic advantages. Simultaneously, real time autonomous

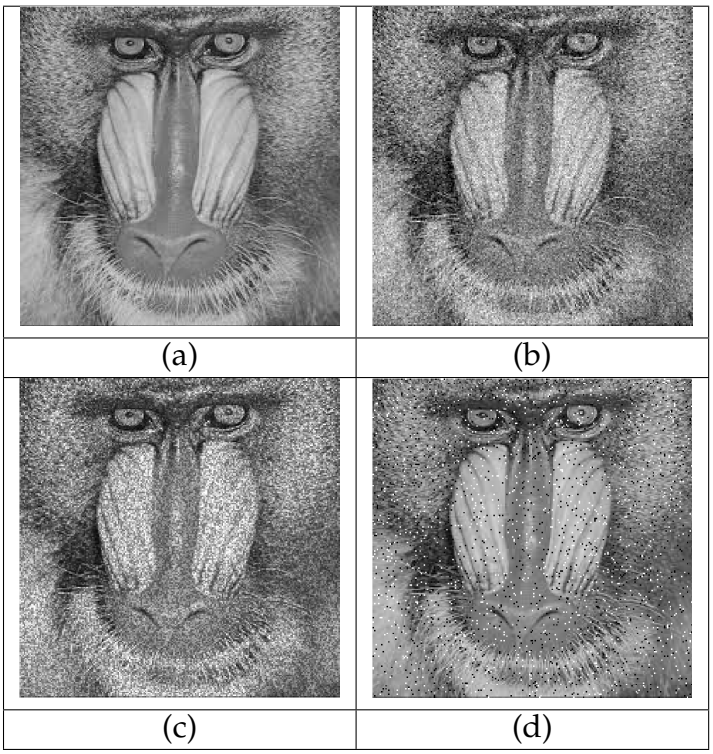

(a) (b)

(c) (d)

Table 2.3 (a)Original image (b) Image with gaussian noise (c) Image with multiplicative noise (d) Image with salt and peper noise

sophisticated are being developed in order to complete human abilities. As seen in the previous sections, image processing turned out to be a powerful signal processing area, and its evolution lead to the creation of a human visual system based discipline: computer vision.

Computer vision is a science discipline that focuses on giving the machines the ability to see their environment, collect data, interpret the information contained in it, and make decisions. Research in computer vision has been carried out to develop mathematical techniques to recover 3D shape and appearance of objects using digital cameras and images [88]. Among the numerous computer vision applications and additionally to the image processing purposes, one can mention a few [89]:

- Robotics: For industrial inspection, surface measurement, manipulator guidance and vehicle guidance.
- Image understanding: developing systems able to look at a scene and describe the objects present in it.

Object detection challenges

The major task in computer vision is object detection and recognition. This section introduces the main challenges in object detection. Figure 2.13 (a) represents a famous monument in Algiers, Algeria. The picture was taken facing the monument, during the daylight, with very few object around it. However, whilst taking a picture, many challenges can be faced:

- Illumination variations: an object photographed during the day is more visible than the same object photographed at night, see Figure 2.13 (b).
- Background: the background surrounding the targeted object can be constantly changing, and can contain too many objects.

Figure. 2.13 Black and white image pixel colour range

- Occlusions: when objects present in images in front of the main object, they can mask it partially, see Figure 2.13 (c).

- Point of view changes: a 3D object can be photographed from many points of view, see Figure 2.13 (d).

- Scale changes: when the distance between the targeted object and the photographer increases, capturing the object's details is more challenging, see Figure 2.13 (e).

OpenCV library

OpenCV stands for open source computer vision. It is a programming library aimed to provide real time computer vision functions [90]. It was released under a BSD license (Berkeley Software Distribution), which is a free permissive license family with minimal commercial and educative restrictions [91, 92].

2.5 Summary

In this chapter, an overview of the different concepts that constitute S2SVLC system were presented. Firstly, a review of wireless communications development was outlined, including the progress from RF technologies to wireless optical communications and new short range technologies, as well as the basic concept of visible light communications. Then, since the main devices used in the S2SVLC system was the smartphone screen and the smartphone camera, the smartphone technology was presented, where both the hardware and software were exposed. Finally, given that the main techniques behind the development of S2SVLC were image processing based, a prerequisite theoretical knowledge for photography, image processing and computer vision was outlined. Digital images were described with the different colour spaces, and the analogy between signal processing and image processing was explained. Image processing and computer vision purposes, applications and challenges were also introduced as all these background notions were necessary to the reader to fully understand the concept of camera communications.

Chapter 3

Mobile Visible Light Communications

3.1 Introduction

In Chapter 2, a general overview of wireless optical communications was discussed, and VLC was presented. The smartphone technology was also thoroughly introduced, including both hardware (screens, microprocessors, cameras, sensors) and software (platforms, applications) components. In this chapter, the parts showed in the previous chapter are linked together in this chapter in order to present the background theory of the S2SVLC concept. Firstly, previous work is reviewed, where several LED to camera communication as well as screen to camera systems are cited. Furthermore, several challenges related to S2SVLC are identified and discussed and the most relevant works are summarized where their main achievements and disadvantages are outlined.

3.2 Review of camera based visible light communication systems

VLC has been experiencing a significant amount of research for the past few years and has grown continuously to potentially become an alternative to RF communications technologies [59]. Nowadays, liquid-crystal display (LCD) screens, Smartphones and digital cameras are widely used in infrastructures and by individuals [37].

In addition, smartphone VLC (SVLC) is a good candidate to replace NFC in popular short range communication applications such as contactless payment and devices pairing [93], since NFC is only supported by a limited number of devices, whereas SVLC is only software based and work with most of the commercial hardware. Additionally, many works have been reported on Android implementations of VLC based communication systems. For instance, [93] introduces a near field communication where the transmitter is implemented on an Android phone with the screen split into 4 different colours for data encoding and transmission while the Rx is a colour sensor implemented on an Arduino board.

This trend has led to camera based communication, a recent research area in VLC for short range communications. In this section, camera communications are separated into two categories, systems using simple light sources for transmissions, and systems using LCD or LED screens for transmission.

3.2.1 Light source to camera communications

Many works have been reported in the LED-to-Camera communication area, and this section presents a review of some of these works.

[94] presents an LED-to-camera communication system where the transmitter

is a board containing 16 LED for data transmission where each LED consists of a red-green-blue (RGB) chip, and the Rx is a standard smartphone camera. It is based on the colour shift keying (CSK) modulation scheme, and allows multiple users to access the network, by using the code division multiple access (CDMA) technology. The CDMA technology is used in second generation (2G) and third generation (3G) wireless communications. It utilizes all the available spectrum to allow more users and supports 10 times more users than the first generation (1G) with the same spectrum. It enables users to use the same frequency and communicate at the same time [95].

Moreover, experiments are carried out in order to evaluate the system and the CSK-CDMA based VLC system is compared to OOK, and showed its superiority keeping the low error rate with two receivers. The experimental work showed that the system can achieve a low error rate (BER < 10-6) with a 3-dB gain. Additionally, the system currently transfers 240 bits per second using a 30frame/second camera rate, which could be 8 times higher using the 240 frame/second based slow motion option existing in the iPhone 6 plus.

More works exploring recent smartphone cameras capabilities were reported. For example, in [96] a CMOS mobile phone built in camera sensor was used to capture the data from a visible LED light source. The modulation scheme adopted for this system is a simple OOK, and the camera rolling shutter is used for data transmission.

Rolling shutter is a mechanism typically used in CMOS cameras for image capturing. In general, different parts of the sensor are exposed to light, at different times. Pixels constituting the camera sensor are split into rows, and the rows are exposed one by one to the light, consecutively from the top to the bottom. Therefore, the top part of the sensor captures a different sequence from the bottom part

of the sensor. This process is applied to reset the sensor in sequence as well. When the reset process moves down through the image, the readout process starts again following the same fashion [97].

Using the rolling shutter produces an effect often seen as a negative one, which is skew scenes on images representing moving objects. However, this property can be explored in wireless communications, in order to transmit data between an LED and a mobile phone camera. The LED light flashes while transmitting a binary stream (ON for 1 and OFF for 0), whilst the camera captures this data. In fact, the delay between the two processes of reading out and resetting the different arrays in the camera sensors while the transmitter (LED light) flashes, constitute a frame containing several black and white bands, see Figure 3.1. The top half of the figure shows the LED on and off states, whereas the bottom half of the figure represents the CMOS camera output.

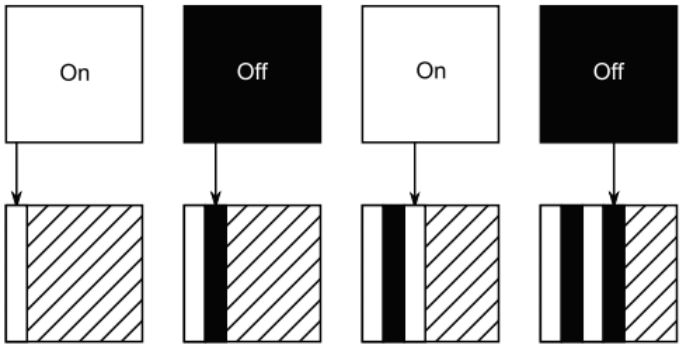

Figure. 3.1 Rolling shutter process and data acquisition

Although the average currently-available CMOS cameras offers a capture rate varying between 20 and 30 frames, multiple bits can be transmitted in one single frame, which allows the system to perform at a higher rate than the receiving camera. Whilst the OOK modulation scheme is adopted, every single bit is converted into a Manchester coded symbol before data transmission. The Rx on the other side captures YUV format file, using an implemented Android application. Based on

the luminance component, Y, extracted from the acquired images, the Rx performs a down-sampling before recovering the data.

Moreover in [98], another LED to camera communication system is exposed. The system described also uses RGB LEDs to transmit data, and a smartphone built in camera on the receiving side of the communication link. Casio, the Japanese electronics manufacturer exhibited this prototype, PicapicCamera, during the Consumer Electronic Show in Las Vegas, 2012. It offered data recovery from up to five transmitting smartphones to every single Rx. It can also detect the flashing light transmitting the information from up to a 10-meter distance.

The manufacturer exposed the different applications where this system is useful, such as time-sensitive advertising, and stores, shops or train stations can also transmit data to pedestrians using low cost light sources or existing monitors. It also represents a simple approach to exchange contact details during social events. Likewise, optical camera communications (OCC), a timely VLC topic, has earned a great share of researchers' attention in the last few years. For instance, [99] shows a 1024-QAM optical camera communication system, designed for transmission of location information, using a dual LED and a commercial digital single-lens reflex camera. A similar system was developed in [60], where a single RGB LED and a commercial camera were used as a transmitter and a Rx respectively, demonstrating a link of 150 bps.

3.2.2 Screen to camera communications

With major progress achieved in the light source to camera communication research alongside the dramatic increase in the LED and LCD screens in everyday life, screen to camera communication was put in the research spotlight more than a decade ago, and many works have been reported in the area. This section will expose some of

these works.

For instance, [100] reported a computer vision based screen to camera communication system, where an LCD screen and a commercial webcam were used as Tx and Rx, respectively.

The work presented focuses on two main desirable aspects of the system, its simplicity and its high performance despite the presence of perspective distortions yielding from the variation of the transmitter's angle of view, see Figure 3.2.

Figure. 3.2 Viewing angle in screen to camera optical wireless communication

In this system, the Tx is constituted of 256 LEDs transmitting a coloured signal over 3 channels (RGB), and each LED is an independent channel transmitting an OOK modulated signal. In order to detect the transmitter on the captured frames, four LEDs at the four corners of the Tx are used as a reference. The four reference LEDs blink continuously at a rate independent from the transmitted signal.

On the Rx, a Hough transform [101] based edge detection method is applied to the received frames, in order to locate the reference LEDs, thus helping to remove any perspective distortions before proceeding to data extraction.

Experiments are carried out using a commercial web-camera operating at a 30 fps capturing rate. Each LED transmits at a rate of 20 bps as only two colours are used during transmission for simplicity purposes. An additional operation before data extraction is executed in order to suppress the duplicate data frames.

The experimental work shows the feasibility of a 4-reference based LED system, and its performance in the suppression of perspective distortions and demonstrates a 5 kbps transmission capacity.

Another important work in the screen-to-camera communication area is presented in [102]. The system is designed for 2D colour barcode streaming between low-size screens and low speed cameras, both available on today's smartphones. Once again, the transmitting screen features four corners used for easy localization in case of blurry or distorted received images. Several techniques are explored in order to maximize the system's throughput, such as an adaptive number of transmitting channels for blur suppression. It also introduces a new metric, called degree of blur (DOB), to quantify the blur effect on the received frames. The metric is based on the calculation of the pixel deviation, and poor quality images presenting high DOB are eliminated. A HSV colour enhancement algorithm is also applied before further processing for sharper cells.

The system offers real time data transmission. Therefore, time consumption is an important parameter and needs to be as low as possible. For that purpose, a fast corner detection technique is adopted. Unique patterns are added to the corners of the transmitted frames, in different colours (red, green and blue), which facilitates the corner detection step. The corners feature different colours in order to help with the code direction. The system also offers to overcome perspective distortions. In order to do so, time reference blocks are added to the transmitted frames, for an easy code segmentation.

The system is implemented on Android platform and multiple experimental tests are carried out. It is evaluated on its performance in terms of decoding rate, block size and throughput, and shows a performance of up to 172 kbps transmission rate. Furthermore, the work presented in [103] also explores a screen to camera

communication link. The system uses a 32-inch LCD screen transmitter and tackles several synchronization issues between the camera and the transmitting screen as well as noise effects including blurring and distortions. It claims to offer a data transmission link of up to 12 Mbps capacity at a 10-meter distance. It also offers a wide angle of view of 120° at which the transmission speed reaches 8 Mbps. The transmitted signal is modulated using the OFDM scheme, where instead of converting bits to voltage, the bits are converted to luminance on the screen.

On the Rx the first step is the image background suppression. The latter is achieved by detecting the four corners of the transmitting screen on the received frames. Corner detection is a major challenge in computer vision and has been widely studied in the past [104]. Many of these algorithms were applied to 2D barcode decoding, but the one applied in this scheme is the data matrix corner detection [105]. The perspective distortion is also considered in this system and a correction is therefore implemented. Using symbol redundancy, the blur effect is attenuated on the received images. This work also focuses on the frame synchronization and presents two phenomena:

- Frame splitting: which occurs whilst the transmitting screen refreshes the displayed frame containing data, causing the screen to display the bottom of the previous frame and the top of the current frame. This effect is overcome by forcing the screen to finish rendering before displaying the data frame.

- Frame shadowing: the camera captures a linear combination of two consecutive frames. In order to ensure that at least one captured frame contains the original transmitted data frame, the camera rate is twice higher than the transmitting screen rate, following Nyquist sampling theorem.

The system is evaluated with experimental tests, and the impacts of several parameters is quantified: distance, angle of view and blur as well as smartphone model.

The results show that such a system offers a great array of applications within a short range communication area.

In [106], the capacity of Smartphone camera (SC) Communications considering the inherent distortions and the varying the distance between the Tx and receiver Rx is investigated. In fact, the system represents a visual MIMO system as it is a VLC system based on computer vision. It focuses on the system's mobility, and offers to localize the transmitter and recover the data despite the mobility effect on the transmitted signal. The modulation scheme adopted is kept simple, and OOK is applied to the original signal. Moreover, RF technology communication concepts such as inter-symbol interference and path loss are applied to camera communication, and a channel model is proposed, where the perspective distortion is the main parameter attenuating the signal. The system also addresses the occlusion issue, which is the situation where an non desired object is present in the camera field of view, occluding thus the transmitter and attenuating the signal. This attenuation is overcome by adapting the block size and increasing it, and compromising the signal throughput.

Once again, the experimental tests also included evaluation in terms of distance, perspective distortion and rotation angle as well as the throughput by varying the transmitted block size.

The results show the capability of this system to suppress perspective distortions. It also demonstrated the system's potential in short range communications, as it offers high speed downloading and streaming.

Another work explores the camera rolling shutter is presented in [107]. It introduces a system that relies on generic screens for transmission, and off the shelf smartphone cameras for data reception and decoding. The system aims to detect active coloured tags on ordinary displays using personal smartphones, at large dis-

tances, up to 4 meters, and from different angle of views. It relies on image processing techniques for the transmitter's tracking, such as Hough transform, and considers the effect of dynamic tags on the human eye, and establishes frequency threshold depending on that are human visual system fusion-frequency dependant.

Moreover, a bi-directional mobile-LCD communication link is investigated in [108]. Both Tx and Rx are smartphone devices. The transmitter and the Rx are in a face-to-face position (line-of-sight channel) and experiments were carried out to evaluate the effect of reflection noise on the screens during the communication. It also addresses the security question and proposes a mathematical model according to the system's geometric parameters in order to avoid eavesdropping.

The following work is a direct application of dynamic visual codes in real life. In fact, [109] demonstrates a camera based VLC link within an aircraft cabin, where successive 2D visual codes were displayed on the in-flight entertainment screen and captured by the camera of passengers smartphones. The performance evaluation of this system shows that it is capable of transmitting up to 120 kbps per passenger, offering also the required aircraft intrinsic security given that the system has no physical effect on the on-board system.

Another notable work relating to camera based VLC is presented in [110] where a general wireless optical channel model is exposed. The model considers multiple input/multiple output (MIMO) pixelated wireless optical communication, aiming to achieve high speed short range communication, in which a line-of-sight is available. An experimental prototype is presented as a proof of concept where a 512x512 sized transmitter is used. The capacity was estimated to 22.4 kb/frame. The work aimed to evaluate the potential of pixel-based wireless optical communication systems and shows its immense gains.

Table 3.1 summarizes the most important features of the most relevant works, to

help for a better analysis of the problem investigated.

The S2SVLC system therefore aims to widen the viewing angle, to increase the distance from a few centimeters to a few tens of centimeters, to adapt the VLC to small screens and smartphone processors and achieve a high data rate.

	Transmitter	Receiver	Specifications	Achievements	Disadvantages
[102]	Smartphone	Smartphone	Main objective: optimize throughput by increasing the number of cells per frame Distance: 5 to 9 inch	172.6 kbps Blur assessment and color enhancement method Accurate bit (high bit success rate at low cell size)	Low distance Low viewing angle
[103]	32 inch LED screen	Camera	Distance: up to 10 meters	Addresses perspective distortions and blur High data rate though it uses low rate camera (up to 14 MP) Performance independent of ambient light)	High distance and throughput while using a 32 inch transmitting screen. The data rate may decrease dramatically with smaller transmitter or a smartphone processor
[111]	8x8 LED matrix	Smartphone	5 to 30 cm	Rotation compensation Uses alignment for orientation purposes.	For multiuser use. 1280 bps (5120 bps achievable with 120 fps) Light metering for camera focus. Relatively low distance given the low data rate.
[112]	Infrared LED	Surveillance camera on the ceiling	49 fps (1296x730) to 90 fps (640x480) Distance: 0.5 to 3m Exposure time varied from min to max.	45 bps Distance: up to 3m. Asynchronous use	Very low transmission rate.

Table 3.1 Most relevant work feature summary

3.3 Advantages of S2SVLC

There are a number of advantages that make the research for screen to camera communications worthy of further and future development. This section enumerates several ones:

- The dramatic improvement in smart devices in the last decade has made the majority of these devices equipped with LED flash, front and rear high quality cameras, which created a phenomenal potential of pragmatic visible communication implementation. Therefore, investigating on a S2SVLC system is timely and important as it takes the advantage of widely-used screens, available in public places and personal devices.

- An S2SVLC system is portable as it can be readily implemented on Smartphones, without any hardware modifications or additions.

- Any type of digital data can be converted into transferable images consisting of thousands of bits per image then displayed in one smartphone screen. Similar to a dynamic 2D barcode, it offers the possibility to transfer a significant amount of data on a display as small as a Smartphone screen.

- A digital camera imaging lens consists of multiple photodetectors and the incident photons. The received signal can be divided into a number of pixels described with an illumination level, individually. Therefore, each pixel can be considered an individual light-based channel.

- It also offers the potential of transmitting three times the size of the transmitter's screen, using RGB images.

- Additionally, a S2SVLC system is an independent end to end communication system as it only relies on the screen and the camera on the hardware side,

and signal and image processing techniques on the software side, to transmit and receive data and does not rely on any other technology such as the use of a server.

3.4 Challenges of S2SVLC

Many factors make camera communication challenging, and this section exposes the major ones:

- Hardware limitations

  The potential of any optical camera communication system is defined by the camera specifications. Most of available smart devices cameras operate at a 30 fps rate, which ultimately limits the achievable communication rate.

- Synchronization

  In order to establish a communication between a dynamically changing display and a camera, synchronization is necessary. In other words, transmitting a long binary stream using a screen requires the display of a high number of frames consecutively. Updating the display on the screen requires a refreshing time and the shutter speed must be considerably smaller than the transmitting screen refreshing rate in order to avoid capturing the transitive frames. This condition reduces the number of invalid received frame without suppressing them entirely. Therefore, processing the frames in order to select the usable ones is time consuming, and needs to be performed effectively for limited transmission rate decrease.

- Mobility

  Screen to camera system are aimed to be implemented on mobile personal de-

vices, utilized by dynamic users. Consequently, the system's ability to transmit and recover data in an actively changing environment is a requirement.

- Real time processing

  Screen to camera communication systems are aimed for users on the move to instantly exchange information. These systems are required to transmit, receive and process data in real time. Given that they rely on computer vision and image processing techniques, adopting low time consumption algorithms can be a complex objective to achieve. However as the smartphones are more powerful and more memory, the real-time aspect could be no longer a main issue in future development

- Security

  Using visible light to transmit data, and in this case a screen to display information, means allowing this data to be accessed by undesirable users. Subsequently, the security question in terms of data modulation is fundamental.

3.5 Summary

In this chapter, the fundamentals of S2SVLC were outlined, starting with the existing camera communication systems, either based on LEDs or screens for data transmission. The different challenges of S2SVLC were also exposed, as well as an overview of the most relevant works, with their most important achievements and disadvantages.

Chapter 4

Smartphone to Smartphone Visible Light Communications

4.1 Introduction

The S2SVLC system consists of using two smartphones for data transmission and reception. Data is represented by a binary stream, which is then encoded into black and white cells to an image. The bicoloured scenario was chosen for simplicity purposes. The latter is then displayed on the Tx screen. On the receiving side, the smartphone's camera is used to capture the displayed images, and recover the transmitted data. Figure 4.1 depicts a typical S2SVLC system.

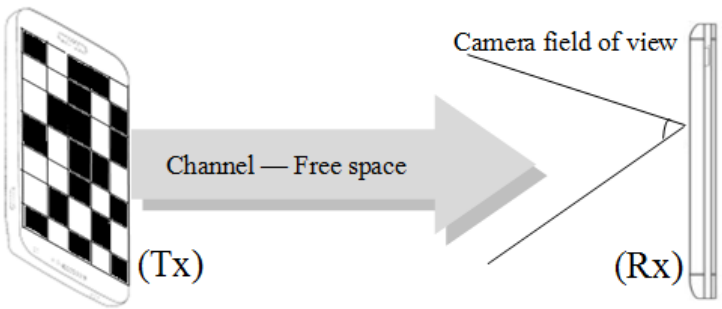

Figure. 4.1 Typical smartphone to smartphone VLC system

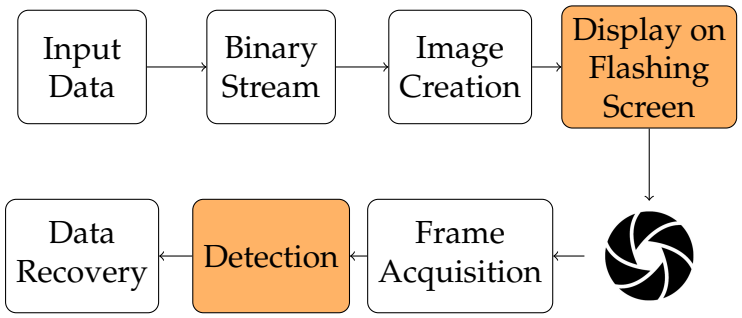

Figure. 4.2 S2S VLC system block diagram

This system is based on computer vision. Therefore, the main challenge in the implementation, is the detection of the targeted object, the Tx in this case, on the received frames. Consequently, a precise detection method is necessary in order to be able to remove the background noise effectively. Other image processing tools are used during the data recovery process to remove other noises such as inter-symbol interference, which will be thoroughly explained in the following sections. Figure 4.2 describes a general block diagram of the system.

This chapter contains a full description of the S2SVLC system developed in this work. Two Tx's detection techniques were used and are explained in details in section 4.5. The first one is based on the object detection algorithm SURF[113], the second was uses a flashing screen to transmit data, and on the receiving side, a frame subtraction followed by Canny edge detector[114] and Hough transform[115] to detect the Tx before recovering the data.

4.2 Modulation schemes

RF signal is complex and bipolar. However, VLC signal is real valued and unipolar. Therefore, a VLC system can only be realized as an intensity modulated direct detection (IM/DD) system [116] [34], and the well-developed modulation schemes dedicated to RF communications cannot be applied to VLC systems. In this section

we introduce some popular modulation schemes that can be used in VLC.

4.2.1 On-Off Keying

On-off-keying (OOK) is one of the most popular modulation schemes due to its simplicity as it is highly simple to implement[117] [118]. It is the simplest form of amplitude shift keying (ASK) modulation. The carrier is switched on and off to represent the binary symbols “1” and “0” respectively. Although this is not the most efficient modulation scheme in terms of data throughput, it is widely used for simplicity purposes, especially in the development and testing phases of a new system, which was the case in this scheme. The OOK symbols are replaced by cells, and one cell is a square shaped group of pixels illuminating the same colour. Applying OOK in this case means using solely two colours on the display: Black (for 0) and White (for 1).

4.2.2 Pulse amplitude modulation

In a regularly timed sequence of a signal, Pulse Amplitude Modulation (PAM) scheme varies the amplitude of a series of signal pulses for its transmission. The pulse amplitudes are to choose from a specific alphabet at the Tx. It is widely used in VLC [119] and has been analyzed for its ability to increase data throughput [120] [121]. Applying Using an LED light for data transmission in a VLC system implies dimming the emitted light according to the transmitted data. Applying PAM in this scheme would be translated into using multiple colours to transmit data, but only in the black to white range. In other words, instead of transmitting one single bit per cell, more can be transmitted by using different grey levels. For example, in order to duplicate the system’s throughput, two grey levels (high and low) can be used in addition to black and white, in order to transmit four different binary

combinations (00, 01, 10, 11).

4.2.3 CSK modulation

White light can be generated using LEDs in two different ways. The first one uses blue LEDs with yellow phosphor, which remains ineffective in VLC as it slows down the process of switching on and off. The second one combines three coloured LEDs (red, green and blue) simultaneously [38][30]. CSK modulation can be applied to S2SVLC by transmitting RGB images containing coloured cells, where the colour of each cell can be encoded in 3 bits, which increases the potentially achievable system's throughput. Moreover, combining CSK and PAM in S2SVLC offers great chances of increasing the system's data rate. However, RGB images are stored in bigger files than binary images. Therefore, the data rate decreases with the higher execution time.
Other RF modulation schemes are applied to VLC such as OFDM in order to improve the VLC data rate effectively [122][123]. However, this is not applicable in this scheme as the different symbols are independent and convey different data.

4.3 Data modulation and image creation

The system block diagram is presented in Figure 4.2. In the Tx side, the input data is converted into a binary stream using ASCII code. An image is then created with a number of black and white cells where '0' and '1' in the binary stream are represented with black and white cells, respectively.

Initially the input information is converted into the corresponding binary stream which is then used to create an image composed of a number of cells, where each cell contains a number of pixels. Pixels within the same cell have the same intensity.

The image creation step is equivalent to signal modulation in this scheme. There are three options when modulating the input signal:

(a) Black/white cells

Cells'colours are either black or white, representing one data bit. The output of the modulation is a matrix of M rows and N columns ($M \times N$) representing pixels' intensity of either 0 or 255 corresponding to black and white respectively. Figure 4.3 depicts an example of a binary stream converted to a black and white image.

(b) Graylevel cells

For the grayscale, every consecutive 8-bit binary pattern is represented by a value between 0 and 255. The output is also a M×N matrix.

(c) RGB cells

In a colour format, pixels are represented by three different colour components: red, green and blue; hence each cell representing 24-bit of the input data stream. The output is three-dimensional matrix of $M \times N \times 3$ elements.

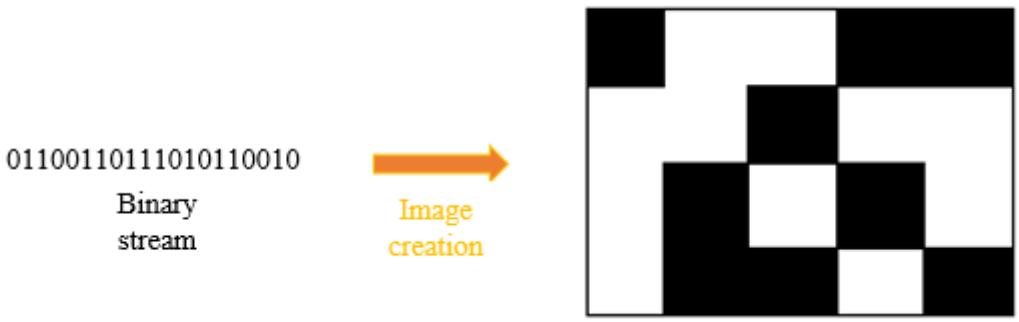

Figure. 4.3 Conversion of binary stream to a displayable image

4.4 SURF based method

4.4.1 Pre-learnt header

As mentioned in the chapter introduction and in Chapter 3, the main challenge in this system is the detection of the Tx, which is the targeted object in this case. The SURF based method is a first attempt to suppress the background noise and detect the Tx on the received frames.

In the previous section, Figure 4.4 described the general block diagram of the system. The first three components of the Tx consisting of converting the input data stream to a transmittable image. The last step on the Tx side is the display as represented in Figure 4.4. In order to ensure an accurate detection on the Rx side, a detection frame (i.e., pilot signal) is first displayed, which is known by both sides of the communication link, the data images generated earlier will be displayed after that. The detection frame is periodically transmitted with the transmission interval depending on the degree of mobility of Tx and Rx.

4.4.2 Keypoint extraction

Object detection is an important application in computer vision, which gives the machines the ability to observe the environment, retrieve and analyze data, and make decisions accordingly. Object detection is a very challenging topic especially in dynamic environments where a number of parameters that need considering when selecting an algorithm for object detection. The most important parameter is the targeted object variations on different images since pictures can be taken under various conditions including illumination, scale, viewpoint and background clutter. For instance, recognizing an object in nighttime can be more challenging than in daytime. Other aspects can be challenging as well such as viewpoint, scale, tar-

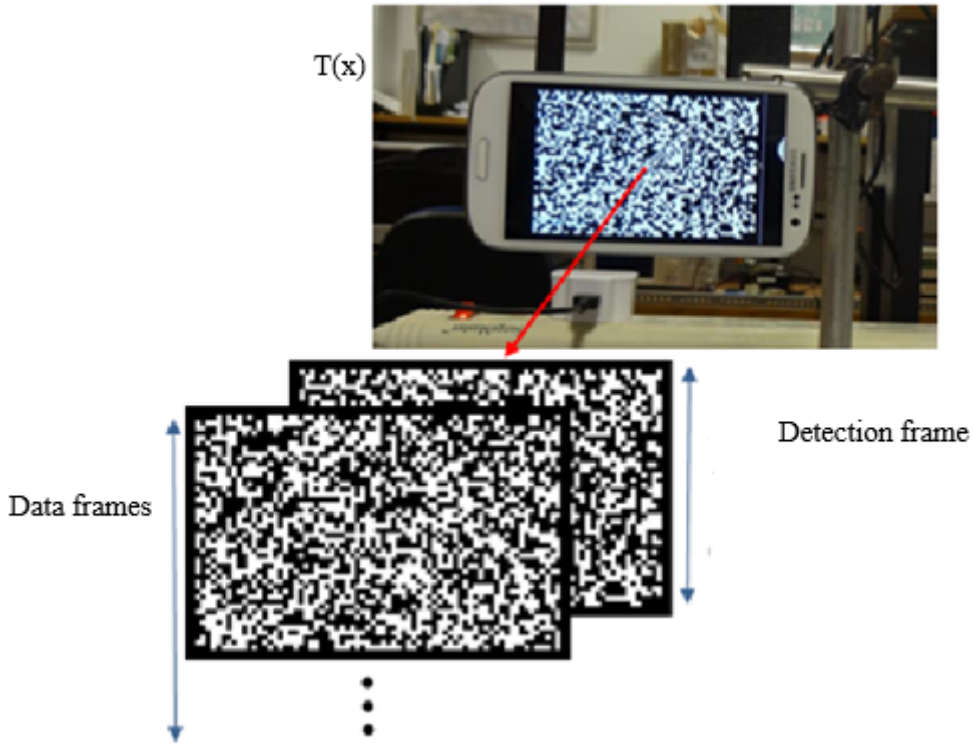

Figure. 4.4 Detection and data frames

geted object occlusion and background clutter. [124]

Different types of object detection algorithms exist as outlined in [125]. One of the most robust classes uses the concept of keypoints, which describe extra specific properties of an image such as important changes in intensity and orientation of pixels, T junctions, corners and others. Keypoints include then a set of specific properties of the image, such as the intensity and orientation. In this scheme, SURF algorithm is chosen since it is an object detection and recognition algorithm, and is invariant to the scale and rotation of the tracked object that is being used in real time applications [113] [126].

SURF can be divided into three steps. First of all, keypoints need to be selected all of over the image. A keypoint could be a T-junction, a corner, a stain . . . etc. This same step is executed multiple times in order to keep only the strongest keypoints.

In other words, the keypoints that are selected the most in the different detection steps. Then, using the neighborhood of the selected keypoint, a unique and distinctive descriptor is calculated. The descriptor needs to be robust against noise and geometric and photometric distortions. Though descriptors are unique, two keypoints from different images, which point to the same area in the same object, have close descriptors. The similarity of the keypoints for the received and the original images determines the accuracy of the targeted object localization.

In keypoint-based feature extraction methods, the execution time depends mainly on the size of the descriptor. Therefore, since SURF was developed for real time performance, a 64-element descriptor is calculated for each keypoint, which is considerably lower than similar methods like SIFT [127] or ORB [128] without compromising the performance [129].

Integral image

The integral image algorithm represents the image in a digital format there each pixel is represented by the sum of all the pixels on its upper left side. It is represented by the following equation [130]:

$$ii(x,y) = \sum_{x' \leq x, y' \leq y} i(x', y') \tag{4.1}$$

Figure 4.5 illustrates the conversion of an RGB image into its integral image. The objective of such an algorithm is to facilitate the pixels' sum calculation within a rectangle in the image.

Fast hessian detector

The Hessian matrix is used in SURF for its fast and precise performance. SURF detects zones of the image where the pixels' intensity changes abruptly. It uses

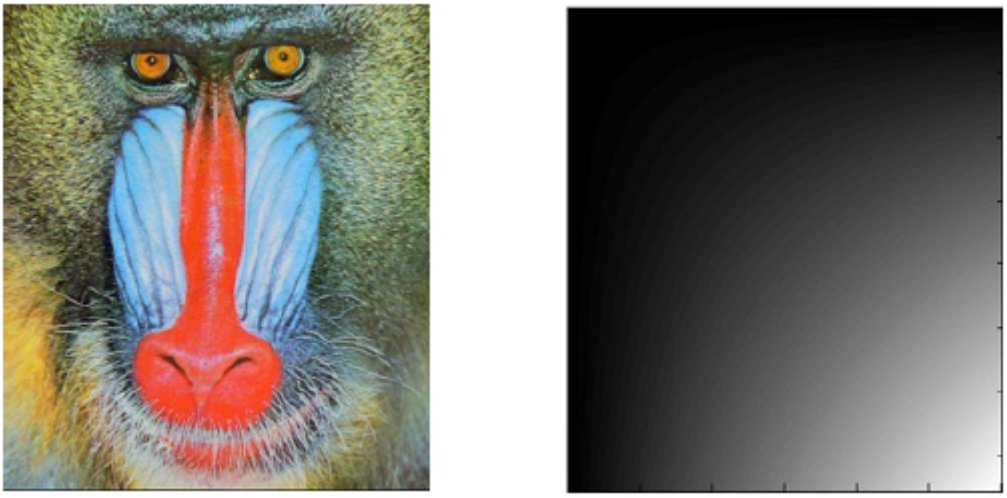

Figure. 4.5 Example of an integral image

the Hessian matrix based on the calculation of partial second derivative for this purpose.

For a given pixel p in an image I, the Hessian matrix $H(p,\sigma)$ at the scale σ is represented as follows [130]:

$$H(p,\sigma) = \begin{vmatrix} L_x x(p,\sigma) & L_x y(p,\sigma) \\ L_y x(p,\sigma) & L_y y(p,\sigma) \end{vmatrix} \tag{4.2}$$

where $L_x x(p,\sigma)$ is the result of the convolution of the Gaussian second derivative $fracd^2 g(\sigma)dp$ with the image I in pixel p.

If the determinant of the Hessian matrix is positive, then both eigenvalues of the matrix are positive, which means that there is an extremum. The only keypoints selected at the end are the ones that represent maxima in a 3x3x3 neighbourhood.

4.4.3 Keypoint description

Once the strongest keypoints selected, the following step is the descriptors calculation. Figure 4.7 illustrates the previous step. This step itself consists of two more

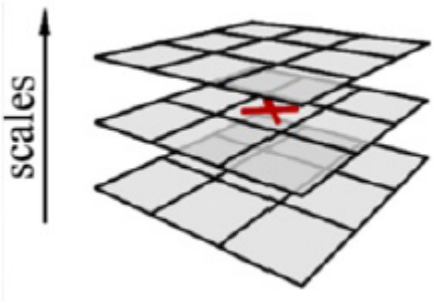

Figure. 4.6 Localisation of a keypoint in a 3x3x3 pyramid

steps:

Figure. 4.7 An example of keypoint detection using Fast Hessian

Orientation assignment

In order to make the algorithm invariant to rotation, its dominant orientation is identified. The SURF descriptor describes the pixels' intensities in the neighbourhood of each keypoint. The x and y Haar wavelet responses is calculated in a neighbourhood of 6 σ where σ is the scale at which the keypoint was detected.

Haar wavelet This algorithm mentions Haar wavelet but in reality, it uses the Haar-like feature. It is similar to Haar wavelet, thus the name. This technique defines rectangular and adjacent zones in the image. The sums of the pixels within the black and the white rectangle are calculated. The difference between the black rectangle and the white rectangle sums represents the Haar-like feature. Figure 4.8

depicts Haar-like feature calculation rectangles. The responses x and y are repre-

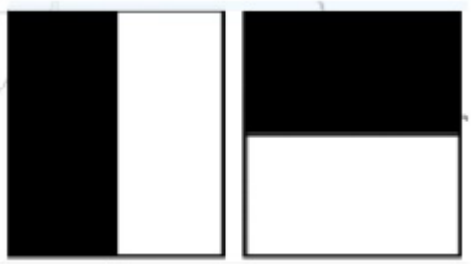

Figure. 4.8 Haar-like feature calculation: x response (left) and the y response (right)

sented by vectors. They are used to calculate the dominant orientation. Figure 4.9 illustrates the window used for the dominant orientation determination. A window (grey area) covering an angle of $\frac{\pi}{3}$ is dragged and the sum of the x and y responses (blue dots) are calculated within this window. A two element vector (red arrow) is then obtained with the sum of the x and y responses. The longest vector represents the dominant orientation.

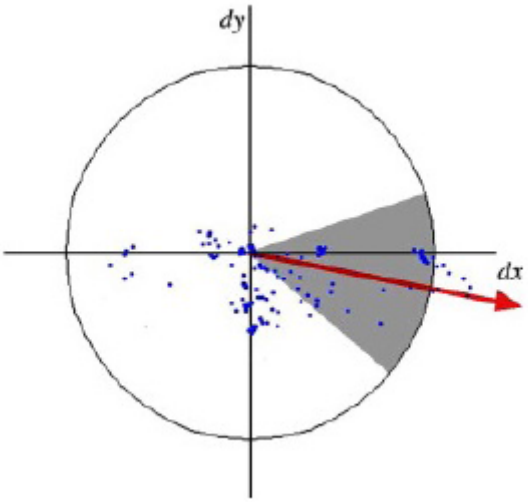

Figure. 4.9 The window used for orientation assignment

Descriptor components

The first step of the descriptor calculation consists of defining a square region around the keypoint. The square window is oriented according to the keypoint orientation. The size of the window is 20σ. Figure 4.10 illustrates this process.

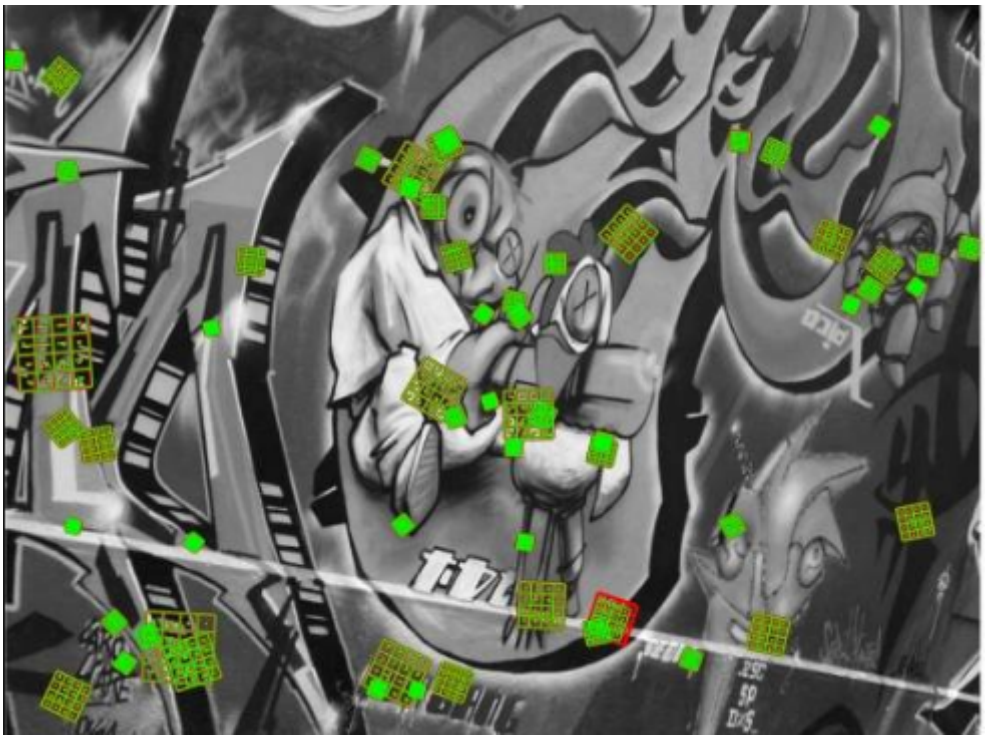

Figure. 4.10 Graffiti details: square windows with different scales

Each region is divided into 4×4 sub-regions. For each subregion, pseudo-Haar wavelet is calculated. The horizontal and vertical responses will be named dx and dx respectively. The sum of the vertical and the horizontal responses of each sub-region will represent the first components of the descriptor. In order to have more information in the descriptor, the sum of the absolute values of the horizontal and vertical responses $|dx|$ and $|dy|$ are calculated. This step is illustrated by Figure 4.11.

Since each square window is divided into 4x4, and each sub-region is described by 4 features, each keypoint is represented by 64 components (4x4x4). Figure 4.12 represents the features of three different sub-regions. A homogeneous region po-

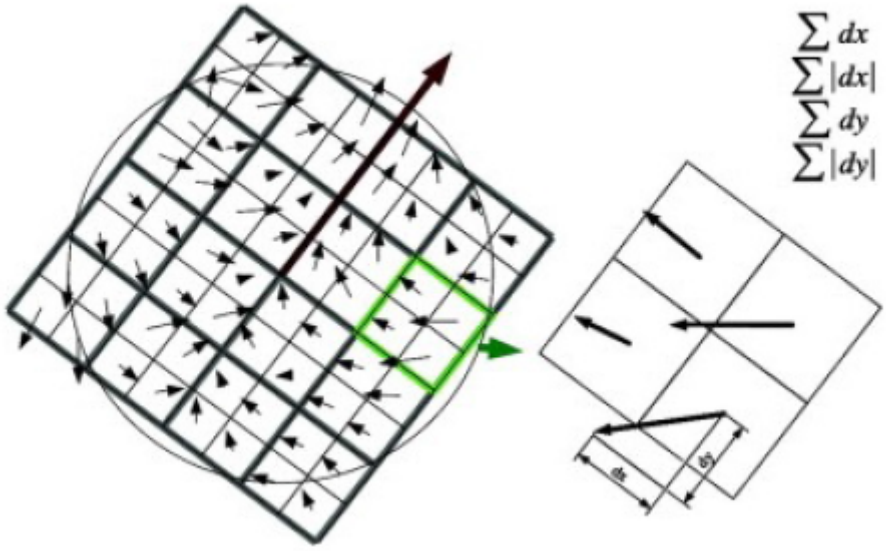

Figure. 4.11 4 Features of each subregion are calculated. For clarity purposes, the sub-region is divided into 2×2

sitioned on the left, all the values are relatively low. The sub-region in the middle presents multiple changes on x-axis, therefore |dx| is the only high value. If the intensity changes gradually as in the third region, dx and $|dx|$ are both high.

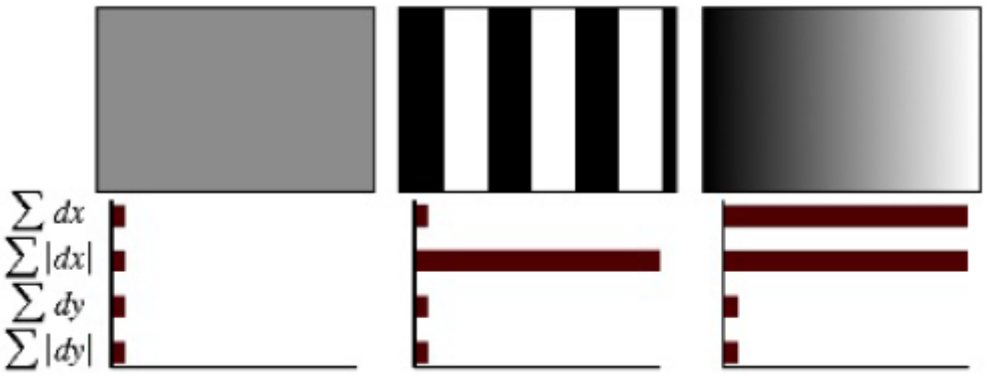

Figure. 4.12 Feature comparison of 3 different sub-regions

4.5 Keypoint matching

Object detection and identification consists of three steps: Keypoints selection, keypoints description and then keypoints matching. In this work, the matching between images has been carried out using a simple Euclidian distance between the descriptors. For a given keypoint from the original detection frame, the Euclidian distance is computed between its descriptor and all descriptors of the captured detection frame. This calculation yields a vector the size of the number of keypoints extracted from the detection frame, and each element is the euclidian distance between the original keypoint descriptor and the extracted descriptor. These distances are then sorted in an ascending order, where the best match relates to the top distance, which is the smallest. In other words, this operation consists of selecting a keypoint from the detection frame that is the closest to the keypoint extracted from the original frame.

4.6 Flashing Screen based Method

4.6.1 Frame Subtraction

In section 4.3, the system block diagram was introduced. The SURF based method and the flashing screen have similar steps in terms of data generation and image creation on the transmitting side. The only difference remains in the last step, which is the display. In this method, the Tx screen flashes between two different brightness levels, high BH and low BL. The flashing screen generates a square wave signal

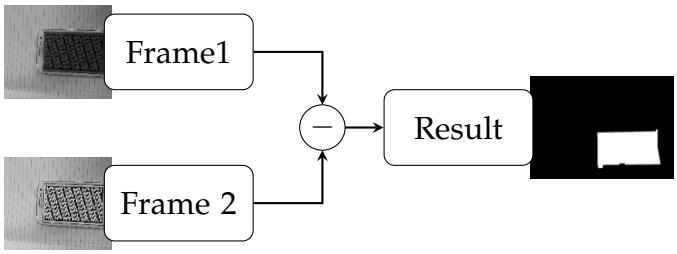

Figure. 4.13 Frame subtraction process

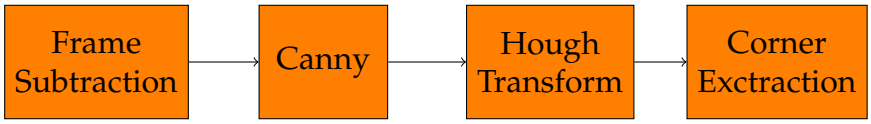

Figure. 4.14 Flashing screen method detection block diagram

b(t) described by the following equation:

$$b(t) = \begin{cases} B_H \text{ when } nT \leq t \leq nT + T_b \\ B_L \text{ when } nT + T_b \leq t \leq (n+1)T \end{cases} \tag{4.3}$$

where T_b and T_d are the durations of B_H and B_L, respectively, and $n = 0, 1, 2, ...$ T is the square wave period and:

$$T = T_b + T_d. \tag{4.4}$$

The Tx screen toggles between B_H and B_L and the camera captures successive frames containing either a low or high brightness transmitting screen. The subtraction between these two frames is the area covered by the Tx, as shown in Figure 4.13, where the two frames 1 and 2 are consecutive.

Once the Tx is located on the picture with the frame subtraction, several image processing techniques are applied before the data recovery. The block diagram in Figure 4.14 illustrates the process in details.

Following the frame subtraction, the Canny edge operator is applied to the output image. Canny is one of the most popular and efficient edge detection operators

[131]. It calculates the grayscale image gradient and the pixels forming an edge are those having the highest gradient response [132]. The output is a binary image containing the strongest edges. Using Hough transform, the lines consisting of the Tx's edges are detected. Hough transform is an effective approach to detect and connect the lines present in a binary image [115] as it groups pixels of the image into known geometric shapes, straight lines for example. When the borders are detected on an image, in some cases it is useful to extract straight lines.

Both Canny edge detector and Hough transform are explained thoroughly in the following sections. The corner's extraction is then possible, and an image warping is executed using a projective transformation [133].

The Rx's camera captures the frames at a frequency f_s. In order to optimize the data transmission rate, only one dark frame is transmitted for the detection of a number of bright frames containing data. Therefore, the Tx localization is calculated once to be applied to a few frames, as shown in Figure 4.15.

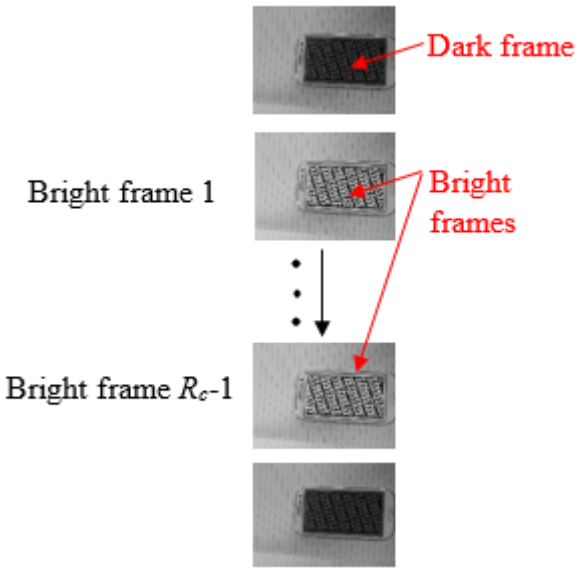

Figure. 4.15 Successive frames transmission

In addition, since the camera is the Rx in this communication system, the signal

sampling frequency is the same as the camera rate f_s. Therefore, the duration T_d of the dark frame has to satisfy the following condition:

$$T_d \geq \frac{1}{f_s}. \tag{4.5}$$

Otherwise, the dark frames can be missed during the image acquisition which compromises the detection. In order to increase the system's throughput,T_d must be as short as possible as there is no data transferred during this laps, and T_b on the other hand must be as long as possible in order to maximize the data transmission per cycle T. Figure 4.16 illustrates this process.

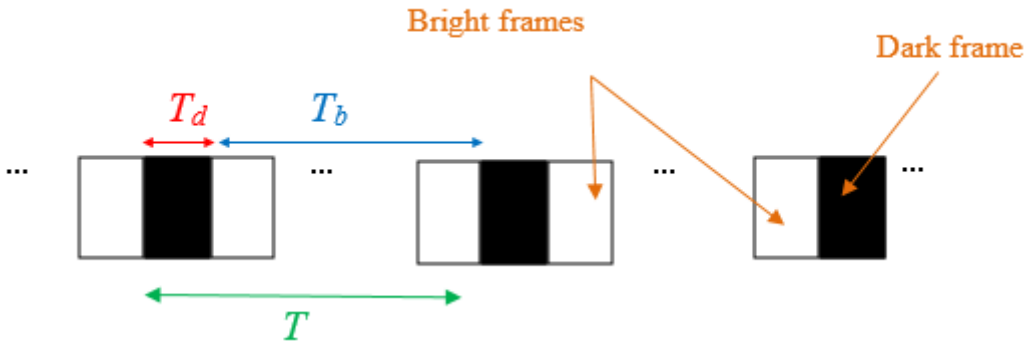

Figure. 4.16 Transmitting screen flashing cycle

4.6.2 Canny Edge Operator

An edge in a digital image is a boundary between region of different color, intensity or texture. It represents a discontinuity where the brightness changes abruptly [134]. Edge detection has a significant contribution in feature detection [89] since it reduces the amount of information in the image to keep only the relevant data. It is based on the second derivative of a Gaussian in order to reduce the noise on the image.

The author of this method based it on three important criteria [135]:

Detection: Maximizing the probability of detecting the actual edge and lowering the probability of the detection of a non-edge, even in the case of a weak edge. This criterion corresponds to signal-to-noise ratio since both probabilities are monotonically increasing.

Localization: The detected edge should be as close as possible to the actual edge.

Number of responses: only one response should be provided per actual edge. Canny Edge operator is applied to the result of the frame subtraction, in order to detect the Tx's borders.

4.6.3 Hough Transform

Hough transform is based on a parametric space, which is called Hough space. This space simplified line detection as it performs a local detection rather than a global one. Although, every curve that can be described with parameters, can be detected by Hough transform, it focuses mainly on straight lines. Moreover, in S2SVLC, the aim is to detect straight lines. Therefore, the following explanation will be limited to this case. Besides, the required number of parameters to describe a straight line is two. Consequently, two parameters will constitute Hough space. These parameters are the ones appearing in the general equation of a straight line within the Cartesian referential:

$$\rho = xcos\theta + ysin\theta \tag{4.6}$$

where ρ is the magnitude

and θ is the orientation of the normal vector to the straight line in a Cartesian referential

These parameters are illustrated in Figure 4.17 (a). This way, a straight line described by the pair (ρ,θ) passing through the point (x,y) in the image space, can be illustrated in the Hough space by only one point.

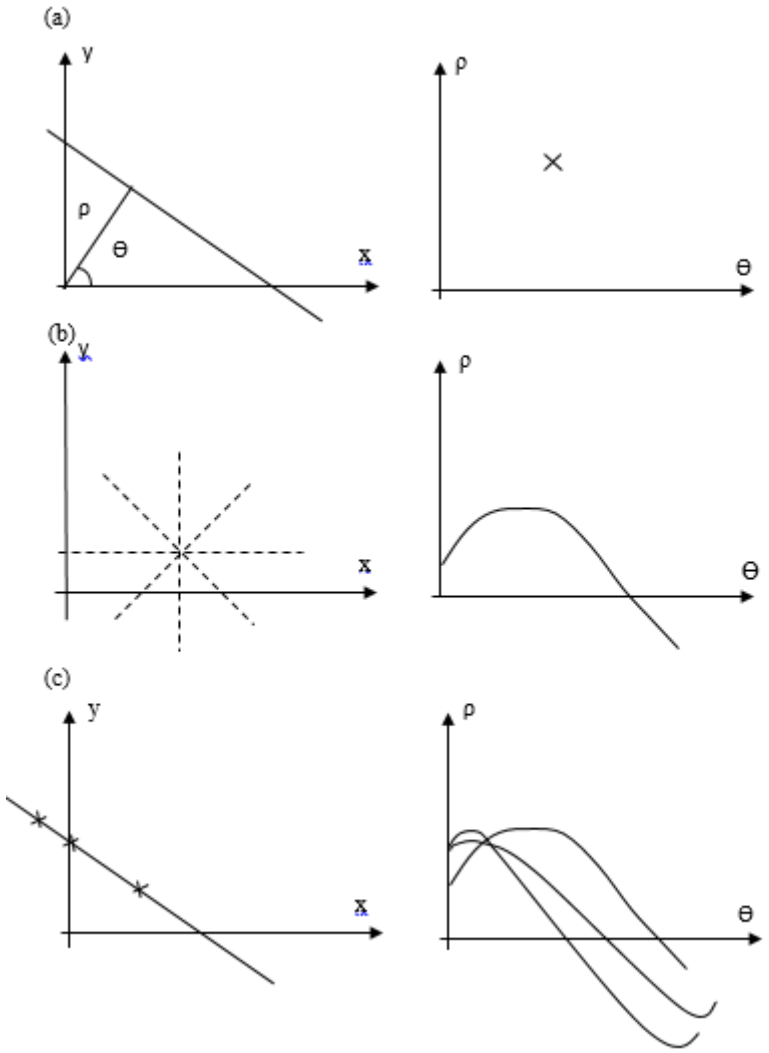

Figure. 4.17 Correspondences between the Cartesian space (left) and Hough space (right)

The normal formulation of a straight line is preferable to a Cartesian formulation $y = ax + b$ because unlike the (a,b) space, the (ρ,θ) space is bounded and homogeneous [136].

There is an infinite number of straight lines passing through a same point (x,y) and the only difference between these lines is the orientation. This beam is represented by a sinusoidal curve in the Hough space (Figure 4.17 (b)). When several points, they form a straight line that is represented in the Hough space by the intersection of multiple sinusoids (Figure 4.17).

4.7 Data Recovery

4.7.1 Perspective Correction

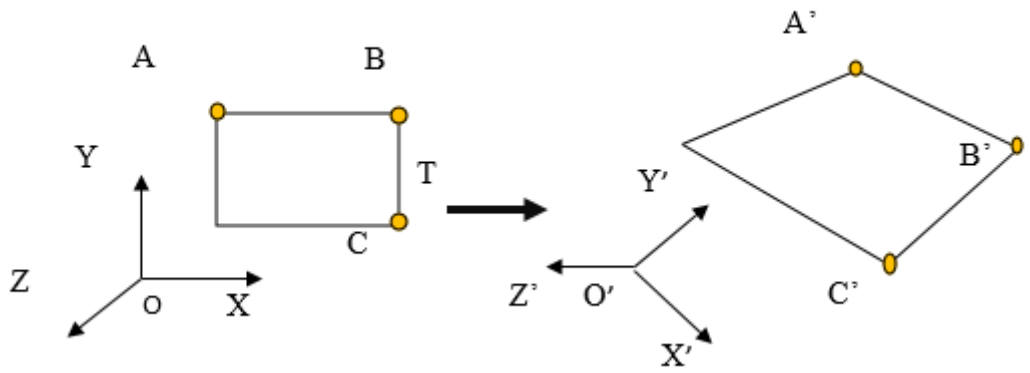

Figure. 4.18 Rectangle distorted with a projective transformation

In Figure 4.18, A is a point in the OXYZ frame of reference and A′ is its projective transformation in the OX′Y′Z′ frame of reference, where:

$$A = TA'. \tag{4.7}$$

The point A homogeneous coordinates are: (AX, AY, AZ) whereas the point A′ homogeneous coordinates are: (A′X,A′Y,A′Z). The transformation matrix T = [tij] where T is an invertible 3x3 matrix and the relationship between the coordinates of

both points is given by the following equation:

$$\begin{matrix} A_x \\ B_x \\ A_z \end{matrix} = \begin{bmatrix} t_{11} & t_{12} & t_{13} \\ t_{21} & t_{22} & t_{23} \\ t_{31} & t_{32} & t_{33} \end{bmatrix} \times \begin{matrix} A'_x \\ B'_x \\ A'_z \end{matrix} \tag{4.8}$$

In order to determine all 9 elements of T matrix, 9 equations are needed. These equations can be obtained using the 3 points A, B and C and their respective projective transformation A', B' and C'. The elements of T are then determined by simply resolving the system of multiple equations for multiple unknowns.

4.7.2 Binarization

Otsu Method

Binarization is the process of converting a grayscale image into a black and white image using thresholding [114]. Two different thresholding methods applied separately were investigated in this work. A hard threshold selection will be explained in the system description section, and a soft thresholding method using Otsu method which relies on the image histogram to compute an optimal binarization threshold value [137].

Otsu method is based on a statistical separation of image pixels in two classes in order to binarize the image. The threshold is calculated using moments of the first two orders which are average ave and standard deviation std [138].

In addition, in order to obtain a result independent from the dimensions, the histogram H is normalized as:

$$H_n = \frac{n_i}{N}, \tag{4.9}$$

where n_i represents the number of pixels at illumination level i in the image and

N is the total number of pixels on the image at the intensity k:

$$ave(k) = \sum_{i=1}^{k} i \times H_n(i), \tag{4.10}$$

For $k = 1, \ldots, 255$.

$$std(k) = \sum_{i=1}^{k} H_n(i), \tag{4.11}$$

For each value of k the following is calculated:

$$s^2(k) = std(k).(1 - std(k)).[(ave(255).std(k) - ave(k))]^2, \tag{4.12}$$

The value of k that maximises the function s is considered as the optimal threshold value to binarize the image because it maximizes the separability in the resultant classes in gray levels [31]. The threshold value k is the one that verifies the condition:

$$s^2(k) = max(s^2(k)) \tag{4.13}$$

Hard Thresholding Method

The cells on the data frames are equally distributed between black and white thanks to the probabilities of 0 and 1 of random signal. Given that p_b is the probability of black cells and p_w is the probability of white cells, we have:

$$p_b = p_w = \frac{1}{2}. \tag{4.14}$$

For a hard decision binarization, the threshold T_b represents the theoretic mean

value of the cells intensity:

$$T_b = (\frac{1}{2}0) + (\frac{1}{2}255), \tag{4.15}$$

$$T_b = 127. \tag{4.16}$$

Given I the received image of size M × N:

$$\begin{cases} \text{if } I(i,j) > T_b \text{ then } I(i,j) = 255 \\ \text{else } I(i,j) = 255, \end{cases} \tag{4.17}$$

where $0 < i \leq M$ and $0 < j \leq N$. However, hard thresholding selection does not take into account the different light conditions, thus the Tb might not be ideal in case there is ambient light noise effect. In fact, the binarization threshold and the process performance are strongly dependent on the ambient lighting.

4.7.3 Quantization

When all the pixels are either black or white, a quantization to the whole cell is applied. If 50% of the pixels in one cell are black, then the remaining pixels will be converted to black. On the other hand, the whole cell will be put to white if white pixels represent 50% or more. These processes are illustrated in Figure 4.19 where a cell is highlighted before and after quantization.

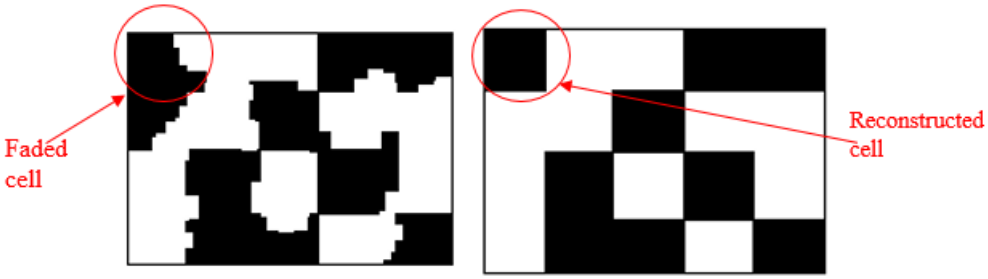

Figure. 4.19 A cell before and after quantization

4.8 Signal attenuation parameters

In this section, the different parameters affecting the signal's strength while transmitted through the channel are enumerated.

4.8.1 Perspective distortion

The S2SVLC system is designed for mobile communications. It is vital for the system to include a Tx's detection robust to the smartphones movements. Figure 4.20 depicts the different scenarios that are challenging for the Tx's detection. The more important the movements are, the more challenging the detection is, and therefore the more attenuated is the signal.

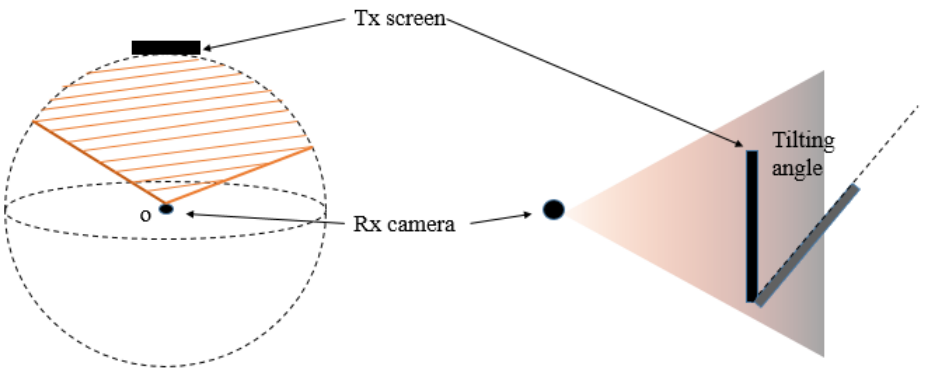

Figure. 4.20 Tx and Rx orientation

4.9 Perspective correction attenuation

In order to reduce the perspective distortion attenuation, a perspective correction is performed as explained in the previous sections.

Before correcting the perspective, a cumulative error affects the system's performance while executing the previous steps, the Tx detection and corner extraction.

Although the perspective correction method is effective, it still comes with an additional effect to the attenuation already accumulated, and this section details how the projective transformation can affect the signal.

Moreover, an easy way to compare the transmitted signal to the received signal, is to calculate the percentage of similarity between the transmitted frame and the received frame by image overlapping. Figure 4.21 (a) represented two frames overlapping, the first one is the frame initially transmitted (orange), the second one is the received frame, after performing the frame subtraction, corner extraction as well as the perspective correction. A perfect case scenario is when the 4 corners of the initially transmitted frame fully overlap the 4 corners of the received frame, where the percentage of similarity is 100%. However, as mentioned before, this is a physical system and a 100% signal recovery is rare given the cumulative error due to the slight inaccuracies throughout the algorithm execution. The error yielding from the perspective correction inaccuracy is described here, using only two corners from the transmitted frame and the received frame, for simplicity purposes. The similarity between these two corners can be translated into the intersection surface between the two. On Figure 4.21 (b) and (c) illustrated these two corners. The error can be separated into a rotation around the centre of the cell, see Figure 4.21 (b) and a translation, see Figure 4.21 (c). The intersection I_c between the transmitted cell C_t and the received cell C_r shown in Figure 4.21(b) can be estimated by simply calculating the overlapping area between C_r the received cell and C_t the

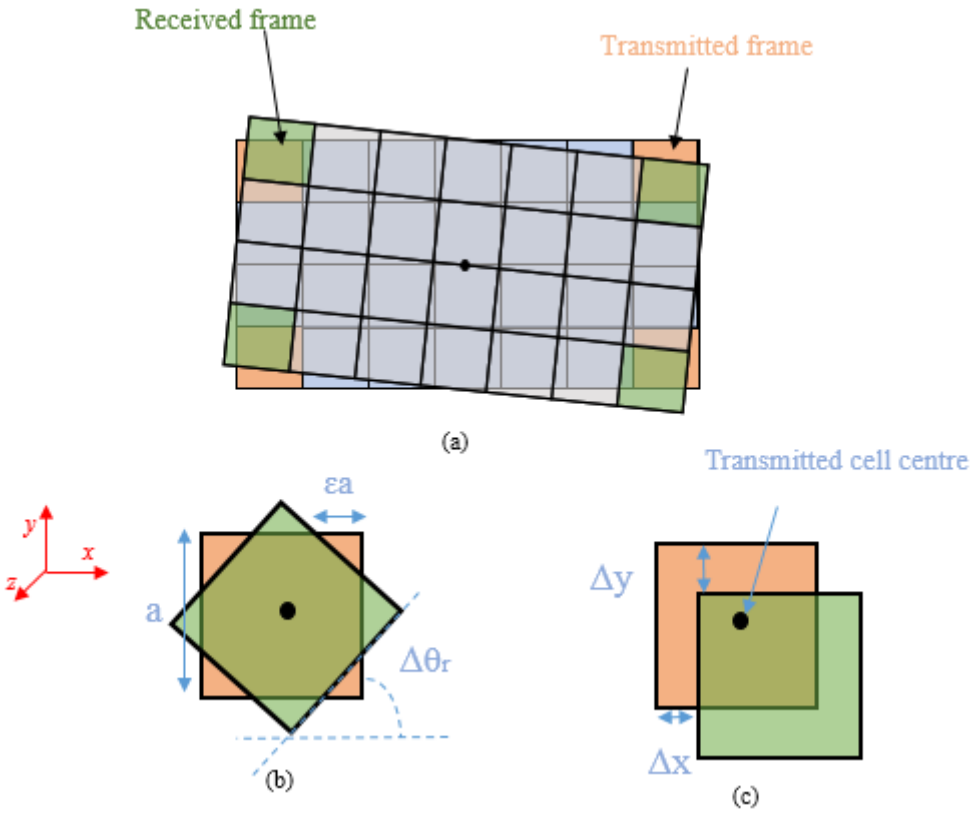

Figure. 4.21 Perspective distortion inaccuracy

transmitted cell. This area can be derived as follows:

$$I_c = a^2 - 4 \times \varepsilon^2 \times a^2 \times tan\Delta\theta_r, \tag{4.18}$$

$$I_c = a^2 \times (1 - 4 \times \varepsilon^2 \times tan\Delta\theta_r), \tag{4.19}$$

Therefore, a full recovery of the signal is only possible when the error-angle $\Delta\theta_r$ equals 0.

On the other hand, I_c in Figure 4.21(c) can be calculated as follows:

$$I_c = (a - \Delta x)(a - \Delta y). \tag{4.20}$$

The intersection between the two cells is consequently full, only when the translation is null.

4.9.1 Inter symbol interference attenuation

As the distance between the Tx and the Rx, the total number of transmitted cells as well as the ambient light change during the communication, the borders of the transmitted cells fade, and they become indistinguishable. This phenomenon can be translated into inter symbol interference (ISI). The ISI effect is reduced using quantization, as described in [139], where each cell is processed individually using the a thresholding method where the a cell is considered as "black" if half of the pixels comprised in the cell are black, and converted to "white" otherwise. The ISI in this system can be represented by a coefficient c_{ISI} where:

$$I_c = c_{ISI} \times a^2, \tag{4.21}$$

and $0 < c_{ISI} < 1$.

Therefore, the signal is fully recovered only if c_{ISI} equals 1.

4.10 Summary

In this chapter, the S2SVLC concept was introduced. A block diagram was depicted and every single step was detailed including data modulation, Tx's detection, noise suppression and data recovery. Two different versions of the system developed in this work were thoroughly described. The first method, which is based on a frame header for the detection of the Tx, used the object detection algorithm SURF. The

second one, relies on a Tx with a flashing screen, and uses different image processing tools to detect the Tx and recover the data. The most important ones are Canny edge operator and Hough transform. This method was developed in order to reduce the SURF-based method unnecessary complexity. Then, the data recovery process was described, which is based on two different methods of image binarization, as well as a quantization process that is meant to remove inter symbol interference. The final section exposed the most important parameters that contribute to the signal attenuation, such as the perspectrive correction inaccuracies as well as the ISI effect.

Chapter 5

Experimental Work

5.1 Introduction

In this Chapter 4, the S2SVLC system was introduced and the main subset of this system was outlined as the detection of the Tx by the Rx's camera. For this purpose, two different versions of the developed systems were described, and this chapter is devoted to one of those methods. In the first one which is based on SURF method, a keypoint extractor and descriptor is used for object detection. In this method, a header is first displayed on the Tx's screen before data frames are transmitted subsequently. The header is pre-learnt by both sides of the communication as it is used for the detection of the Tx's on the received frames. In this chapter, the performance of the SURF based method will be evaluated. Key parameters were used for the investigation such as distance, rotation and tilting angle. In the first set of experimental work, the tilting angle is equal to 0 and the rotation angle was in the range of [-30°,30°], as it outside this range, the bit success rate drops dramatically. However, in the second experiment set, improvements were made and a projective transformation was used, the rotation covered all 360° and the tilting angle reached 75° with an acceptable recovery rate.

5.2 System set up

5.2.1 System flowchart

The system is numerically evaluated using Matlab. Figure 5.1 shows the flowchart of system operation and hence the associate code. As stated in Figure 5.1 in section 4.4.1 of Chapter 4, a detection frame is displayed first on the Tx's screen for accurate detection purposes, and then the data frame is displayed straight away. On the receiving side, the first step consists of data capturing. The receiver's camera will first capture the detection frame which will be used to locate the Tx, and then it will capture the data frames. Once recognised, the detection frame is processed in the Tx's detection block. The SURF algorithm is applied to both the captured detection frame and the original detection from, and the SURF keypoints are extracted. These keypoints are then described and compared using the matching method described in Section 5 of Chapter 4. If the total number of the matched keypoints is insufficient (the threshold is determined empirically), the detection is impossible and the process will be stopped. On the other hand, if there are enough matched keypoints, the next step of data recovery will be proceeded.

As mentioned in the chapter's introduction, two sets of experimental work will be carried out. The data capturing and the Tx's detection steps are the same for both cases. However, the data recovery step is improved in the second set. The key differences between the two sets in the recovery step are the 'geometric transformation'and the 'quantization'modules. The key differences between the first set and the second set are highlighted in Table 5.1.

In the first set, after the detection of the keypoints, the bounding box around the detected keypoints (see Figure 5.2) is used to calculate a 2D transformation matrix, which will be used to recover received data frame. Whereas in the second set, the

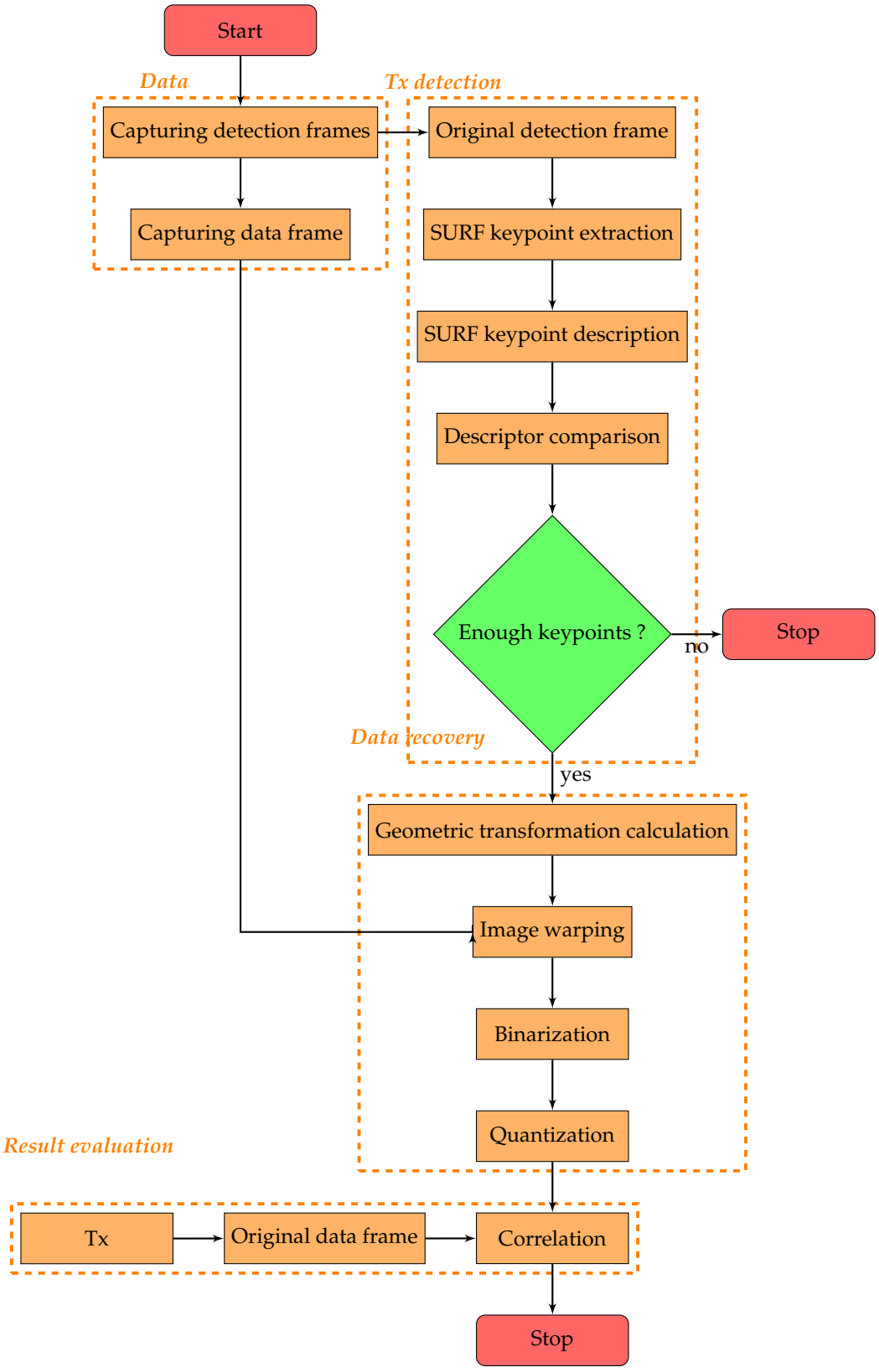

Figure. 5.1 System flowchart

	First set	Second set
Rotation angle	[-20°,+20°]	[-20°,+20°]
Tilting angle	0°	[-50°,+20°]
Tx	iPhone 4	LG G3
Receiver	HTC One back camera Sony QX-10	Samsung Galaxy S3 back camera Samsung Galaxy S3 front camera Sony QX-10
Geometric transformation	2D	3D
Quantization process	\	used

Table 5.1 Key differences between first set and second set

detected keypoints are used to calculate a 3D transformation matrix, in order to give more mobility capability to the smartphones. The quantization module is only introduced in the second set for cell reconstruction.

5.2.2 The set up

Two mobile devices are used to carry out the experiment work. The transmitting smartphone is used for displaying the data matrix in black/white image whilst the built-in camera of the receiving device is used to capture the displayed data. In the setup, the Tx is located at a fixed position, whereas the Rx is able to move along the z-axis. The background of the captured image might include other irrelevant objects located around Tx. Both Tx and Rx are exposed to the normal office lighting conditions (400 lux) using fluorescent lamps which is the ambient background noise. In both sets of experimental work, we carry out measurement by varying the transmission distance d, rotating the angle θ, as well as the total number of cells transmitted in one frame (see Figure 5.3). Additionally, the geometric transformation introduced in the second set is three dimensional. Therefore, the Tx and the Rx do not need to be in a parallel position for an accurate data transmission, and a tilting angle is allowed. The system will also be evaluated according to the tilting angle α (see Figure 5.4). The Tx is tilted with α ranging from 0° to 75° where

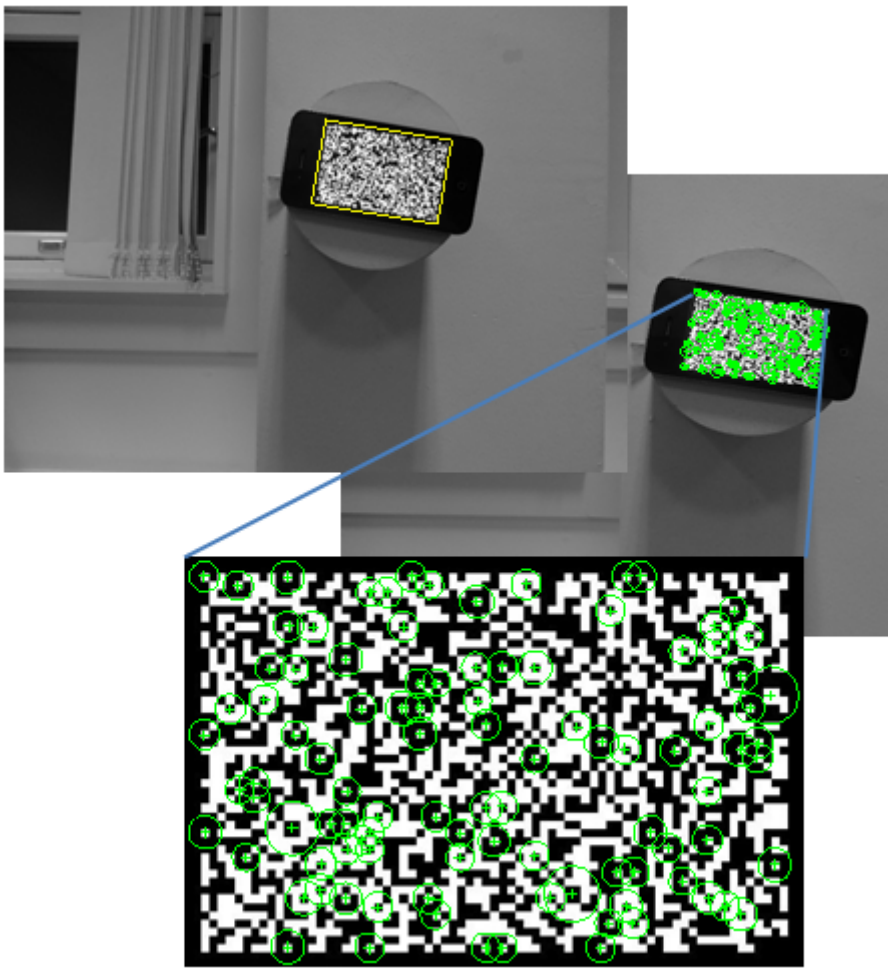

Figure. 5.2 Keypoints determination at the receiver

0° is the initial position where both Smartphones are in parallel planes. Additionally, in chapter 4, section 4.7.2, two different binarization methods were described (Otsu method and the hard-thresolding method). These two methods are evaluated and compared in this set. Otsu binarization method was referred to as the Soft Thresholding method (ST) whereas the second one was referred to as the Hard Thresholding method (HT).

In the first set of experimental work, we use two cameras to capture the transmit signal at the receiver. The first camera is the HTC One Smartphone camera, which is the main interest of our investigation for object detection. The second camera is

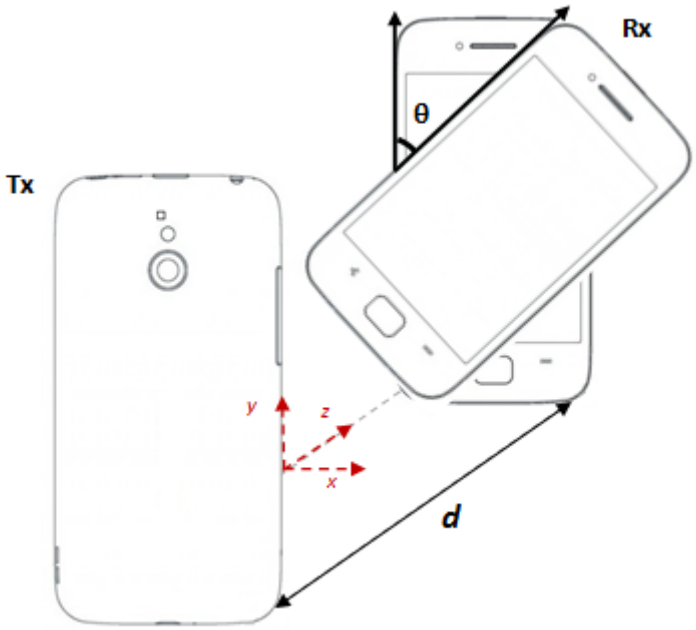

Figure. 5.3 S2SVLC: Distance and rotation angle

Figure. 5.4 S2SVLC: Tilting angle

Sony QX-10 with better optics and resolution [140] is used as a reference to compare the quality of the image of the first camera. There is no optical image stabilizer (OIS) for both cameras and snapshots from both cameras are taken under the same test condition for comparison purpose.

In the second set, we have used Samsung Galaxy S3 Smartphone back and front

cameras to capture the image from the Tx mobile, in addition to the Sony QX-10 camera as a reference camera to compare with the Galaxy S3 camera performance. There is no optical image stabilizer (OIS) in both S3 cameras and snapshots from both cameras are taken under the same test conditions for comparison purpose. Table 5.2 shows the key parameters of the experiment setup.

Parameters	**First set**	**Second set**
Number of cells (MxN)	3750 (75 x 50)	3750 (75 x 50)
Number of pixels per cell	7 x 7	10 x 10
Number of cell colour states	2 (black and white)	2 (black and white)
Tx smartphone screen resolution	640 x 960 (3.5 inches)	1280 x 720 (4.8 inches HD super AMOLED)
Rx smartphone front camera resolution	Not evaluated	1.9 Megapixel
Rx smartphone back camera resolution	4 Megapixel [141]	8 Megapixel
Reference camera (Sony QX-10)	18 Megapixel	18 Megapixel
Link length **d**	10 cm to 110 cm	10 cm to 110 cm
Parallel rotation angle θ	-30° to 30°	0° to 360°
Parallel rotation angle α	0°	0° to 75°
Measured ambient light level (lux) / normal office lighting	570 (Note: ISO office standard lighting level is 400 lux)	570

Table 5.2 Experimental parameters

5.3 Comparison with previous work

In this section, we compare the S2SVLC to similar systems, described in camera based communication under perspective distorsions [106], Pixnet [103] and COBRA [102]. Some key properties are listed in Table 5.3.

	Pixnet	**Cobra**	**Link with perspective distortions**	**S2SVLC**
Tx	32 inch LCD screen	5 inch smartphone screen	21.5 inch LCD screen	4.8 inch smartphone screen
Receiver	Off-the shelf camera	Smartphone camera	Tablet camera	Smartphone camera
Cells colours	Black/ white	Coloured	Black/white	Black/white
Distance	Up to 14m	5 inch	5 m	Up to 1.2 m
Number of cells	81x81	800 x 400	15 x 15	Up to 170 x 120

Table 5.3 Experimental parameters

5.4 Low rotation angle and parallel position

5.4.1 Distance

Figure 5.5 shows the successful rate of data recovery against the spacing between the two cameras d and θ set to 0° in the first set. The figure depicts the performance of the system when the images are captured by the HTC phone's camera for d up to 76 cm. Over the short range (10 - 50 cm) the success rate is 80%, starting to reduce from $d > 50$ cm. For $d > 76$ cm very little data recovery is observed. This is due to the resolution of HTC camera which is limited (4 Mega pixels whilst the object is much smaller at $d > 60$cm). Therefore the HTC device cannot clearly distinguish the individual cells.

In contrast the reference camera Sony QX-10 has a much higher resolution (18 Megapixel) and better optics lens. The communications range can be extended up to 100 cm with good results of 93% and 80% correct data recovery at d of 10 cm and 1 m, respectively, thus demonstrating the system performance highly depends on

the camera quality (resolution and lens). Moreover, a huge gap is noticed between the front camera compared to the other cameras. This is expected as its resolution is very low (1.9 Megapixel compared to 8 and 18 Megapixel).

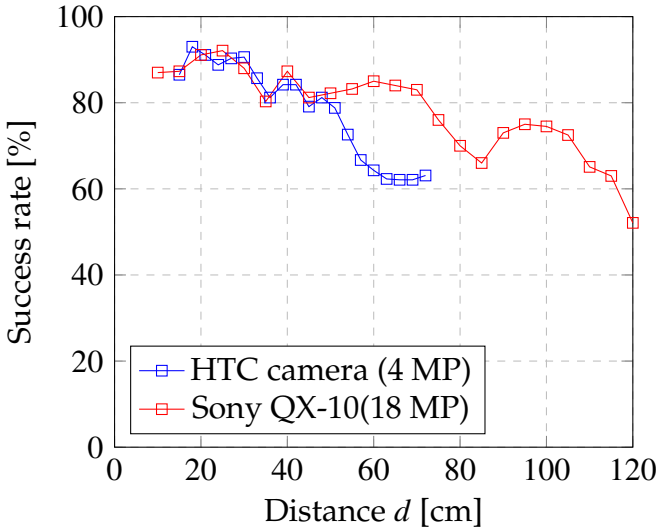

Figure. 5.5 Bit success rate against distance d

5.4.2 Rotation

The second geometrical test is carried out by varying the rotation angle θ to evaluate the performance of the received data recovery, see Figure 5.3. For the HTC camera d is kept at 28 cm to ensure high success rate as shown 5.6. Both cameras display similar performances with the success rate is slightly above 80% over the range of -17° to +17°.

5.4.3 Number of cells

In the final test of this first set, the transmission capacity is measured as a function of the increase number of transmitting cells ($N \times M$). For d = 16 cm, the success rate is plotted against the total number of cells as shown in 5.7. The success rate drops

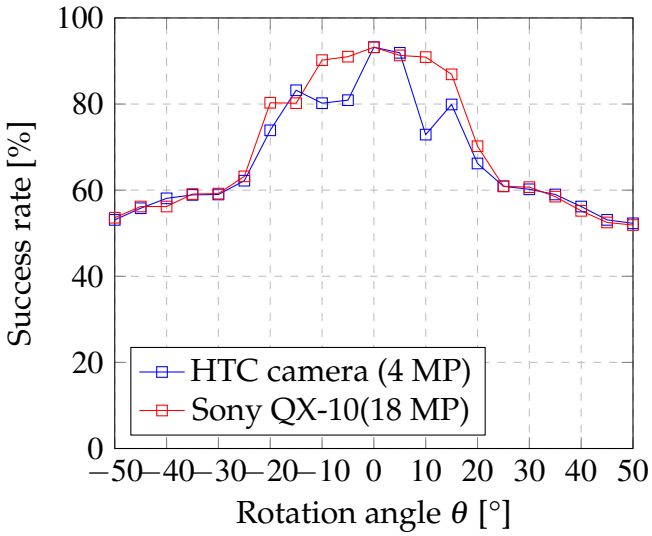

Figure. 5.6 Bit success rate against rotation θ

sharply for both cameras due to the fact that the Tx phone has a low resolution so that the cell itself is not very clear and sharp, which makes the data recovery more challenging.

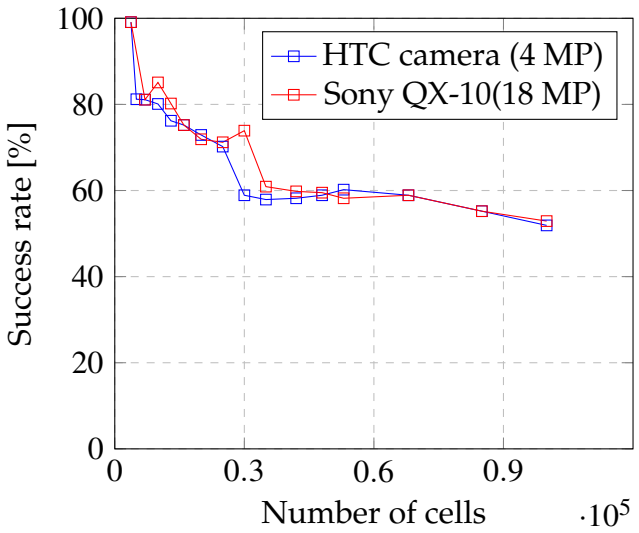

Figure. 5.7 Bit success rate against number of cells increase

5.4.4 Conclusions

The result obtained over the range d = 10 – 50 cm ($\theta = 0^{\circ}$) shows a stable performance (Figure 5.5) of S2SVLC. There are 3750 black/white cells being transmitted per frame (i.e. 3750 bits). At the standard camera rate of 30 fps, we could achieve the total data rate of 112.5 Kbps. Maintaining the 80% correctness the data rate could be three times higher where 10,000 cells can be used, thus offering 300 kbps. The data rate could be significantly increased if higher quality phones are used (higher camera resolution for data capturing and bigger screens for data transmission) and the cells are in grey scale or colours instead of only black and white.

5.5 Non parallel position and full rotation

5.5.1 Distance

Figure 5.8 shows the performance of data recovery using three cameras. The communications link distance d between the two smartphones is varying between 10 cm and 120 cm. The Samsung back camera reaches 98% data recovery over the short range (10 – 50 cm). On longer distances, the bit success rate drops to 60% until the detection is not possible anymore as the number of keypoints detected is insufficient after 70 cm. It is worth noting that the number of keypoints correctly matched (as explained in section 4.5) between the original detection frame and the captured detection frame reduces when the distance between the Tx and the Rx increases. When this number is lower than a threshold empirically set (5 correctly matched keypoints in this case), the Tx cannot be detected anymore.

The Samsung front camera achieves a data recovery greater than 85% within the range of 10 to 25 cm. The performance drastically decreases as the number of keypoints is not sufficient for the Tx's detection when the distance is overr 30 cm.

This result was expected given the low resolution (1.9 Megapixel) of the front camera compared to the back camera (8 Megapixel). In contrast the reference camera Sony QX-10 has a much higher resolution (18 Megapixel) and better optics lens. The communications range can be extended up to 110 cm where the detection is still possible (sufficient number of matched keypoints) even though the bit success rate decreases, thus demonstrating the system performance highly depends on the camera quality (resolution and lens). Nonetheless, the results in the short range (10 – 60cm) are good and very close to the results obtained with the back camera of the smartphone, as they vary between 85 and 100%.

In order to binarize the data correctly regardless of the background light and the Tx's screen illumination, an automatic solution for optimal threshold calculation is developed and implemented. Here the Otsu method is adopted for optimising the system performance [138].To evaluate the reliability of this method that is applied within this system, the performance of Otsu method is investigated using both soft decision thresholding method (ST) and hard decision thresholding method (HT).

The captured images are washed out when the Tx is exposed to the ambient light (570 lux) in the standard office lighting. As a result, the black colour is brighter and the process with hard threshold will tend to favour it to 'white colour'. Consequently, the soft threshold value should be closer to 255 and greater than the hard threshold to allow more accurate separation between cells of different colours and a better recovery.

Overall, the Otsu method gives better results than the hard thresholding method.

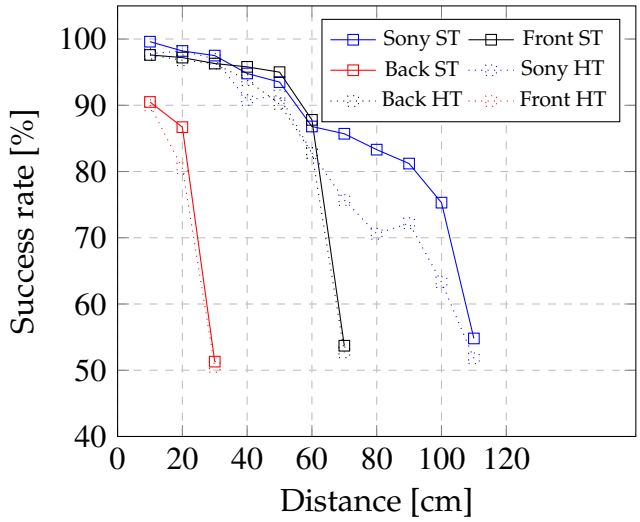

Figure. 5.8 Bit success rate against distance *d* and comparison of HT and ST

5.5.2 Parallel rotation

The second geometrical test is carried out by varying the angle of rotation of the Tx where both Smartphones are in parallel planes, to evaluate the performance of the receiver data recovery, see Figure 5.9. For all of three cameras the distance d was kept at 15cm as all camera performances are very good at this distance which allows the investigation of the rotation with minimum distance effect. Both Sony camera and Samsung back camera display similar performances where the success rate is near 100% on the range (0° to 360°). The Samsung front camera shows fairly good performance. It slightly decreases when the angle increases towards 180° and reaches the 90% recovery again when the angle is closer to 360°°.

5.5.3 Tilting angle - Non parallel rotation

We further investigate the system performance against the tilted positions of the Tx (see Figure 5.10). Both Sony camera and Samsung back camera achieved good results within the range between (0 and 50°). The performance drops slightly at 60°. The detection is not achieved after that as the number of keypoints is not sufficient.

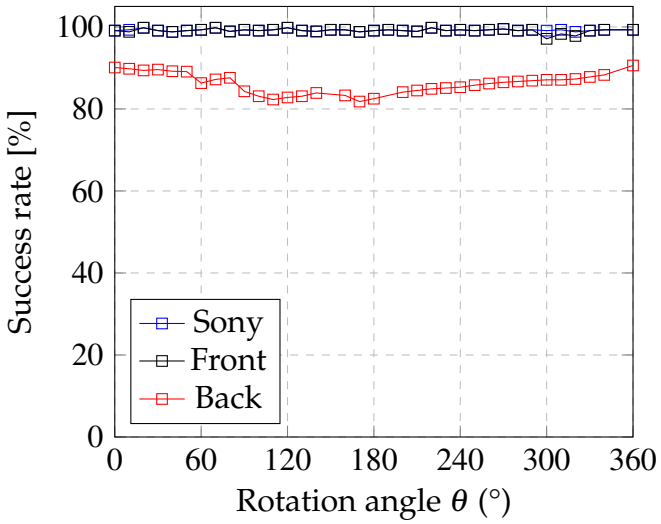

Figure. 5.9 Bit success rate against rotation angle θ and comparison of HT and ST

The Samsung front camera has a low resolution and therefore less immunity against the different mobility parameters. It achieves an acceptable results only in the range (0° to 20°). These results again indicate the importance of camera quality on the system performance. In this case, the results obtained with Otsu method and the hard decision thresholding method presented consequent difference making Otsu method a better choice again.

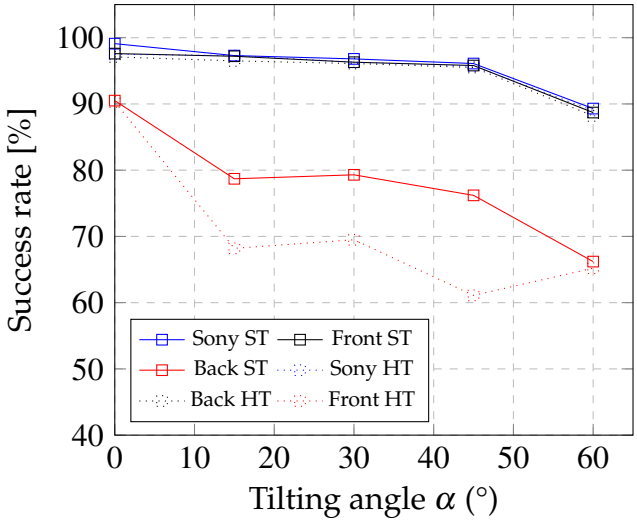

Figure. 5.10 Bit success rate against tilting angle α and comparison of HT and ST

5.5.4 Number of cells

Experiments are carried out with the variation of the number of cells displayed on the Tx's screen to extensively evaluate the performance of the receiving capability with different threshold schemes. The number of cells was varied from 3,000 to 100,000 over a 15 cm link distance.

For the reference Sony camera and Samsung Back camera, the performance decreases slightly when increasing the number of transmitted cells until it drops after 90,000 cells. On the other hand, the Samsung front camera is more affected by the number of cells increase and the recovery rate drops under 70% at 30,000 cells transmitted.

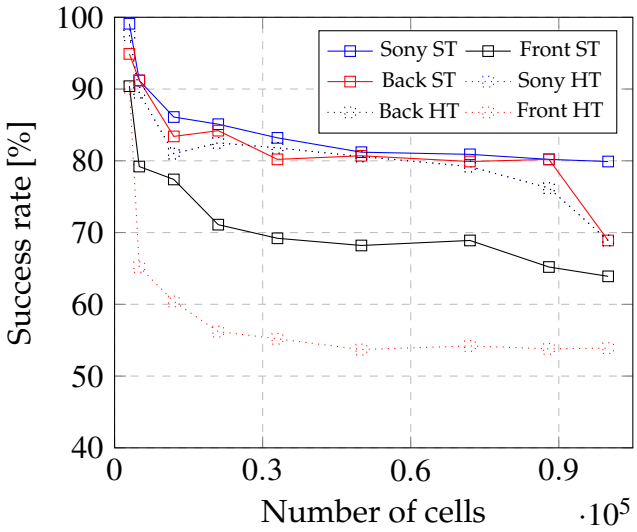

Figure. 5.11 Bit success rate while increasing the number of transmitted cells and comparison of HT and ST

5.6 Summary

In the previous chapter,an S2SVLC system based on a keypoint extractor and descriptor named SURF was described. This method was thoroughly evaluated in

this chapter and two sets of experimental work were carried out. The first set represented the initial implementation of the system. Multiple parameters were investigated, such as distance, total number of cells transmitted as well the rotation angle. The geometric transformation used in this set was bi-dimensional and therefore, both Tx and Rx needed to be in a parallel position as three-dimensional distortions could not be suppressed. In the second set of experimental work, the system was improved using different techniques. First of all, a three dimensional geometric transformation was used which allowed a certain tilting angle and a wider rotation angle. Then, a quantization step was introduced in order to reduce the inter symbol interference effect. Finally, on top of the hard thresholding method, Otsu method was used, which is a soft thresholding method in order to have a system independent of the ambient light. Both methods were evaluated and compared regarding their performances in terms of bit success rate. The comparison of these methods was outlined with the results of all the mobility parameters investigated.

Overall, the tests were carried out in various mobility conditions in S2SVLC such as the distance between the Tx and the Rx, the Tx rotation and tilting angles as well as the total number of cells transmitted. The proposed system offered the suppression the path loss, inter-symbol interference and perspective distortions. The obtained results outlined a reasonable performance of standard smartphones and the benchmark for short range data communications with different camera performance.

It is noted that new generation of smartphones present higher quality features in terms of screen and camera resolution, thus offering a higher potential for this system to perform high speed data transmission.

Chapter 6

Implemented Smartphone to Smartphone VLC System

6.1 Introduction

In chapter 5, an initial implementation of S2SVLC was presented. It was achieved on Matlab for simplicity purposes. SURF algorithm was used for the Tx's detection and a detection frame known by both sides of the communication was required. However, SURF is an over-complex algorithm for this type of application. Additionally, although it was designed for real-time use, other simpler and less time consuming options can be considered in this scheme. In this chapter, one of these options is investigated and the detection method is updated. In order to enhance the S2SVLC portability and simplify the detection process, a new detection method is developed. Firstly, the data is encoded into black and white cells and displayed on the Tx's flashing screen followed by a frame subtraction to locate the Tx's on the received frames. The remaining steps are similar to the system developed in Chapter 5. However, the end-to-end system is fully developed where its functionalities are entirely implemented on Android devices instead of an off-line processing as

in Chapter 5. The proposed S2SVLC system evaluated in this chapter offers inherent advantages in terms of portability and simplicity of implementation as it does not require any hardware modifications on the devices used. Before proceeding with the system's evaluation, an initial experimental work is reported in order to characterize the devices used, such as the screen's rise and fall times.

6.2 System flowchart

The system flowchart is depicted in Figure 5.1. First the receiving camera captures all the transmitted frames. The captured frames are saved on the Rx memory. Then, the Tx's location is calculated for the first time, using the first dark frame detected by the Rx. A frame subtraction is applied to every two pair of consecutive frames. The resulting frame is then converted to a binary image, and the number of white pixels is calculated and compared to a threshold determined empirically. If both those frames are bright, the number of white pixels is low. If the pair of frames used represent a dark frame and a bright frame, this number is high.

When a dark frame is calculated, the system executes the remaining step described in Chapter 4. In other words, a Canny edge operator and a Hough transform are applied to the binary image resulting from the frame subtraction. The Tx's edges are then determined and the Tx's location is then calculated. The Tx location is used to apply the perspective correction on the received frames for reconstruction purposes. The final step consists of the bit extraction, which is simply the extraction of the data contained in the received frames. This step is explained in the following section.

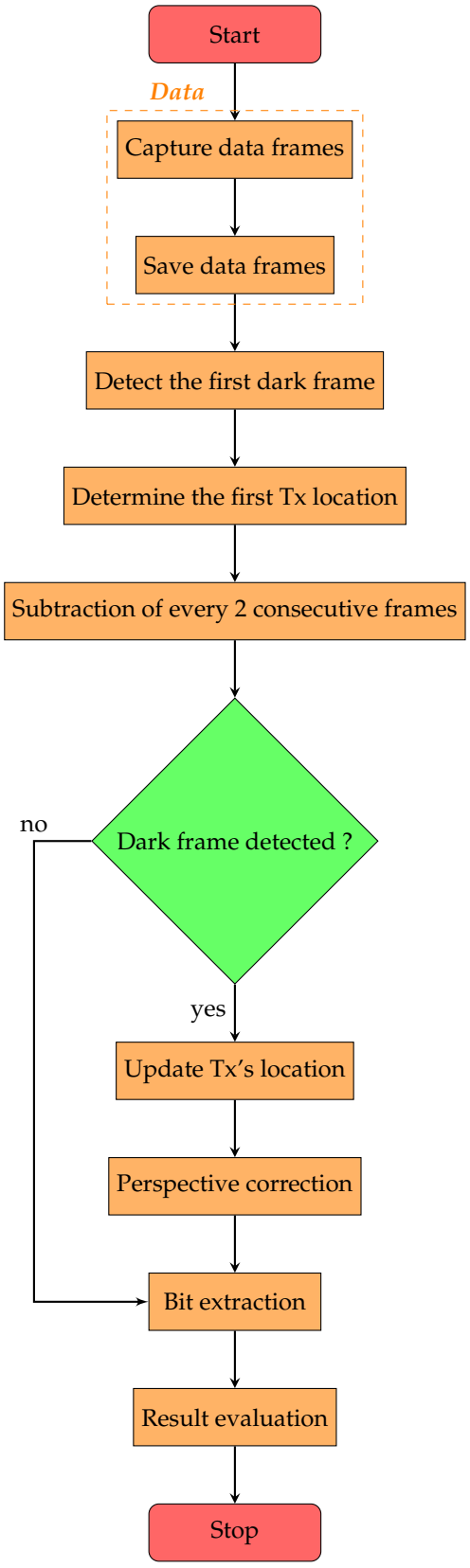

Figure. 6.1 System flowchart

6.3 Bit extraction

Figure 6.2 illustrates the Tx's mobility within the Rx's FOV.

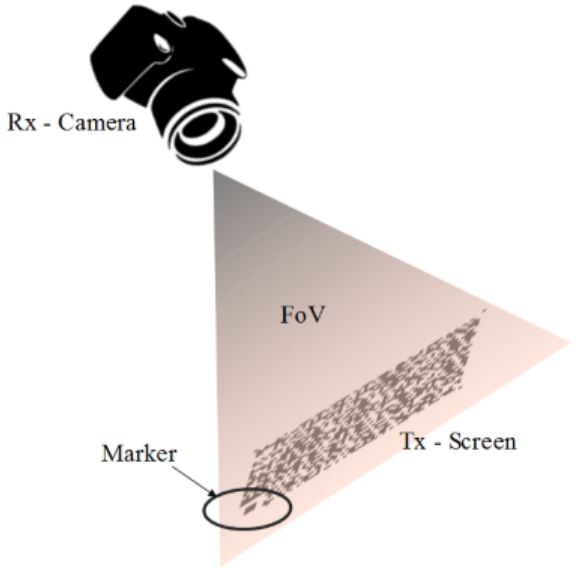

Figure. 6.2 Tx and Rx rotation

The order in which the lines and corners are extracted is unpredictable, and depends essentially on the detected lines strength. Therefore, data extraction requires an additional step in order to determine the starting point of the extraction. The proposed system is designed to adapt to high mobility including rotations around the three axes. Therefore, when the captured screen is reconstructed, it can be in any one of the four directions represented in Figure 6.3. Hence, a specific marker known by both sides of the communication link is added to the displayed frame on the transmitting side.

Unlike the QR code extraction technique [142] and Cobra detection method [102], the marker is only used after the Tx detection and corner extraction, to help with the recovery of the transmitted bits.

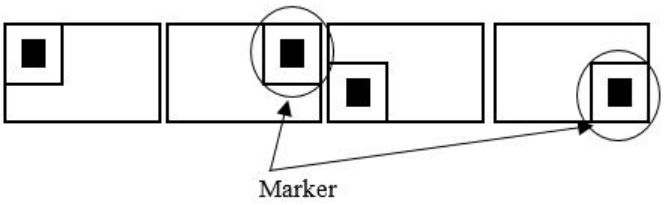

Figure. 6.3 Tx and Rx rotation

6.4 Experimental set up

6.4.1 Device characterization / Screen rise and fall times

Before any further investigation on the smartphone to smartphone communication system, the device electrical and lighting characterization is required. In this section, experimental tests on the transmitting screen performances are presented. Using a lux meter, the illumination of a Samsung Galaxy S3 is measured order to determine the screen's illumination rise and fall times when it flashes on and off (see Figure 6.4).

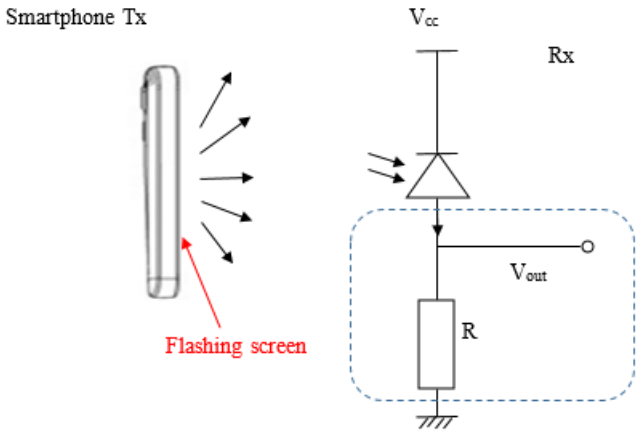

Figure. 6.4 Smartphone screen illumination measurement set up

In other words, when the screen toggles between a low level brightness, B_L, and a high brightness level, B_H, and vice versa, and these transitions require an execution time. During this experimental test, the Tx screen changes the brightness

continuously. The emitted signal, when the screen flashes, can be modeled with a square wave signal. In practice, we measured the rise time of the flashing screen at different brightness levels (from 20% to 100%), using a photodiode as shown in Figure 6.4. The results obtained for 20%, 60% and 100 are depicted in Table 6.1 showing that even if the rise times for all the cases are very close, the transition is more visible when the brightness is higher. For instance, in Table 6.1 (a), B_H = 100%, the brightness decreases from B_H to a transitive state, where the photodiode response is twice higher than the minimum brightness level (0.01 mV and 0.005mV respectively) yielding in a screen fall time of 0.02 s. However, when B_H = 20%, the brightness changes smoothly between B_H and B_L and the screen fall time is insignificant.

6.4.2 Flashing screen measurements

Initially, an investigation focusing on two detection parameters is carried out: the high brightness level of the flashing screen and the transitions appearing in the captured images resulting from the screen rise time. The duration of the dark frame is also investigated. The determination of these parameters is necessary for the continuation of the work. The results obtained are presented in this section. The proposed system is implemented using Android Studio. The Rx application converts a text into a frame and displays it on the screen, which is flashing. Note that the Rx was implemented using Android Studio and OpenCV library. This application allows the user to start the data acquisition and to stop it using a push button. The frames are saved for further processing (detection) and data recovery. In order to achieve a high detection rate both B_L and B_H are different. In the first experimental test carried out, we measure the detection rate while varying the Tx's screen brightness from 10% to 100% of the maximum for 4 different transmission spans of 10,

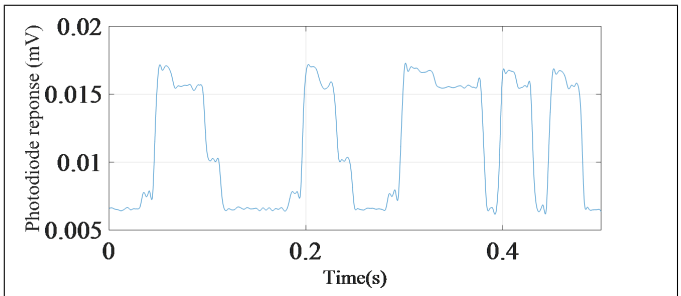

(a) (10-100%)

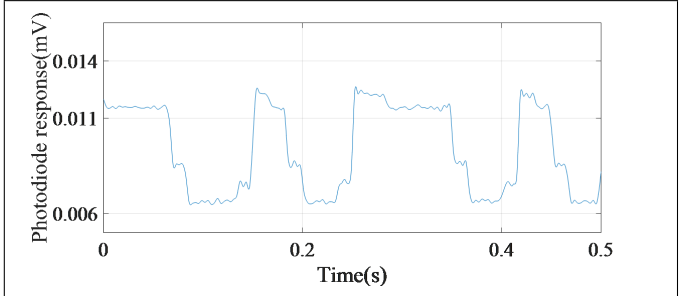

(b) (10-60%)

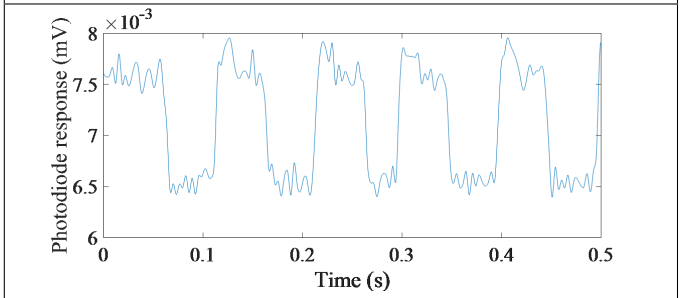

(c) (10-20%)

Table 6.1 Screen brightness variations (a) 10-100%, (b) 10-60% and (c) 10- 20% brightness

Parameter	Value
Tx	Samsung S3
Maximum brightness	224 Candela [3]
B_L	10%
Rx	LG G3
Camera frame rate (Rc)	11 frames/second
Dark frame duration (Tb)	110ms
Bright frames duration (Td)	890ms
Cell colours	Black/White
Number of cells per frame	1500

Table 6.2 Hardware implementation informaton

20, 30 and 40 cm. Table 6.2 shows the key parameters adopted in the experimental work.

The results obtained are depicted in Figure 6.5. As expected, for low values of B_H (i.e., 20 or 30%) the detection is almost impossible as the difference between B_H and B_L is extremely low. However, for B_H = 50% or higher the detection rate is extremely high for all distances reaching 100%. Moreover, for B_H = 40% the detection rate reaches 100% only for the distance d = 10cm. However, the detection rate decreases with the distance reaching only 43% at a distance of 40 cm. These results show that in order to detect the Tx an image flashing between 10 and 50% for the distance < 40 cm is sufficient. A higher level of B_H would lead to the energy wastage without achieving significant performance improvement. For instance in Figure **??** (a) and for B_H = 100% the brightness decreases from B_H to a transitive state, where the photodiode response level is twice that of the minimum brightness levels of 0.01 mV and 0.005mV. However, for B_H = 20%, the brightness changes smoothly between B_H and B_L. In order to evaluate the transition appearance during the communications, we performed several image acquisitions while varying B_H from 40 to 100%, as the detection outside this range is nearly impossible (see Figure 6.5). Ten acquisitions of 20 seconds (20 cycles) per a B_H value were per-

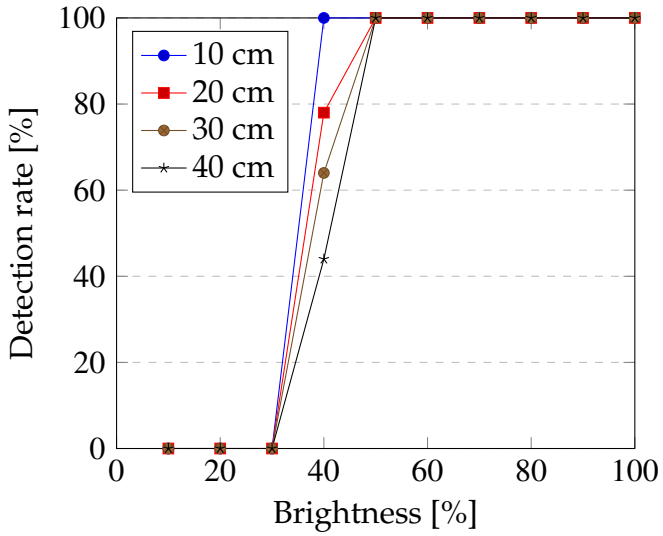

Figure. 6.5 Detection rate against the the Tx brightness for a range of transmission distances

formed, and the number of transition free images was calculated ($\Delta F_D = 0$), which are presented in Figure 6.6. The number of transition free transmissions decreases when the brightness level increases, which is consistent with the previously shown results in Chapter 3 where the device characterization is presented. However, the number of transitions is low and it has little effect on the transmission.

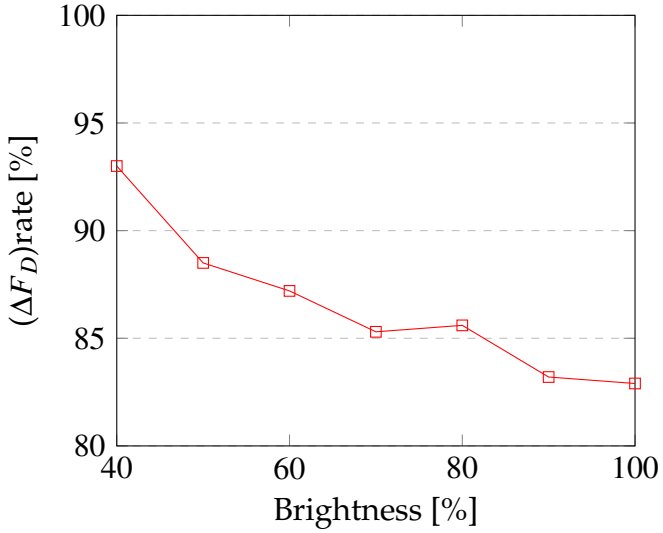

Figure. 6.6 Transition free dark frame transmissions when varying the Tx

6.4.3 Software development

The system presented in this chapter is implemented on Android platform. On the Tx, a mobile application is developed where the user can enter a text to transmit it. The text is then converted to a binary stream, and every single bit is converted to a cell (black if the bit equals 0 and white if not). A bitmap is then formed using the cells and is displayed on the screen, see Figure 6.7.

Figure. 6.7 Transmitting application interface

Whilst displaying the data frame, the application also makes the screen flash, by increasing and decreasing the screen's brightness constantly. On the Rx, a mobile application is developed where the user can start and stop capturing frames. The received frames are then processed one by one, where the Tx's location is updated every time a dark frame is received. Table 6.3 outlines information about the software development.

Parameter	Value
Tx OS version	Android Jelly bean 4.3
Rx OS version	Android Marshmallow 6.0
Graphic library	Open CV 2.4
Integrated Developing environment	Android studio 1.2.1

Table 6.3 Software development information

6.4.4 Investigated parameters

Three scenarios can be investigated in this experimental setup in order to evaluate the system's performance in a dynamic environment. In the first scenario (which is also the most promising case) all the transmitted frames are different, and they are updated at the camera rate, see Figure 4.16. In the second scenario, the data displayed on the transmitting screen is updated every time the screen flashes. In other words, a dark frame F_D is displayed followed by n number similar bright frames. Then, another dark frame F_D is displayed followed by a new bright frame. Both cases 1 and 2 require a screen refreshing time to update the data displayed on the screen. Given that this parameter is not considered in this scheme as the investigation will focus mainly on the post-processing operated by the Rx, the simplest case was implemented on the Tx, where all the transmitted frames F_n are identical. Several parameters, presented in Figure 6.8, were investigated in this paper in order to evaluate the system's performance. These parameters include the distance d between the Tx and the Rx, the rotation angle θ, the tilting angle α as well as the Tx's translation within the Rx FOV.

Table 6.4 represents the parameters used in the experimental work. In [143], an investigation focused on two detection parameters was carried out: the high brightness level of the flashing screen and the transitions appearing in the captured images resulting from the screen rise time. Whilst displaying the data frame, the application also makes the screen flash, by increasing and decreasing the screen's

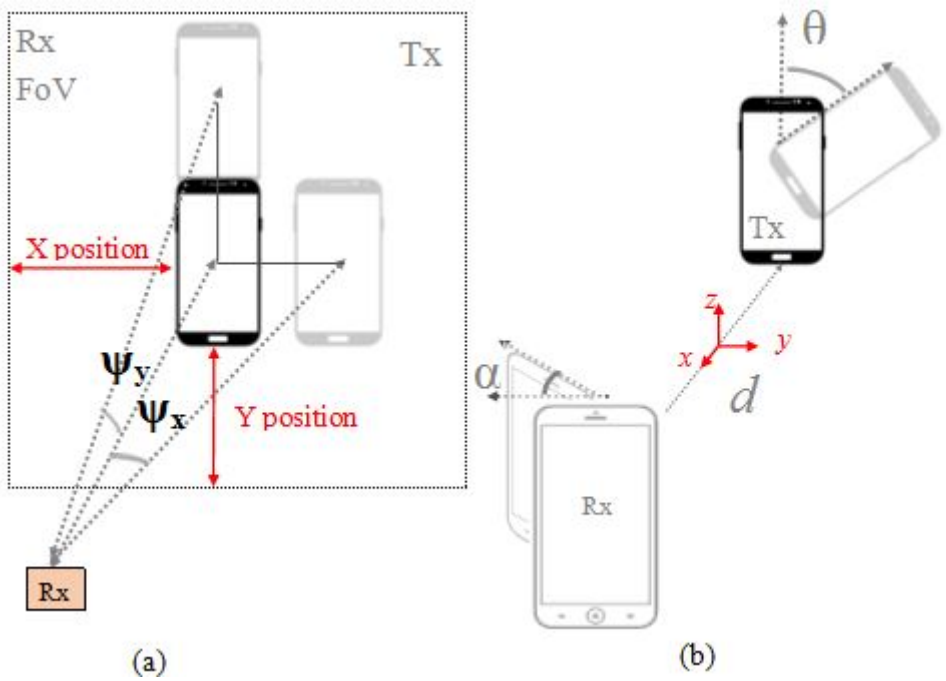

Figure. 6.8 Investigated parameters

brightness constantly. The flashing screen requires a rise time when it flashes between B_L and B_H on the Tx. This screen rise time is measured using a photodiode when B_H= 50% of the maximum brightness. It is represented in Figure 6.4.

The duration of the dark frame was also investigated and the optimal parameters are used in the work presented here. The cell size used in this scheme is also presented in the table. The cell area is given in mm^2 as the number of pixels in one cell has no effect on the system whereas the cell size does.

	Parameter	**Value**
Channel configuration	Distance (d) Rotation angle θ Tilting angle α	12 cm to 51 cm 0° to 180° -90° to 90°
Tx	Device B_L B_H	1280x720 (Samfsung Galaxy SIII) 200 ms 800 ms
Rx	Device Data rate Cell size	13 Megapixel (LG G3) 2048 bit/frame 2.8 mm^2

Table 6.4 Experimental parameters

6.5 Results and discussions

6.5.1 Distance

The first parameter to be investigated is the effect of the distance d (see Figure 6.8) between the Tx and the Rx on the system's performance. The other experimental parameters were fixed throughout the distance range (θ = 0 °, α = 0°, cell size = 2.8 mm^2) while d varies. The initial distance value is d = 12 cm. Figure 6.9 shows the bit success rate (BSR) against the distance d. Within the range [12 cm, 34 cm] the BSR is highly promising as it remains between 93 and 100%. In the range [34 cm, 45 cm], the BSR drops below 90% but remains reasonable as above 80%. The experiment final distance investigated was 52cm as the BSR drops below 80% and is no longer acceptable, given that the transmitted cells are either black or white, and two different images can present a BSR of 50%.

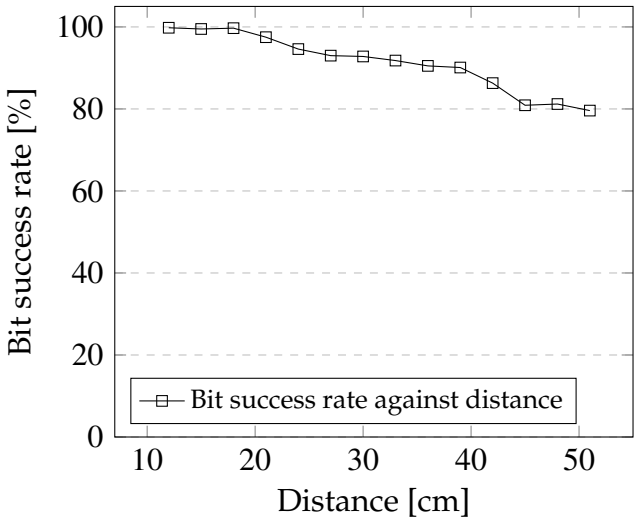

Figure. 6.9 System performance against distance

6.5.2 Translation

The second experiment to be carried out is the Tx translation within the Rx FOV. The FOV was sampled into a number of X and Y positions. Again, the only parameter that varies is the position of the Tx within the Rx FOV. The other parameters remain constant throughout the experiment (θ = 0 °, α = 0°, cell size = 2.8 mm^2, d = 28 cm). The Tx X position varies between 10 and 85% of the FOV width, and the Y position varies between 10 and 85% of the FOV height. Although the higher BSR was obtained at distances lower than d = 28 cm, this distance allowed the FOV to obtain more samples from the FOV, thus evaluating more positions.

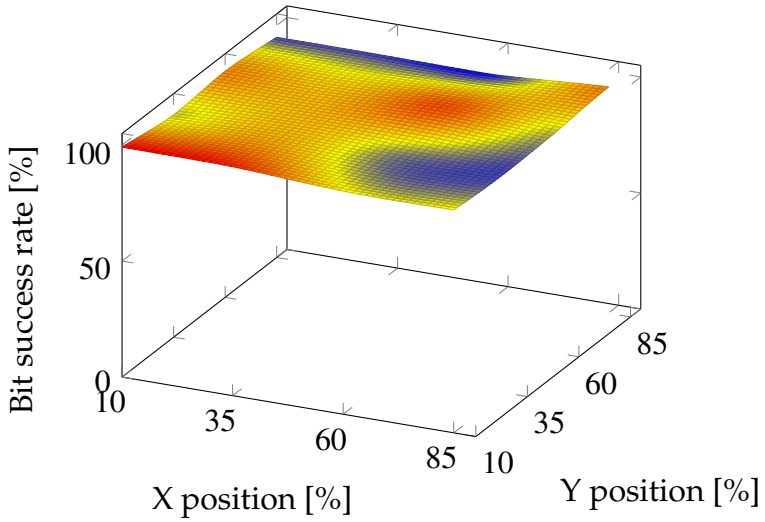

Figure. 6.10 System performance against translation

The results are presented in Figure 6.10. The BSR remains relatively flat as it varies between 92 and 96% data recovery, demonstrating that the system performance is invariant to the Tx translation within the Rx FOV.

6.5.3 Rotation

indent The next experiment is related to the rotation angle θ. Both the Tx and the Rx are in a parallel position, but the Tx is rotated around the z-axis, see Figure 4.13. The angle θ is varied within the range [0°,180°], whilst the other parameters are fixed (α = 0°, cell size = 2.8 mm^2, d = 18 cm). The results are depicted in Figure 6.11. Once again, the BSR remains reasonably stable and reaches up to 100% data recovery, showing that the system is robust to parallel rotation.

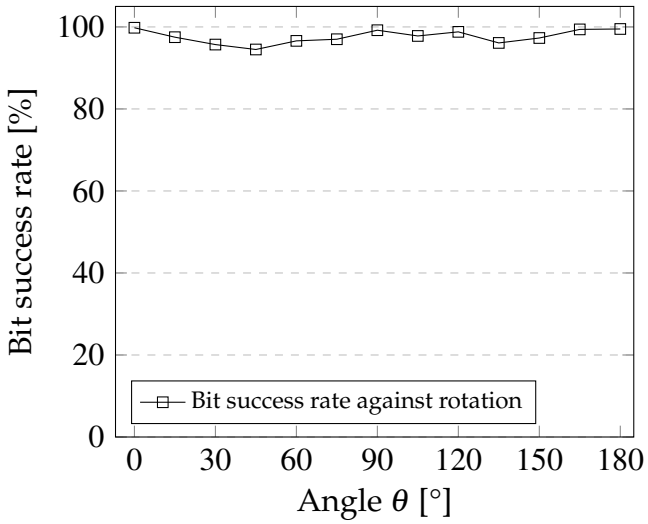

Figure. 6.11 System performance against rotation

6.5.4 Tilting

Another geometric experiment is carried out, investigating the effect of the tilting angle α (see Figure 6.8) on the system performance. The angle α is varied within the range [-60°, +60°] whilst the other parameters remain the same (θ = 0 °, cell size = 2.8 mm^2, d = 21 cm). The results are depicted in Figure 6.12.

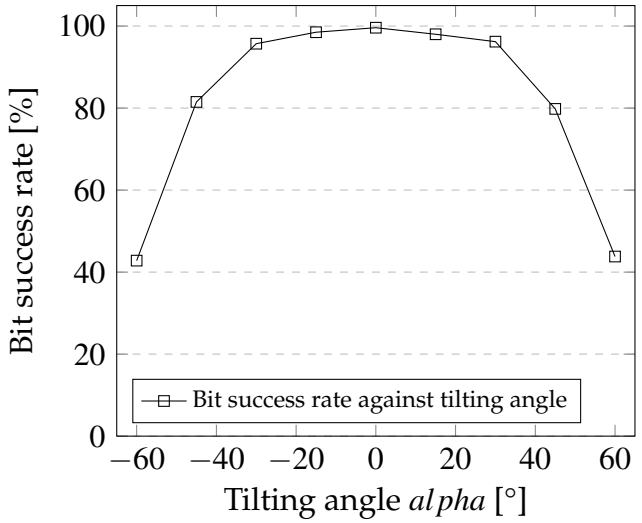

Figure. 6.12 System performance against tilting

The BSR obtained when α varies between -30° and +30° is fairly high and above

95% data recovery. However, outside the [-30°, 30°] range, the BSR decreases dramatically to 80% at -45 and +45°, and below 50% at -60 and +60°.

6.5.5 Cell size

The final parameters investigated in this paper, is the cell size. By decreasing the cell size, the total number of cells transmitted per frame increases. Three cell sizes are used: 2.80 mm^2, 0.70 mm^2 and 0.17 mm^2, over three distances: 12 cm, 22 cm and 32 cm. The other experimental parameters remain constant (θ = 0 °, α = 0°). Overall, the BSR decreases with the distance, and drops from above 90% to approximately 85% for the three different sizes, demonstrating that a reasonable BSR can be achieved at a lower cell size, thus transmitting more data per frame. Nevertheless, the BSR decreases to 70% for the 2.8 mm^2 size and the 0.7 mm^2 size, and to below 60% for the 0.17 mm^2, which is no longer acceptable.

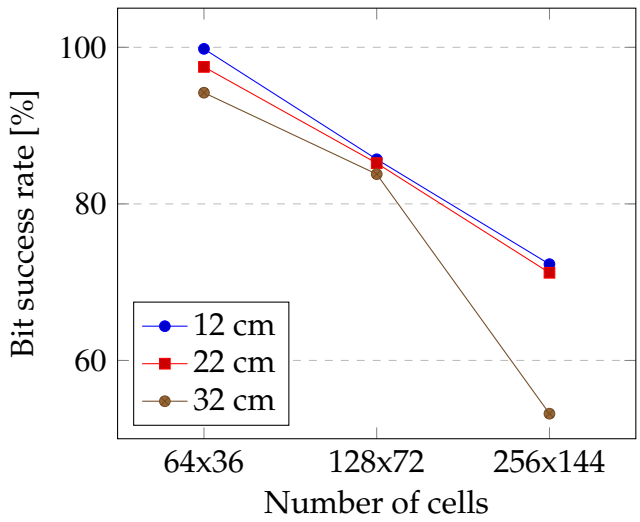

Figure. 6.13 System performance against the number of cells transmitted

Cell size	COBRA	S2SVLC
15 to 20	Nearly 100%	Nearly 100%
10 to 15	Nearly 100%	Nearly 100%
5 to 10	50%	94%

Table 6.5 S2SVLC and COBRA cell size comparison

6.6 S2SVLC and COBRA

In This section, S2SVLC and COBRA [102] are compared. Among the similar works cited in the literature review, COBRA is the system that resembles most S2SVLC, as it implements a communication link between two smartphones over short distances, and similar parameters are investigated (cell size, rotation angle, tilting angle, distance etc.). In order to compare these two systems, results were extracted from Hao2012, and the key observations are summed up in the following sections.

6.6.1 Cell size result comparison

Table 6.5 depicts the comparison of COBRA and S2SVLC performances against block size. Note that block size in this scenario refers to the size in pixels of one side of the squared cell, used to transmit the data. When the block size decreases while the camera resolution remains constant, its extraction becomes harder which affects the system's performance. Although the performance of both systems is similar and extremely high when the block size varies between 10 to 20 pixels, the Cobra bit success rate drops drastically when the block size decreases to below 10. On the other hand, S2SVLC's performance remains high and 94% of the data is correctly recovered at a block size of 5 pixels.

Rotation angle	COBRA	S2SVLC
30°	Nearly 100%	Nearly 100%
45°	Nearly 100%	Nearly 100%
60°	Nearly 100%	Nearly 100%
90°	Nearly 100%	Nearly 100%

Table 6.6 S2SVLC and COBRA rotation angle result comparison

6.6.2 Tilting angle

In terms of tilting angle, the COBRA system shows the better performance, as the bit success rate remains extremely high between 15 and 75° tilting angle, and when the block size varies between 12 and 15 pixels. The performance drops when the block size decreases below 11 pixels. The S2SVLC system however shows a high bit success rate only between 15 and 35° tilting angle.

6.6.3 Rotation angle

The performance comparison of both systems in terms of rotation angle is summarized in the Table6.6. The rotation angle has a negligible effect on both systems and the bit success rate remains extremely high in both cases.

6.6.4 Distance and throughput

The COBRA system achieves the highest throughput (around 90kbps) over a distance of 12 cm with 10-pixel sized cells. The system throughput decreases (lower than 90 kbps) as when either the block size or the distance increase. However, S2SVLC achieves similar data rate performing over longer distances (up to 50 cm) and using only black and white cells. S2SVLC could potentially achieve three times the current data rate by replacing the black and white cells with coloured cells of 8 different colours (Red, green, blue, black, white, cyan, yellow, magenta), where

each cell would represent three bits instead of one single bit.

6.7 Summary

This chapter presented the design and implementation of an S2SVLC system, where the transmitting smartphone screen was used to display data, and the receiving smartphone camera was used for data recovery. The data is encoded into black and white images that are displayed on a flashing screen, and a frame subtraction on the Rx allows an accurate detection of the Tx before recovering the data. In the previous chapter, the SURF-based S2SVLC was investigated and evaluated. However, in this chapter, the detection method was modified as the SURF algorithm is over-complex for this scheme. Therefore, the modifications made aimed to reduce the complexity of the S2SVLC system. The new method relied on techniques used in chapter 5 for path loss, inter-symbol interference and perspective distortions, among them a geometric transformation and a quantization process. A section reporting the device (smartphone) characterization, which included the screen's rise and fall times was first exposed.The system was then evaluated and the results obtained showed reasonable performance, demonstrating a promising system for short range smartphone to smartphone communications. The proposed system can potentially offer a high capacity as one could use the transmission of RGB-colored images instead of solely black and white coloured images. The system's performance is tested and evaluated under different mobility conditions such as the link distance between the Tx and the Rx, the capacity by varying the total number of transmitted cells in each frame as well as the rotations of both the Tx and the Rx devices. Practically, S2SVLC offers a range of new features with a 90° FOV and a reasonable distance range for short range communications (12 to 51 cm). Additionally, the flashing screen facilitated the portability compared to the previous chapter where a detection frame was

needed, and the algorithm can be combined with standard compression techniques and error correction, for data rate enhancement.

Chapter 7

Conclusions and Future Works

7.1 Conclusions

The main objective of studying S2SVLC is to harness the potential of using existing personal communication devices for short range communications, thus offering a complementary communication system to the already saturated RF technology spectrum. The research reported in this thesis relies on this fundamental objective by investigating an image processing based screen to camera communication system, using mainstream smartphone screens and cameras.

S2SVLC is the result of the combination of various basic concepts. It includes fundamental notions of OWC and VLC more specifically, as well as smartphone technology and image processing and computer vision. All these concepts have been introduced in Chapter 2 to facilitate the reader's understanding, commencing with an overview of the progress of RF technology, the birth of wireless communications as well as the basic principles of VLC. The smartphone technology is also presented, starting with a brief telephone history, and exposing the features found in available smartphones that are relevant to S2SVLC as well as the existing smartphone operating systems. This chapter also introduces the reader to the

fundamentals of images processing, including the definition of a pixel and a digital image. It presents digital cameras by highlighting their most important parameters. Finally, Chapter 2 gradually exposes fundamentals of image processing and computer vision, while giving notions on colour spaces, different noises present on digital images. Note that one of the main focuses of this work is the detection of the Tx by the Rx, and therefore, object detection challenges are also explained.

Following the general overview of the fundamental concepts forming S2SVLC, Chapter 3 explained how the tools exposed in Chapter 2 were linked together in order to create camera communications. It overviewed the most remarkable works that took advantage of existing cameras in order to create communication systems, relying on either a light source or an LCD screen for transmission. The chapter also gives several benefits and motivations in the investigation of this system, such as using the widely spread cheap light sources as well as the broadly exploited cameras and screens available in personal devices to transmit thousands of bits in one frame. It also explains that S2SVLC can be easily implemented as its development is purely software based. Moreover, challenges of S2SVLC are also enumerated outlining the most investigated: mobility and real time processing. Additionally, some practical work was carried out in order to characterize the main device used in this work, which is the smartphone. The rise and fall times of the screen are measured and represented. Furthermore, the free-space channel attenuates the signal due to many parameters, including the distance and the Tx's rotation. This attenuation is explained theoretically in the final section of this chapter.

S2SVLC is a communication system and compromises therefore the fundamentals of standard communication systems, such as the signal modulation. Chapter 4 outlines some of the most utilized modulation schemes in VLC. It also links the regular modulation step in communication system block diagrams to the signal mod-

ulation in S2SVLC, where every single bit is converted to a cell, black or white, and all these cells form an image to be transmitted through the smartphone's screen. Then, as stated earlier, the main challenge in the S2SVLC development is the Tx's detection by the Rx's camera. In this thesis, two different methods were investigated. The first one was based on a feature extraction and description algorithm, SURF, which was used to detect a detection frame known by both sides of the communication. The theory behind the SURF algorithm is thoroughly explained. The second method used for the Tx's detection is based on the flashing screen during data transmission. Then, multiple image processing tools are applied to the received frames in order to detect the Tx. These tools (frame subtraction, Canny edge detector and Hough transform) are also exposed in details. The next objective of this thesis is to reconstruct the received frame by correcting the perspective and recover the data. The data recovery process is finally exposed in this chapter, including the perspective correction method which is based on a geometric transformation, as well as the image binarization process which included two options, a hard thresholding method and a soft thesrholding method (Otsu). Finally, a quantization step for cell reconstruction was also added.

The first detection method based on the Speeded Up Robust Feature (SURF) extractor and descriptor is investigated in Chapter 5, and the experimental work is carried out in order to evaluate the system's performance. The algorithm exposed in Chapter 4, section 3, is implemented on Matlab. A random binary stream equally distributed between zeros and ones is generated, and an image is created on Matlab before it is transferred on the transmitting smartphone. The space around the Rx was then sampled in order to recreate several dynamic scenarios including the Tx's rotation and tilting, as well as the variations in the link length and the number of cells transmitted within one frame. The data was collected using three cameras, a

smartphone's back and front cameras as well as a high quality camera for reference. The bit success rate was measured off-line on Matlab. Early results are exposed in the chapter, where the achievability of the system was tested. The rotation of the Tx was limited to [-20°,20°] and tilting angle was null. However, the algorithm was improved as the perspective correction process and the quantization for cell reconstruction were added. Therefore, up to 100% data was recovered through all the rotation interval [0°,360°] using both the reference camera and the smartphone's back camera, the link length reached 70cm using the back camera and 110cm using the reference camera, and the tilting angle was widened to [-50°, +50°] with a reasonable bit success rate.

The ultimate objective of this thesis is to implement the proposed system on a mobile platform, for real time data transmission and reception. The mobile platform used was Android, and the second detection method based on the flashing screen was implemented. This method added more portability to the system as it does not require a pre-known detection frame. On the transmitting side, a mobile application was developed with a user interface that allows to enter a text, which is then used to create an image. The image was displayed on a flashing screen. On the receiving end, the application developed offers the user to start and stop capturing data. The received images are stored and processed after the image acquisition is finished. The frame subtraction, Canny edge detector and Hough transform are applied to the received frames and the data is extracted. As was the case in Chapter 5, the system's implementation on Android was tested and evaluated, with various rotation and tilting angles, distances, and rates per frame. In terms of tilting angle, the bit success rate obtained between [-45°,45°] was acceptable, offering thus a 90° field of view to the Rx. Similar results to Chapter 5 were obtained for the rotation angle, as the bit success rate remained flat throughout the rotation interval

[0°,180°]. The translation within the Rx's field of view was also tested and proved to have no effect on the bit success rate. The distance tested in this scheme varied between 12 and 51 cm, and the channel capacity was evaluated using different cell sizes and distances.

7.2 Future Works

This research work has completed the main objective listed in Chapter 1, which is the implementation of a S2SVLC system on Android platform. However, the amount of time and work required to complete the system's development to its full potential is out of the scope of this work. The following topics are suggested to extend research work reported in this thesis.

Synchronisation

In theory, the most optimal case scenario in screen to camera communication is when a perfect synchronization is achieved:

- Transmitting screen refreshes the displayed data at a rate R_t.
- The receiving camera captures the data at a rate R_r and $R_t = R_r$.

However, the Tx's screen is required to flash for accurate detection purposes, and as shown in 'rise/fall time' experiment, section 3.5, some frames are lost as the threshold set for dark frame detection. Moreover, in order to update the frame displayed on the transmitting screen, a refreshing time is required. Therefore, some frames captured by the camera will contain a combination of two consecutive frames and two combinations may occur [103]:

- The captured frame contains the top of the current from and the bottom of the previous frame.

- The captured frame contains a linear combination of two consecutive frames as the shutter is open for a laps of time sufficient to capture light from the previous and the current frame.

In order to use the system's potential fully, work on the synchronization between the Tx and the Rx is necessary.

Reaching the full potential by and updating data frames at the same rate as the camera acquisition rate is practically unachievable. However, if some experimental work is carried out in this direction, the synchronization limitations can be determined as well as the practical refreshing rate. These results would allow the development of a fully functioning S2SVLC where a real file can be decoded and encoded into images to be transmitted through the S2SVLC channel.

Adaptive threshold for dark frames detection

The transmitting screen flashes for accurate detection purposes. On the receiving side, the algorithm is required to process the incoming frames, and detect the dark frames in order to update the calculated Tx's location on the received frames. Before making the decision on whether the treated frame is dark or bright, the frame subtraction is performed. The resulting frame is then binarized on the amount of white pixels contained in this frame is calculated. If the subtraction is performed between a dark frame and a bright frame, the number of white pixels on the obtained frame is high. It is low if the frames used for subtraction are both bright, or either one of them is not fully dark/bright. Currently, an empirical thresholding value is used to select the cases where a dark frame is followed by a bright frame and vice versa, and reject the other cases. This threshold depends mainly on the distance between the Tx and the Rx, or in other words, it depends on the size of the transmitting screen as seen by the receiving camera. For future work, it would be beneficial to implement a method for adaptive threshold selection. One option can

be suggested, which involves the calculation of all the subtraction frames and their corresponding number of white pixels, and select the highest values over the whole ranges of acquired images. This method would include a thresholding step again. However, the received frames are processed as a package, rather than individually, which provides more information on the distance/screen size, and the threshold selection would be achieved according to this additional information.

Shaking hand

The S2SVLC system is designed for mobile devices communications. Consequently, in a real scenario the users should be able to hold their personal device during the data transmission. Given that the Tx's detection on the received frames depends on two consecutive frames for frame subtraction, a shaking hand holding either the Tx or the Rx would result in a loss in terms of accuracy during the Tx's detection. In order to overcome this problem, 4 additional markers in the shape of a black square were added to the transmitted frames (see Figure 7.1 (a)) , in order to increase the system tolerance to handshaking. Figure 7.1 represents two reconstructed data frames, with a good reconstruction (a) and a less accurate reconstruction in (b). A rapid scanning through the reconstructed image corners permits the detection of the white border, and a similar process is then applied to detect the four markers before the bit extraction. The detection of the markers was developed and implemented on Android platform. However, the mathematical modelling and the practical evaluation of this message have not been achieved yet.

RGB / greyscale images

In order to increase the channel capacity, one of the options is to use coloured or greyscale images for data transmission. Using greyscale images would offer an 8 bit/ cell transmission rate on a 2-D matrix as every grey level is represented by a number between 0 and 255. Given that in Chapter 6 a 100 kbps transmission

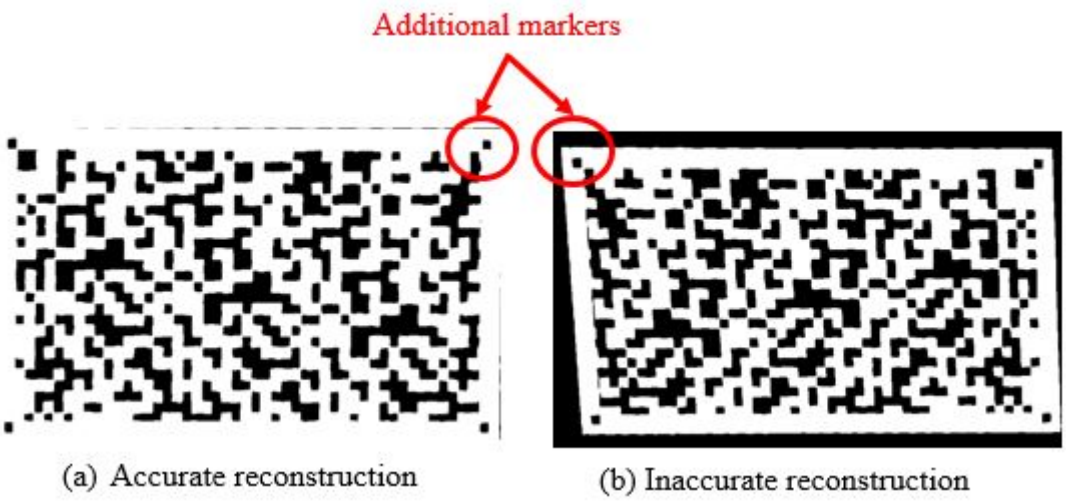

Figure. 7.1 Additional markers against shaking hands

link using black and white images was shown, 8 times the black/white capacity. Moreover, using coloured cells for transmission would allow to convey information over a 3-D matrix where each cell is encoded using three components: red, green and blue. This case would offer even more capacity potential as it would transmit 3 times the data transmitted over the greyscale images.

Extend to more screens and devices

Currently, the only existing implementation of this system is on Android. However, Chapter 6 showed the system's implementation simplicity, portability and flexibility. Therefore, the system can be extended to other mobile platforms such as iOS, as well as other devices such as tablets, or available screens and cameras in public places such as museums and libraries, checkout machines in supermarkets etc.

References

[1] F. Goes, "Chapter-02 anatomy of the human eye," *The Eye in History*, p. 14–24, 2013.

[2] M. K. Mandal, *The Human Visual System and Perception*, pp. 33–56. Boston, MA: Springer US, 2003.

[3] M. Tovée, *An Introduction to the Visual System*. Cambridge University Press, 1996.

[4] A. H. Sakr and E. Hossain, "Analysis of k -tier uplink cellular networks with ambient rf energy harvesting," *IEEE Journal on Selected Areas in Communications*, vol. 33, pp. 2226–2238, Oct 2015.

[5] C. Dehos, J. L. González, A. D. Domenico, D. Kténas, and L. Dussopt, "Millimeter-wave access and backhauling: the solution to the exponential data traffic increase in 5g mobile communications systems?," *IEEE Communications Magazine*, vol. 52, pp. 88–95, September 2014.

[6] T. Hirano, K. Miyazaki, M. Hatamoto, R. Yasumitsu, K. Hama, and F. Watanabe, "Rf-mems for reconfigurable satellite antenna," in *The Second European Conference on Antennas and Propagation, EuCAP 2007*, pp. 1–5, Nov 2007.

[7] "Rf spectrum policy: Future-proof wireless investment through better compliance."

[8] "Valuing the use of spectrum in the eu," Jun 2016.

[9] W. Yuanquan and C. Nan, "A high-speed bi-directional visible light communication system based on rgb-led," *China Communications*, vol. 11, pp. 40–44, March 2014.

[10] H. Marshoud, P. C. Sofotasios, S. Muhaidat, and G. K. Karagiannidis, "Multiuser techniques in visible light communications: A survey," in *2016 International Conference on Advanced Communication Systems and Information Security (ACOSIS)*, pp. 1–6, Oct 2016.

[11] S. Hojo, M. Tokiya, M. Mizuki, M. Miyata, K. T. Kanatani, A. Takagi, N. Tsurikisawa, S. Kame, T. Katoh, T. Tsujiuchi, and H. Kumano, "Development and evaluation of an electromagnetic hypersensitivity questionnaire for japanese people," *Bioelectromagnetics*, vol. 37, no. 6, pp. 353–372, 2016.

[12] L. Kheifets, M. Repacholi, R. Saunders, and E. van Deventer, "The sensitivity of children to electromagnetic fields," *Pediatrics*, vol. 116, no. 2, pp. e303–e313, 2005.

[13] J. C. Lin, "Hypersensitivity responses in humans to electromagnetic fields [health effects]," *IEEE Microwave Magazine*, vol. 14, pp. 30–32, Nov 2013.

[14] N. Cvijetic, D. Qian, J. Yu, Y. K. Huang, and T. Wang, "100 gb/s per-channel free-space optical transmission with coherent detection and mimo processing," in *2009 35th European Conference on Optical Communication*, pp. 1–2, Sept 2009.

[15] T. Song, K. Wang, A. Nirmalathas, T. Liang, E. Wong, and J. Ma, "High-speed optical wireless personal area communication system supporting multiple users," in *2016 IEEE Photonics Conference (IPC)*, pp. 297–298, Oct 2016.

[16] A. Mahdy and J. S. Deogun, "Wireless optical communications: a survey," in *2004 IEEE Wireless Communications and Networking Conference (IEEE Cat. No.04TH8733)*, vol. 4, pp. 2399–2404 Vol.4, March 2004.

[17] Y. Ito, "A new paradigm in optical communications and networks," *IEEE Communications Magazine*, vol. 51, pp. 24–26, March 2013.

[18] G. Wellbrock, T. Wang, and O. Ishida, "New paradigms in optical communications and networks," *IEEE Communications Magazine*, vol. 51, pp. 22–23, March 2013.

[19] D. Kedar and S. Arnon, "Urban optical wireless communication networks: the main challenges and possible solutions," *IEEE Communications Magazine*, vol. 42, pp. S2–S7, May 2004.

[20] R. Paudel, Z. Ghassemlooy, H. Le-Minh, S. Rajbhandari, and B. Livingstone, "Investigation of fso ground-to-train communications in a laboratory environment," in *2011 Second Asian Himalayas International Conference on Internet (AH-ICI)*, Nov 2011.

[21] R. Srinivasan, B. Sriharipprasath, N. Vairamoorthy, K. Baskaran, and K. Kumaravel, "The reliable last mile communication over wireless optical networks in different climate situations - retracted," in *International Conference on Sustainable Energy and Intelligent Systems (SEISCON 2011)*, pp. 610–615, July 2011.

[22] Z. Qu and I. B. Djordjevic, "Approaching terabit optical transmission over strong atmospheric turbulence channels," in *2016 18th International Conference on Transparent Optical Networks (ICTON)*, pp. 1–5, July 2016.

[23] H. Huang, G. Xie, Y. Yan, N. Ahmed, Y. Ren, Y. Yue, D. Rogawski, M. J. Willner, B. I. Erkmen, K. M. Birnbaum, S. J. Dolinar, M. P. J. Lavery, M. J. Padgett, M. Tur, and A. E. Willner, "100 tbit/s free-space data link enabled by three-dimensional multiplexing of orbital angular momentum, polarization, and wavelength," *Opt. Lett.*, vol. 39, pp. 197–200, Jan 2014.

[24] X. Liang, F. Hu, Y. Yan, and S. Lucyszyn, "Link budget analysis for secure thermal infrared communications using engineered blackbody radiation," in *2014 XXXIth URSI General Assembly and Scientific Symposium (URSI GASS)*, pp. 1–3, Aug 2014.

[25] D. R. Wisely, "A 1 gbit/s optical wireless tracked architecture for atm delivery," in *IEE Colloquium on Optical Free Space Communication Links*, pp. 14/1–14/7, Feb 1996.

[26] S. Jia, X. Yu, H. Hu, J. Yu, T. Morioka, P. U. Jepsen, and L. K. Oxenlawe, "Experimental analysis of thz receiver performance in 80 gbit/s communication system," in *2016 41st International Conference on Infrared, Millimeter, and Terahertz waves (IRMMW-THz)*, pp. 1–2, Sept 2016.

[27] D. A. Basnayaka and H. Haas, "Hybrid rf and vlc systems: Improving user data rate performance of vlc systems," in *2015 IEEE 81st Vehicular Technology Conference (VTC Spring)*, pp. 1–5, May 2015.

[28] H. L. Minh, D. O'Brien, G. Faulkner, L. Zeng, K. Lee, D. Jung, Y. Oh, and E. T. Won, "100-mb/s nrz visible light communications using a postequalized white led," *IEEE Photonics Technology Letters*, vol. 21, pp. 1063–1065, Aug 2009.

[29] P. A. Haigh, F. Bausi, H. L. Minh, I. Papakonstantinou, W. O. Popoola, A. Burton, and F. Cacialli, "Wavelength-multiplexed polymer leds: Towards 55 mb/s organic visible light communications," *IEEE Journal on Selected Areas in Communications*, vol. 33, pp. 1819–1828, Sept 2015.

[30] H. L. Minh, D. O'Brien, G. Faulkner, L. Zeng, K. Lee, D. Jung, Y. Oh, and E. T. Won, "100-mb/s nrz visible light communications using a postequalized white led," *IEEE Photonics Technology Letters*, vol. 21, pp. 1063–1065, Aug 2009.

[31] H. L. Minh, D. O'Brien, G. Faulkner, L. Zeng, K. Lee, D. Jung, and Y. Oh, "High-speed visible light communications using multiple-resonant equalization," *IEEE Photonics Technology Letters*, vol. 20, pp. 1243–1245, July 2008.

[32] H. Elgala, R. Mesleh, and H. Haas, "Indoor optical wireless communication: potential and state-of-the-art," *IEEE Communications Magazine*, vol. 49, pp. 56–62, September 2011.

[33] F. Jin, X. Li, R. Zhang, C. Dong, and L. Hanzo, "Resource allocation under delay-guarantee constraints for visible-light communication," *IEEE Access*, vol. 4, pp. 7301–7312, 2016.

[34] T. Komine and M. Nakagawa, "Fundamental analysis for visible-light communication system using led lights," *IEEE Transactions on Consumer Electronics*, vol. 50, pp. 100–107, Feb 2004.

[35] J. Jiang, Y. Huo, F. Jin, P. Zhang, Z. Wang, Z. Xu, H. Haas, and L. Hanzo, "Video streaming in the multiuser indoor visible light downlink," *IEEE Access*, vol. 3, pp. 2959–2986, 2015.

[36] R. F. Karlicek, "Smart lighting - beyond simple illumination," in *2012 IEEE Photonics Society Summer Topical Meeting Series*, pp. 147–148, July 2012.

[37] Y. Wang, N. Chi, Y. Wang, L. Tao, and J. Shi, "Network architecture of a high-speed visible light communication local area network," *IEEE Photonics Technology Letters*, vol. 27, pp. 197–200, Jan 2015.

[38] J. Vucic and K. D. Langer, "High-speed visible light communications: State-of-the-art," in *OFC/NFOEC*, pp. 1–3, March 2012.

[39] P. H. Binh and N. T. Hung, "High-speed visible light communications using znse-based white light emitting diode," *IEEE Photonics Technology Letters*, vol. 28, pp. 1948–1951, Sept 2016.

[40] J. J. D. McKendry, R. P. Green, A. E. Kelly, Z. Gong, B. Guilhabert, D. Massoubre, E. Gu, and M. D. Dawson, "High-speed visible light communications using individual pixels in a micro light-emitting diode array," *IEEE Photonics Technology Letters*, vol. 22, pp. 1346–1348, Sept 2010.

[41] K. Ebihara, K. Kamakura, and T. Yamazato, "Layered transmission of space-time coded signals for image-sensor-based visible light communications," *Journal of Lightwave Technology*, vol. 33, pp. 4193–4206, Oct 2015.

[42] D. K. Misra, *Filter Design*, pp. 333–391. John Wiley & Sons, Inc., 2004.

[43] A. Dornan, *The Essential Guide to Wireless Communications Applications, Second Edition: From Cellular Systems to Wi-Fi*. Upper Saddle River, NJ, USA: Prentice-Hall, Inc., 2nd ed., 2002.

[44] R. Ludwig and G. Bogdanov, *RF circuit design : theory and applications*. Upper Saddle River, NJ : Prentice-Hall, [2nd.ed] ed., 2009. Includes bibliographical references and index.

[45] J. Vincent, P. Borderies, J. R. Poirier, and V. Gobin, "Long-range three-dimensional ground wave propagation modeling over flat, irregular terrain," *IEEE Transactions on Antennas and Propagation*, vol. 64, pp. 1900–1906, May 2016.

[46] L. Zhou, X. Xi, J. Liu, and N. Yu, "Lf ground-wave propagation over irregular terrain," *IEEE Transactions on Antennas and Propagation*, vol. 59, pp. 1254–1260, April 2011.

[47] S. F. Mahmoud and Y. M. M. Antar, "High frequency ground wave propagation," *IEEE Transactions on Antennas and Propagation*, vol. 62, pp. 5841–5846, Nov 2014.

[48] Y. Erhel, D. Lemur, M. Oger, J. L. Masson, and F. Marie, "Evaluation of ionospheric hf mimo channels: Two complementary circular polarizations reduce correlation.," *IEEE Antennas and Propagation Magazine*, vol. 58, pp. 38–48, Dec 2016.

[49] K. Saha, *The Earth's Atmosphere: Its Physics and Dynamics*. Springer Berlin Heidelberg, 2008.

[50] J. M. Moran and B. R. Rosen, "Estimation of the propagation delay through the troposphere from microwave radiometer data," *Radio Science*, vol. 16, pp. 235–244, March 1981.

[51] S. H. Cho and J. R. Wait, "Electromagnetic wave propagation in a laterally nonuniform troposphere," *Radio Science*, vol. 13, no. 2, pp. 253–253, 1978.

[52] A. Saakian, *Radio Wave Propagation Fundamentals*. Artech House Remote Sensing Library, Artech House, 2011.

[53] V. Granatstein, *Physical Principles of Wireless Communications*. Taylor & Francis, 2007.

[54] M. Uysal and H. Nouri, "Optical wireless communications—an emerging technology," in *Transparent Optical Networks (ICTON), 2014 16th International Conference on*, pp. 1–7, IEEE, 2014.

[55] F. R. Gfeller and U. Bapst, "Wireless in-house data communication via diffuse infrared radiation," *Proceedings of the IEEE*, vol. 67, pp. 1474–1486, Nov 1979.

[56] M. A. Khalighi and M. Uysal, "Survey on free space optical communication: A communication theory perspective," *IEEE Communications Surveys Tutorials*, vol. 16, pp. 2231–2258, Fourthquarter 2014.

[57] A. A. Huurdeman, *Telex*, pp. 510–514. Wiley-IEEE Press, 2003.

[58] P. A. Haigh, F. Bausi, H. L. Minh, I. Papakonstantinou, W. O. Popoola, A. Burton, and F. Cacialli, "Wavelength-multiplexed polymer leds: Towards 55 mb/s organic visible light communications," *IEEE Journal on Selected Areas in Communications*, vol. 33, pp. 1819–1828, Sept 2015.

[59] D. C. O'Brien, L. Zeng, H. Le-Minh, G. Faulkner, J. W. Walewski, and S. Randel, "Visible light communications: Challenges and possibilities," in *2008 IEEE 19th International Symposium on Personal, Indoor and Mobile Radio Communications*, pp. 1–5, Sept 2008.

[60] P. Luo, M. Zhang, Z. Ghassemlooy, H. L. Minh, H. M. Tsai, X. Tang, L. C. Png, and D. Han, "Experimental demonstration of rgb led-based optical camera communications," *IEEE Photonics Journal*, vol. 7, pp. 1–12, Oct 2015.

[61] "Ieee standard for local and metropolitan area networks–part 15.7: Short-range wireless optical communication using visible light," *IEEE Std 802.15.7-2011*, pp. 1–309, Sept 2011.

[62] M. Marinoni, A. Biondi, P. Buonocunto, G. Franchino, D. Cesarini, and G. Buttazzo, "Real-time analysis and design of a dual protocol support for bluetooth le devices," *IEEE Transactions on Industrial Informatics*, vol. 13, pp. 80–91, Feb 2017.

[63] N. Q. Mehmood and R. Culmone, "A data acquisition and document oriented storage methodology for ant+ protocol sensors in real-time web," in *2016 30th International Conference on Advanced Information Networking and Applications Workshops (WAINA)*, pp. 312–318, March 2016.

[64] N. E. Madhoun and G. Pujolle, "Security enhancements in emv protocol for nfc mobile payment," in *2016 IEEE Trustcom/BigDataSE/ISPA*, pp. 1889–1895, Aug 2016.

[65] W. Z. Khan, H. M. Zangoti, M. Y. Aalsalem, M. Zahid, and Q. Arshad, "Mobile rfid in internet of things: Security attacks, privacy risks, and countermeasures," in *2016 International Conference on Radar, Antenna, Microwave, Electronics, and Telecommunications (ICRAMET)*, pp. 36–41, Oct 2016.

[66] G. Constable and B. Somerville, *A Century of Innovation: Twenty Engineering Achievements that Transformed Our Lives*. Joseph Henry Press, 2003.

[67] "Number of smartphone users worldwide 2014-2020."

[68] M. Lu, C. Lai, T. Ye, J. Liang, and X. Yuan, "Visual analysis of multiple route choices based on general gps trajectories," *IEEE Transactions on Big Data*, vol. PP, no. 99, pp. 1–1, 2017.

[69] A. Berenguer, J. Goncalves, S. Hosio, D. Ferreira, T. Anagnostopoulos, and V. Kostakos, "Are smartphones ubiquitous?: An in-depth survey of smartphone adoption by seniors," *IEEE Consumer Electronics Magazine*, vol. 6, pp. 104–110, Jan 2017.

[70] T. c. Chiueh, H. Lin, A. Chao, Anthony, T. G. Wu, C. M. Wang, and Y. S. Wu, "Smartphone virtualization," in *2016 IEEE 22nd International Conference on Parallel and Distributed Systems (ICPADS)*, pp. 141–150, Dec 2016.

[71] F. M. Tseng and Y. L. Liu, "Combining scenario analysis with the diffusion model and the competitive model for analyzing the development of the smartphone operating system," in *2012 Proceedings of PICMET '12: Technology Management for Emerging Technologies*, pp. 1581–1590, July 2012.

[72] "Android just hit a record 88% market share of all smartphones."

[73] A. Bruckstein, "On optimal image digitization," *IEEE Transactions on Acoustics, Speech, and Signal Processing*, vol. 35, pp. 553–555, Apr 1987.

[74] B. Shahrasbi and N. Rahnavard, "Model-based nonuniform compressive sampling and recovery of natural images utilizing a wavelet-domain universal hidden markov model," *IEEE Transactions on Signal Processing*, vol. 65, pp. 95–104, Jan 2017.

[75] M. Sonka, V. Hlavac, and R. Boyle, *Image Processing, Analysis, and Machine Vision*. Thomson-Engineering, 2007.

[76] W. Wang, H. Liu, J. J. Zheng, and J. A. Yang, "Integrated blur image quality assessment based on human visual perception," in *2015 International Conference on Computer Science and Applications (CSA)*, pp. 119–124, Nov 2015.

[77] "Bbc bitesize - gcse physics - the electromagnetic (em) spectrum - revision 1."

[78] E. C. Lalor, R. B. Reilly, B. A. Pearlmutter, and J. J. Foxe, "A spectrum of colors: Investigating the temporal frequency characteristics of the human visual system using a system identification approach," in *2006 International Conference of the IEEE Engineering in Medicine and Biology Society*, pp. 3720–3723, Aug 2006.

[79] W. K. Pratt, *Digital Image Processing (2Nd Ed.)*. New York, NY, USA: John Wiley & Sons, Inc., 1991.

[80] D. Amitrano, V. Belfiore, F. Cecinati, G. D. Martino, A. Iodice, P. P. Mathieu, S. Medagli, D. Poreh, D. Riccio, and G. Ruello, "Urban areas enhancement in multitemporal sar rgb images using adaptive coherence window and texture information," *IEEE Journal of Selected Topics in Applied Earth Observations and Remote Sensing*, vol. 9, pp. 3740–3752, Aug 2016.

[81] F. Albiol, A. Corbi, and A. Albiol, "Geometrical calibration of x-ray imaging with rgb cameras for 3d reconstruction," *IEEE Transactions on Medical Imaging*, vol. 35, pp. 1952–1961, Aug 2016.

[82] R. Mancuso, S. Smorfa, and M. Olivieri, "A novel high-quality yuv-based image coding technique for efficient image storage in portable electronic appliances," *IEEE Transactions on Consumer Electronics*, vol. 54, pp. 695–702, May 2008.

[83] R. J. Patan, M. Chakraborty, and S. S. Devi, "Blind color image de-convolution in yuv space," in *2016 International Conference on Communication and Signal Processing (ICCSP)*, pp. 1551–1555, April 2016.

[84] R. Jain and P. K. Johari, "An improved approach of cbir using color based hsv quantization and shape based edge detection algorithm," in *2016 IEEE International Conference on Recent Trends in Electronics, Information Communication Technology (RTEICT)*, pp. 1970–1975, May 2016.

[85] M. Berthier, S. E. Asmar, and C. Frélicot, "Binary codes k-modes clustering for hsi segmentation," in *2016 IEEE 12th Image, Video, and Multidimensional Signal Processing Workshop (IVMSP)*, pp. 1–5, July 2016.

[86] R. Lukac and K. Plataniotis, *Color Image Processing: Methods and Applications*. Image Processing Series, CRC Press, 2006.

[87] T. Moeslund, *Introduction to Video and Image Processing: Building Real Systems and Applications*. Undergraduate Topics in Computer Science, Springer London, 2012.

[88] R. Szeliski, *Computer Vision: Algorithms and Applications*. New York, NY, USA: Springer-Verlag New York, Inc., 1st ed., 2010.

[89] R. J. Schalkoff, *Digital Image Processing and Computer Vision: An Introduction to Theory and Implementations*. New York, NY, USA: John Wiley & Sons, Inc., 1989.

[90] G. Bradski and A. Kaehler, *Learning OpenCV: Computer Vision in C++ with the OpenCV Library*. O'Reilly Media, Inc., 2nd ed., 2013.

[91] Itseez, "Open source computer vision library." https://github.com/itseez/opencv, 2015.

[92] Itseez, *The OpenCV Reference Manual*, 2.4.9.0 ed., April 2014.

[93] J. Niu, W. Song, C. Liu, L. Shu, and C. Chen, "Necas: Near field communication system for smartphones based on visible light," in *2014 IEEE Wireless Communications and Networking Conference (WCNC)*, pp. 2426–2431, April 2014.

[94] S. H. Chen and C. W. Chow, "Color-shift keying and code-division multiple-access transmission for rgb-led visible light communications using mobile phone camera," *IEEE Photonics Journal*, vol. 6, pp. 1–6, Dec 2014.

[95] Qualcomm, "Wireless evolution and engineering." https://www.qualcomm.com/invention/technologies/wireless, 2016.

[96] C. Danakis, M. Afgani, G. Povey, I. Underwood, and H. Haas, "Using a cmos camera sensor for visible light communication," in *2012 IEEE Globecom Workshops*, pp. 1244–1248, Dec 2012.

[97] "Image Sensors & Processors, howpublished = http://www.onsemi.com/powersolutions/taxonomy.do?id=2209&lctn=header, note = Accessed: 2017-01-03."

[98] 2012-01-10-01, "Casio unveils prototype of visible light communication system using smartphones at ces - 2012 - news - casio."

[99] P. Luo, M. Zhang, Z. Ghassemlooy, H. L. Minh, H. M. Tsai, X. Tang, and D. Han, "Experimental demonstration of a 1024-qam optical camera communication system," *IEEE Photonics Technology Letters*, vol. 28, pp. 139–142, Jan 2016.

[100] T. Nguyen, N. T. Le, and Y. M. Jang, "Practical design of screen-to-camera based optical camera communication," in *2015 International Conference on Information Networking (ICOIN)*, pp. 369–374, Jan 2015.

[101] R. O. Duda and P. E. Hart, "Use of the Hough transformation to detect lines and curves in pictures," *Commun. ACM*, vol. 15, no. 1, pp. 11–15, 1972.

[102] T. Hao, R. Zhou, and G. Xing, "Cobra: Color barcode streaming for smartphone systems," in *Proceedings of the 10th International Conference on Mobile Systems, Applications, and Services*, MobiSys '12, (New York, NY, USA), pp. 85–98, ACM, 2012.

[103] S. D. Perli, N. Ahmed, and D. Katabi, "Pixnet: Interference-free wireless links using lcd-camera pairs," in *Proceedings of the Sixteenth Annual International Conference on Mobile Computing and Networking*, MobiCom '10, (New York, NY, USA), pp. 137–148, ACM, 2010.

[104] J. R. Parker, *Algorithms for Image Processing and Computer Vision*. New York, NY, USA: John Wiley & Sons, Inc., 1st ed., 1996.

[105] I. O. for Standardization and O. I. de Normalisation, *Information Technology - Automatic Identification and Data Capture (AIDC) Techniques - Harmonized Vocabulary*. International Standard ISO/IEC, ISO/IEC, 2005.

[106] A. Ashok, S. Jain, M. Gruteser, N. Mandayam, W. Yuan, and K. Dana, "Capacity of pervasive camera based communication under perspective distortions," in *2014 IEEE International Conference on Pervasive Computing and Communications (PerCom)*, pp. 112–120, March 2014.

[107] G. Woo, A. Lippman, and R. Raskar, "Vrcodes: Unobtrusive and active visual codes for interaction by exploiting rolling shutter," in *2012 IEEE International Symposium on Mixed and Augmented Reality (ISMAR)*, pp. 59–64, Nov 2012.

[108] B. Zhang, K. Ren, G. Xing, X. Fu, and C. Wang, "Sbvlc: Secure barcode-based visible light communication for smartphones," *IEEE Transactions on Mobile Computing*, vol. 15, pp. 432–446, Feb 2016.

[109] T. Fath, F. Schubert, and H. Haas, "Wireless data transmission using visual codes."

[110] S. Hranilovic and F. R. Kschischang, "A pixelated mimo wireless optical communication system," *IEEE Journal of Selected Topics in Quantum Electronics*, vol. 12, pp. 859–874, July 2006.

[111] W. A. Cahyadi, Y. H. Kim, Y. H. Chung, and C. J. Ahn, "Mobile Phone Camera-Based Indoor Visible Light Communications With Rotation Compensation," *IEEE Photonics Journal*, vol. 8, no. 2, pp. 1–8, 2016.

[112] T. C. Bui and S. Kiravittaya, "Demonstration of using camera communication based infrared LED for uplink in indoor visible light communication," in *2016 IEEE Sixth International Conference on Communications and Electronics (ICCE)*, pp. 71–76, 2016.

[113] T. N. Shene, K. Sridharan, and N. Sudha, "Real-time surf-based video stabilization system for an fpga-driven mobile robot," *IEEE Transactions on Industrial Electronics*, vol. 63, pp. 5012–5021, Aug 2016.

[114] B. Su, S. Lu, and C. L. Tan, "Robust document image binarization technique for degraded document images," *IEEE Transactions on Image Processing*, vol. 22, pp. 1408–1417, April 2013.

[115] D. Fang, Z. Nanning, and X. Jianru, "Primal sketch of images based on empirical mode decomposition and hough transform," in *2008 3rd IEEE Conference on Industrial Electronics and Applications*, pp. 2521–2524, June 2008.

[116] D. Tsonev, S. Videv, and H. Haas, "Light fidelity (li-fi): towards all-optical networking," 2013.

[117] J. Vučić, C. Kottke, S. Nerreter, K. Habel, A. Büttner, K. D. Langer, and J. W. Walewski, "230 mbit/s via a wireless visible-light link based on ook modulation of phosphorescent white leds," in *2010 Conference on Optical Fiber Communication (OFC/NFOEC), collocated National Fiber Optic Engineers Conference*, pp. 1–3, March 2010.

[118] D. F. Zhang, Y. J. Zhu, and Y. Y. Zhang, "Multi-LED Phase-Shifted OOK Modulation Based Visible Light Communication Systems," *IEEE Photonics Technology Letters*, vol. 25, no. 23, pp. 2251–2254, 2013.

[119] J. Y. Wang, J. B. Wang, M. Chen, and X. Song, "Dimming scheme analysis for pulse amplitude modulated visible light communications," in *Wireless Communications & Signal Processing (WCSP), 2013 International Conference on*, pp. 1–6, 2013.

[120] L. Grobe and K. D. Langer, "Block-based PAM with frequency domain equalization in visible light communications," in *2013 IEEE Globecom Workshops (GC Wkshps)*, pp. 1070–1075, 2013.

[121] K. I. Ahn and J. K. Kwon, "Capacity Analysis of M-PAM Inverse Source Coding in Visible Light Communications," *Journal of Lightwave Technology*, vol. 30, no. 10, pp. 1399–1404, 2012.

[122] L. Wei, H. Zhang, and B. Yu, "Optimal bit-and-power allocation algorithm for VLC-OFDM system," *Electronics Letters*, vol. 52, no. 12, pp. 1036–1037, 2016.

[123] C. Ma, H. Zhang, M. Yao, Z. Xu, and K. Cui, "Distributions of PAPR and crest factor of OFDM signals for VLC," in *2012 IEEE Photonics Society Summer Topical Meeting Series*, pp. 119–120, 2012.

[124] S. V. Kothiya and K. B. Mistree, "A review on real time object tracking in video sequences," in *2015 International Conference on Electrical, Electronics, Signals, Communication and Optimization (EESCO)*, pp. 1–4, Jan 2015.

[125] C. Schmid and R. Mohr, "Local grayvalue invariants for image retrieval," *IEEE Transactions on Pattern Analysis and Machine Intelligence*, vol. 19, pp. 530–535, May 1997.

[126] A. M. Salazar, I. M. de Diego, C. Conde, and E. C. Pardos, "Evaluation of keypoint descriptors applied in the pedestrian detection in low quality images," *IEEE Latin America Transactions*, vol. 14, pp. 1401–1407, March 2016.

[127] D. G. Lowe, "Distinctive Image Features from Scale-Invariant Keypoints," *Int. J. Comput. Vision*, vol. 60, no. 2, pp. 91–110, 2004.

[128] E. Rublee, V. Rabaud, K. Konolige, and G. Bradski, "ORB: An efficient alternative to SIFT or SURF," 2011.

[129] L. Juan and O. Gwon, "A Comparison of SIFT, PCA-SIFT and SURF," *International Journal of Image Processing (IJIP)*, vol. 3, no. 4, pp. 143–152, 2009.

[130] P. Viola and M. J. Jones, "Robust real-time face detection," *Int. J. Comput. Vision*, vol. 57, pp. 137–154, May 2004.

[131] H. Xiangjian, L. Jianmin, W. Daming, J. Wenjing, and W. Qiang, "Canny edge detection on a virtual hexagonal image structure," in *Pervasive Computing (JCPC), 2009 Joint Conferences on*, pp. 167–172, 2009.

[132] C. Akinlar and E. Chome, "Cannysr: Using smart routing of edge drawing to convert canny binary edge maps to edge segments," in *2015 International Symposium on Innovations in Intelligent SysTems and Applications (INISTA)*, pp. 1–6, Sept 2015.

[133] R. Hartley and A. Zisserman, *Multiple View Geometry in Computer Vision*. New York, NY, USA: Cambridge University Press, 2 ed., 2003.

[134] M. Sonka, V. Hlavac, and R. Boyle, *Image Processing, Analysis, and Machine Vision*. Thomson-Engineering, 2007.

[135] J. Canny, "A Computational Approach to Edge Detection," *IEEE Trans. Pattern Anal. Mach. Intell.*, vol. 8, no. 6, pp. 679–698, 1986.

[136] C. Briot, *Briot and Bouquet's Elements of Analytical Geometry of Two Dimensions*. Bibliolife Reproduction, BiblioBazaar, 2009.

[137] D. Liu and J. Yu, "Otsu method and k-means," in *2009 Ninth International Conference on Hybrid Intelligent Systems*, vol. 1, pp. 344–349, Aug 2009.

[138] N. Otsu, "A Threshold Selection Method from Gray-level Histograms," *IEEE Transactions on Systems, Man and Cybernetics*, vol. 9, no. 1, pp. 62–66, 1979.

[139] R. Boubezari, H. L. Minh, Z. Ghassemlooy, and A. Bouridane, "Smartphone Camera Based Visible Light Communication," *Journal of Lightwave Technology*, vol. 34, no. 17, pp. 4121–4127, 2016.

[140] Magnes, Jannyrocks, mbk2554, Dobbo, Fajo, E. OSO, i. D. H. One, and Kevo, "Sony dsc-qx30 lens-style camera with 30x optical zoom," Dec 2014.

[141] "Htc one (m8) - user manual - support | htc united kingdom."

[142] L. Belussi and N. Hirata, "Fast qr code detection in arbitrarily acquired images," in *2011 24th SIBGRAPI Conference on Graphics, Patterns and Images*, pp. 281–288, Aug 2011.

[143] R. Boubezari, H. L. Minh, Z. Ghassemlooy, and A. Bouridane, "Novel detection technique for smartphone to smartphone visible light communications," in *2016 10th International Symposium on Communication Systems, Networks and Digital Signal Processing (CSNDSP)*, pp. 1–5, July 2016.